Title
Multisectored Ultrasound Applicators for Thermal Therapy

Permalink
https://escholarship.org/uc/item/9t32m225

Author
Kinsey, Adam M

Publication Date
2007-05-29

Peer reviewed|Thesis/dissertation

Multisectored Ultrasound Applicators for Thermal Therapy

by

Adam Merritt Kinsey

DISSERTATION

Submitted in partial satisfaction of the requirements for the degree of

DOCTOR OF PHILOSOPHY

in

BIOENGINEERING

in the

GRADUATE DIVISIONS

of the

UNIVERSITY OF CALIFORNIA, SAN FRANCISCO

And

Multisectored Ultrasound Applicators for Thermal Therapy

Copyright 2007

by

Adam Merritt Kinsey

Abstract

Multisectored Ultrasound Applicators for Thermal Therapy

by

Adam Merritt Kinsey

Doctor of Philosophy in Bioengineering

University of California, San Francisco/Berkeley

Chris J. Diederich, Ph.D., Dissertation Research Director

Sarah J. Nelson, Ph.D., Chair

Heat treatments can be used as an adjunct to radiotherapy or chemotherapy or as a stand-alone alternative to surgery. Despite the therapeutic effects of heat, acceptance of thermal therapy in the clinic has been slow because of a lack of accurate control of heating distributions. Many different types of heating modalities and devices have been developed to deliver thermal therapy. Recent advancements in non-invasive temperature monitoring, in particular, MR, give an increased understanding of the spatial deposition of heat delivery in tissue. Ultrasound offers excellent spatial energy deposition and increased heating penetration due to its short wavelength. External, intracavitary, and interstitial ultrasound heating devices can deliver accurate thermal treatments when coupled with MR temperature monitoring. This work presents the development and evaluation of novel interstitial and transurethral ultrasound thermal therapy

applicators designed for use with MR temperature monitoring. Multisectored tubular ultrasound transducers were developed and incorporated into the devices to deliver conformal thermal treatments in the angular and radial dimensions. To provide three dimensional control of the heating distribution, multiple multisectored transducers were incorporated along the length of the applicators. The devices were constructed of MR compatible materials and do not require any movement or manipulation during treatment to deliver a conformal heating distribution. Acoustic characterization of the multisectored ultrasound applicators was conducted using force-balance acoustic efficiency measurements and rotational acoustic beam profiles. In this work, 2D and 3D biothermal models were modified and developed to evaluate the heating characteristics of these devices. For verification of the model and thermal lesion evaluation, *ex vivo* tissue studies were completed. Finally, *in vivo* experiments under MR guidance and MR temperature monitoring were conducted in canine thigh muscle for the interstitial devices and canine prostate for the transurethral applicators. The *in vivo* studies displayed the ability of multisectored ultrasound applicators to conform thermal therapy to a target area during treatment according to feedback from MR temperature images and. This work details the design, development, biothermal model characterization, *ex vivo* tissue evaluation, and *in vivo* MR guided evaluation of novel multisectored ultrasound devices and outlines their potential for improving thermal therapy.

To my parents, who have endlessly strived to provide me opportunity and whose love and support have always guided me.

Acknowledgements

Thank you to my family, friends, advisors, and colleagues who have provided me with support and counsel throughout my academic career. Most importantly, I would like to thank my graduate advisor, Dr. Chris Diederich, for his support, guidance, and friendship. Because of Chris, my graduate education was an amazing experience. I am grateful for the knowledge and guidance of my colleagues in the Thermal Therapy Research Group at UCSF, in particular, Dr. Will Nau, Dr. Dan Tyreus, Richard Shu, and Dr. Tony Ross, as their help and friendship have been invaluable to my academic career.

There have been many others who have shaped me and my education. Thank you to the members of my dissertation and qualifying exam committees; Dr. Sarah Nelson, Dr. Jeff Lotz, and Dr. Penny Sneed. I would like to thank Dr. Kim Butts Pauly, Dr. Viola Rieke, and Dr. Graham Sommer at Stanford. Thank you to the Joint Graduate Group in Bioengineering at UCSF and UCB.

Most of all, I am grateful for the support of my family. I would like to thank Erica Ludlum for her support and encouragement. Thank you to my sister, Sarah Kinsey, for always challenging me and cheering me forward. My parents, Merritt and Lois Kinsey, have always strived to offer me the greatest of opportunities, for which I am forever grateful. Their love has shaped my life and career.

Table of Contents

List of Tables

List of Figures

Chapter 1

Introduction

1.1 Hyperthermia

From relieving sore muscles to reconstructing tissues to treating cancer, the therapeutic effect of heat on the body has been explored for centuries. Medical treatment with heat can be separated into two categories; hyperthermia and thermal ablation (also referred to herein as high-temperature thermal therapy.) Hyperthermia is most commonly used for cancer treatment as an adjuvant to radiotherapy[84,103] and recently, chemotherapy.[8,57] By heating tissue 2-8 ^oC above steady-state internal body temperature (37 ^oC), the cells become sensitized to radiation and chemotherapy, increasing the efficacy of treatment. In the case of radiation, this occurs through thermal denaturization of

enzymes in the cell necessary for the repair of strand breaks.[100] Hyperthermia temperatures can also cause the cells to oxygenate, which can result in the creation of more oxygen radicals when the cells are irradiated.[44] The creation of poisonous oxygen radicals is one of the primary ways in which radiation therapy necroses tissue. Because of this effect, hyperthermia can help destroy hypoxic tissues that are often radiation resistant.[86] When hyperthermia and radiation are delivered concurrently, the amount of cell killing significantly increases in comparison to when the therapies are individually delivered.[84]

Chemotherapy involves poisoning cells with chemical compounds, either natural or synthetic. Chemotherapy is often an effective method of treating cancer because many tumors have a highly vascular periphery where drugs will accumulate. Hyperthermia can cause an increase in blood flow and dilation of blood vessels and, when targeted to tumor cells, results in even more preferential deposition of chemotherapy to the cancer area. In addition, hyperthermia can make cell membranes more permeable to chemical compounds, allowing more of the accumulated drugs to be deposited into the cell.[31,37] The combination of hyperthermia and chemotherapy has been shown to increase the efficacy of treatment compared to traditional chemotherapy by more than two-fold.[57,100]

1.2 Thermal Ablation

Bulk cell killing with heat, or thermal coagulative necrosis, involves high

temperatures (> 50 ^{o}C) that irreversibly denature cellular proteins. Similar to hyperthermia, high-temperature thermal therapy can be used in conjunction with radiation and chemotherapy; however, it is typically applied as an alternative to radiation or surgical methods for cancer treatment. Thermal ablation is appealing to investigators and clinicians for a variety of reasons. In most cases, the delivery of heat can be accomplished with a small needle probe or with an external device, making thermal ablation significantly less invasive than surgery. This can reduce major treatment complications and improve mortality rates, possibly resulting in lower costs due to decreased hospital stay. Another key consideration for delivering thermal ablation therapy is that it can be delivered multiple times for the treatment of recurrent cancer or after other treatments fail.

1.3 Thermal Dose

Studies have shown that cell killing with heat is related to the amount of time the treated tissue is at a certain temperature. In other words, delivering lower temperatures for a long period of time can result in a similar thermal lesion to delivering higher temperatures for a short period of time. The time-temperature relationship of cytotoxic heat treatment is known as thermal dose, which can be quantified by the Sapareto-Dewey isoeffect thermal dose equation:[30,99]

$$t_{43} = \sum_{t=0}^{t_{final}} \Delta t \bullet R^{(T-43)}$$

where t_{43} is the thermal dose, expressed in equivalent time (min) at 43 ºC. Thermal dose is determined from the cumulative thermal damage between the beginning of heating ($t = 0$) and the end of treatment (t_{final}). Thermal damage is related to the time between temperature measurements (Δt), the average temperature (T) during Δt, and an empirically derived constant, R. Based on an Arrenhius experimental analysis of cell killing, R is equal to 2 for temperatures below 43 ºC and 4 for temperatures at 43 ºC and above. Thermal coagulative necrosis is often seen when the thermal dose values are $t_{43} > 240$ min, although this can vary depending on the tissue type.[21,32]

1.4 Clinical Heat Treatment

Hyperthermia and thermal ablation have been applied for the treatment of numerous types of cancers. Hyperthermia as an adjunct to radiation therapy has shown improved efficacy in many types of tumors, including melanoma,[85] glioblastoma multiforme,[104] chest wall recurrence of breast cancer,[119] and cervical cancer.[117] In all of these studies, the addition of hyperthermia treatment increased the rates of tumor response and cancer-free survival than radiotherapy alone.

Thermal ablation is being used to treat localized cancerous tissue in sites

such as liver,[2] kidney,[105] brain,[5,74] prostate,[110] and bone.[95] There are many non-oncological uses of high-temperature thermal therapy as well. The diseases and conditions that are treated with heat include prostatic hyperplasia,[71,122] cardiac arrythmias,[121] uterine fibroids,[106] lower back pain,[98] and cosmetics such as dermal tightening.[48] One of the most prolific areas of development of thermal ablation technologies is for treating prostatic disease, primarily as a minimally-invasive alternative to surgical transurethral resection of the prostate (TURP). Heat treatments have demonstrated durability and efficacy close to TURP but with lower morbidity.[12,71] There are no major vessels within the prostate tissue, making heat treatments realistic and consistent. Two types of intracavitary heating applicators, transrectal and transurethral, have been developed to deliver treatment to the prostate. These methods provide advantages for heating the prostate because they minimize the number of tissue interfaces in the heating zone, allowing the heat source energy to be applied directly to the prostate.

1.5 Heating Modalities

Warm water baths and hot springs are two ancient methods for healing the mind and body. While the mechanisms of the therapeutic effect of these prescribed treatments were not known to the ancients, these were two of the first methods for delivering thermal therapy. These methods take advantage of heat

conduction and are still commonly used today both for muscle and joint aches and pains, as well as being a method for whole body hyperthermia. Thermal conduction is the most basic method of heating the body; however, it is not very effective for treating deep-seated localized disease or delivering a large amount of heat energy to a large volume. Heating modalities have been primarily developed with the goal of increasing the penetration depth of heat in tissue without increasing the overall maximum temperatures. The heating modalities outlined here take advantage of the properties of different types of waveforms at different frequencies as they attenuate through tissue.

1.5.1 Radiofrequency

Radiofrequency (RF) is probably the most common method for delivering medical heat treatments because of its ease of use. Also, these devices are the simplest in construction when compared to the rest of the modalities outlined here. RF devices emit electromagnetic waves with frequencies of 0.3-30 MHz. The heating from these devices falls off in tissue with the square of radial distance from the tissue-electrode interface. In other words, while simple to construct and superior to thermal conduction sources, the radial penetration of heating from an RF heating probe is limited. To overcome this limited radial heating depth, many device designs utilize multiple RF sources or cooling near the RF source. These devices are practical and widely used for heat treatments; however, to increase the heating volume and obtain greater control of the heating

disposition, microwave or ultrasound devices should be considered.

1.5.2 Laser

Laser light can be delivered to an internal tissue through the use of fiber-optic cables. Laser excites the tissue and, as the tissue relaxes, heat is generated. The major advantage of using lasers for thermal ablation of tissue is the precision of heat treatment. The tip of a laser source can be on the order of 1 mm, allowing for use as a surgical tool or for fine cosmetic procedures. However, for thermal ablation of a large volume of tissue, such as a primary tumor, the radial penetration of the heating is less than 1 cm. Also, lasers rapidly coagulate tissue, which changes the tissue's optical properties and makes it difficult to heat far beyond the laser source.

1.5.3 Microwave

Microwaves are electromagnetic waves at frequencies of 300 MHz to several gigahertz that cause polar molecules in tissue to rotate at the frequency of the microwaves, which causes viscous heating. In the microwave frequency range, propagation of waves is predominantly radiative as compared to conductive at RF ranges, providing better heating penetration. Microwaves create larger lesions than both RF and laser devices and provide improved spatial control. They also are relatively simple when compared to ultrasound.

Microwave heating devices can be designed to deliver heating patterns with adaptable control, but this control is typically very limited.

1.5.4 Ultrasound

Ultrasound can be delivered to tissue with many different types of devices, including external, intracavitary, and interstitial applicators. Ultrasound waves at high frequencies (1-10 MHz) deposit energy in tissue due to viscous heating from vibrations. In general, due to its short wavelength, ultrasound provides favorable heating radial penetration when compared to the other heating modalities mentioned in this introduction. The attenuation coefficient of ultrasound energy is roughly proportional to frequency, which allows the penetration depth to be varied from <1 cm to >10 cm by changing the frequency. Also, ultrasound can be delivered from a number of different geometrical shapes and sizes. By changing the geometry of the transducer or using electronic focusing of the energy waves, ultrasound offers three dimensional control over the heating deposition. This control is significantly greater than with any of the other heating modalities. The limitations to ultrasound thermal therapy are significant acoustic absorption at bone interfaces, acoustic reflection from gas surfaces, and complex equipment design and treatments.

1.5.4.1 High-Intensity Focused Ultrasound

High-intensity focused ultrasound (HIFU) refers to an external or

intracavitary ultrasound thermal therapy device that either geometrically or electronically focus the ultrasound energy at a treatment site. Typically, these devices have a small focal zone and rapidly ablate a small heating region. To thermally treat a large volume of tissue, the focus can be moved in steps during treatment. The tissue coagulation is almost instantaneous when high power levels are applied, making the thermal damage relatively independent of heterogeneities and changes in the thermal parameters of tissue.[62] Geometrically focused HIFU devices (spherical transducers) can be mechanically scanned to treat large tissue volumes. This offers a high degree of spatial control over the ultrasound energy deposition and resulting heating pattern. It is this spatial control that gives HIFU an advantage over heating modalities to adjust for temperature variations due to tumor irregularities, perfusion heterogeneity, and blood vessels. Mechanically scanned HIFU systems have been used clinically in the past.[55,73]

Most clinical heat treatments with ultrasound are done using HIFU systems that incorporate electronic focusing. This can be accomplished by using several transducer elements (as many as a few thousand) and driving them in a manner that brings the ultrasound waves into phase at a small focus in the tissue. Clever driving techniques have been developed that offer significant advantages over mechanically scanned geometrically focused systems.[41] HIFU phased array systems also provide a great deal of flexibility in treatment setup and planning. By properly controlling the ultrasound energy deposition, complex

beam patterns can be formed to account for phase aberrations and tissue interfaces.[9,42] Very recently, a commercial HIFU device system has been approved for the treatment of uterine fibroids.[77,106]

Intracavitary HIFU devices provide a minimally invasive alternative to surgery in tissue sites and tumors that are near a body cavity. This reduces the number of tissue interfaces in the heating area and makes ultrasound delivery more consistent. Intracavitary applicators can also utilize phased array systems for penetration depth and spatial control. Transrectal devices have been the primary method of delivering ultrasound thermal therapy to prostatic disease. Recent large clinical studies have been completed that demonstrate the effectiveness of transrectal HIFU for treating prostate cancer.[110] Also, many studies have been done inspecting the usefulness of transrectal HIFU for BPH treatment.[111]

1.5.4.2 Interstitial Ultrasound Devices

Interstitial methods are most often used for treating bulky or unresectable deep-seated tumors that are difficult to reach by external methods. While the technique is minimally invasive, it is still the treatment of choice in many sites because the heating source is implanted directly into the tumor, localizing the therapy. With ultrasound, interstitial techniques also overcome some of the limitations of HIFU, such as changes in impedance at tissue interfaces and ultrasound reflection at gas interfaces. This is because the energy is localized to

the tumor, which avoids heating healthy surrounding tissue. Interstitial implants are commonly used to localize radiotherapy, known as brachytherapy, which can be combined with interstitial hyperthermia treatments. Clinical trials utilizing this method of treatment with microwave devices for glioblastoma patients have shown an increase in 2-year survival from 15 % to 31 % as compared to radiotherapy alone.[104]

Interstitial ultrasound applicators have been developed for hyperthermia and thermal ablation treatments. These applicators typically consist of non-focused planar or tubular transducers. The outer electrode on the tubular transducers can be cut to isolate one part of the transducer, creating a directional heating pattern. The diameter of the tubular ultrasound transducers incorporated into interstitial devices is typically 1-3 mm. These applicators have demonstrated improved radial penetration compared to other heating modalities.[33,109] Interstitial ultrasound applicators have been constructed using two basic design templates; catheter-cooled and direct-coupled. Catheter-cooled applicators consist of a transducer assembly mounted on a support structure which can then be inserted into a 13-14 gauge catheter. Water cooling can then be delivered in through the insert and out through the catheter. This cools the tissue surrounding the applicator, allowing the ultrasound energy to penetrate farther into the tissue, and also cools the transducer as it heats up from mechanical inefficiencies. These devices have demonstrated the ability to generate high temperatures (> 50 ^{o}C) at continuous high power levels (>10 W).[81]

Direct-coupled interstitial ultrasound device designs have also been shown to provide excellent heating penetration when compared to other heating modalities. Only a thin layer of protective plastic coating separates the transducer from the tissue, which couples the ultrasound energy directly to the tissue. The applicators can be cooled through the center of the device with air or water.[26,27] Water cooled interstitial ultrasound devices (<3 mm OD) can make thermal lesions up to and beyond 4 cm in diameter in bench top[109] and *in vivo* experiments.[27] Both catheter-cooled and direct-coupled devices can incorporate multiple ultrasound elements along the length of the device to axially control and shape a heating pattern.[33,81] The power to each individual tubular element of multielement applicators can be adjusted to control the tissue temperature along the length of a catheter. The length and number of transducers within an applicator can be selected based upon the overall desired heating resolution and heating pattern size. With a large number of elements, the power deposition pattern does not have to be dependent on the placement of the catheter, which can be a limitation of RF and microwave techniques.

Interstitial devices have also been studied that incorporate planar or slightly focused ultrasound transducers. Studies of devices incorporating linear arrays of planar transducers have been able to flatten the temperature profile and extend the heating deeper into tissue.[18] The applicator must be rotated and the focus scanned to heat a large volume of tissue. This significantly extends the treatment time as compared to treatments using tubular transducers. Planar

transducers can also be incorporated into cylindrical devices; however, the diameter of the device may be too large for practical interstitial purposes.[65,66] Ultrasound phased arrays have been developed for transesophagael thermal therapy.[79] These arrays can provide an accurate method of thermal treatment; however, the device is too complicated and large (10 mm OD) for practical use as an interstitial method.

1.5.4.3 Transurethral Ultrasound Devices

The prostate is an excellent candidate for thermal ablation therapy. By accessing the prostate through the urethra, key tissue interfaces can be avoided. With transrectal devices, the ultrasound energy must travel through the rectal wall and it can be difficult to treat the anterior portion of the gland away from the rectum. Transurethral heating applicators are positioned in the center of the prostate and do not have to deal with tissue interfaces, as they heat from the inside out. Compared to interstitial techniques, this method of prostate treatment is significantly less invasive. Currently, the most common way of treating BPH disease is through the urethra [transurethral resection of the prostate (TURP)]. Also, the majority of thermal ablation treatments of BPH are done with commercially available transurethral microwave (TUMT) devices. However, to heat the whole gland for cancer therapy, the device must be able to necrose tissue up to 2.5 cm in radius from the urethra. Currently, this is the reason the most common method of heating the prostate for cancer treatment is a transrectal

HIFU approach. A HIFU setup is not possible to incorporate into a transurethral device because of size limitations and would still face some of the previously mentioned limitations of HIFU.

As discussed, ultrasound energy can penetrate much farther into the tissue than microwaves. This makes it the obvious choice for incorporating a heating modality into a transurethral device for treating prostate cancer. One of the first transurethral ultrasound devices consisted of an array of four sectored (180°) tubular transducers that were able to extend high temperatures (> 50 °C) more than 1.5 cm in *in vivo* tissue.[35] These devices showed excellent potential for prostate thermal therapy, but the directional heating pattern was fixed and control over the heating pattern was limited. To improve spatial control over the heating pattern conform thermal lesions to the prostate boundary, a very similar sectored (90°) tubular ultrasound was developed that could be rotated during treatment.[96] Recently, much of the research into transurethral ultrasound devices has focused on incorporating a planar transducer that can be rotated during treatment.[16,19,96] This provides a narrow acoustic beam width (~4 mm) and offers slightly better radial penetration than tubular transducers. When rotated, due to the small beam width, the device can very accurately shape a thermal lesion in the prostate. Furthering the same strategy, the beam width becomes even narrower when a slightly focused, curvilinear transducer is incorporated into a device.[97] This allows for even more precise heating; however, as the beam width narrows from a 90° sectored tubular to planar to

curvilinear transducer, the treatment time becomes longer with each step up in precision. The drawbacks of implementing rotating transurethral ultrasound applicators are increased treatment time, increased setup time, and a very complicated driving system. Many of these devices are being designed for use with magnetic resonance (MR) temperature monitoring and require an MR-compatible driving motor for the rotation.

1.6 MR Thermal Imaging

Thermal therapy is becoming more accepted in the clinic for the treatment of solid tumors and tissues. Although heat treatment has been explored for many years, acceptance was slow despite the obvious therapeutic benefits of heat. The main issue was inconsistency in heating distributions and the danger of heating healthy tissue. Now and in the past, temperatures are primarily controlled and monitored with invasive thermocouple probes. These probes provide very accurate temperature measurements, but without a large array of them, they cannot provide precise spatial information about a heating distribution. Within the last ten years, major advancements have been made in thermal dosimetry involving non-invasive spatial temperature maps. These technologies are based on diagnostic imaging modalities. MR imaging is the most research and common method of spatial temperature monitoring.

MR imaging provides an excellent tool for target definition, guidance of

device setup, and post-procedure therapy evaluation.[29] However, the most valuable aspect of using MR as a tool for monitoring thermal treatments is the ease of monitoring temperature changes in tissue. The main methods of monitoring temperature with MR imaging are based on simple tissue properties. The most accurate of these methods is known as diffusion thermal imaging, where the Brownian motion of the molecules in tissue, as described by the diffusion constant, changes exponentially with increases in temperature. This change in the diffusion constant can be observed in MR images on the basis of the signal attenuation in the presence of a pair of strong mutually counteracting gradients.[28] While the accuracy of the temperature change monitored can be less than 1 ^{o}C, this method is not practical for temperature monitoring in patients because it is very sensitive to tissue movement and requires a long period of time to acquire the images. In addition, the temperature sensitivity varies with tissue type.[46,93]

The original method used for monitoring temperature deep within the body with MR takes advantage of the relationship between T1 relaxation time and temperature.[87] T1 is linearly inversely proportional to temperature up to 55 ^{o}C. However, the method is only accurate within 3 ^{o}C, the sensitivity varies in different tissue, and temperature cannot be monitored in tissue that has been previously heated.[46] In the body, these limitations prevent this method of temperature monitoring from being robust, despite being resistant to patient movement.

1.6.1 Proton Resonance Frequency Shift

The most researched and common method for monitoring temperature in the body with MR relies on the linear relationship between the proton resonance frequency (PRF) of water and temperature. The chemical shift of PRF can be calculated from phase information in RF-spoiled gradient echo images as given by:

$$\Phi(T) = \gamma B_o \sigma(T) \cdot TE$$

where φ is the image phase, γ is the gyromagnetic ratio, TE is the echo time, B_o is the main magnetic field, T is temperature, and σ is the PRF shift. Subtraction of a reference baseline phase image before heating from the each sequential image acquisition creates a map of the temperature change as governed by:

$$\Delta T = T - T_{ref} = \frac{\Phi(T) - \Phi(T_{ref})}{\alpha B_o \gamma \cdot TE}$$

where α is the temperature dependency of the PRF shift, and $\alpha = (d\sigma/dT) = {\sim}0.01$ ppm $^oC^{-1}$.

The biggest advantage of the PRF method is that it is mostly independent of tissue composition.[90] One of the important issues associated with the PRF shift method is the inability to measure temperature in fat. High lipid content tissues, such as the breast, cannot be monitored with the PRF method. Fat can also cause artifacts in the temperature measurements in other lower fat content

tissues. The other key issue with the PRF shift MR temperature monitoring is the method's sensitivity to motion in the MR imaging field. This motion can cause errors in the image registration during image subtraction, which could falsely appear as temperature changes in a map. New methods and imaging sequences have been developed to minimize this temperature artifact due to motion. One method developed independently, but concurrently with this work, is referenceless PRF shift thermometry.[94] Taking advantage of the lack of water in fat tissue, so there are no phase changes, the phase in fat can serve as a background phase for each individual temperature image. In other words, the referenceless method removes the need for image subtraction, making it inherently more robust and resistant to tissue or device motion.

Very recently, commercial MR temperature imaging guided thermal therapy became approved for clinical use for the first time in the United States. A HIFU system incorporated with an MR system was approved for the treatment of uterine fibroids.[77,106] This system represents the new objective of thermal therapy; to become a commonly used treatment for benign and malignant tumors in the United States. Coupled with MR temperature imaging for therapy monitoring and treatment verification, the accuracy of thermal therapies should be significantly improved, remedying a problem that has plagued the field for decades. Also, as MR and heating device technology improves, these treatments should become more cost effective and may finally offer a safe, effective, minimally-invasive alternative to traditional surgery.

1.7   Research Objectives

The objective of this dissertation research was to design, develop, and comprehensively evaluate novel ultrasound devices for thermal therapy, with special considerations for guiding and monitoring the heating with MR temperature imaging. In this work, new interstitial and transurethral devices and catheter designs were developed. Multisectored tubular ultrasound transducers were incorporated into these devices to provide dynamic three-dimensional control over the creation of large heating distributions. The devices and transducers constructed in this research are MR-compatible and were designed with the limitations of MR temperature imaging in mind.

1.7.1   Dissertation Content

This work outlines a complete synthesis of new ultrasound thermal therapy devices from construction of the applicators to *in vivo* studies in canines under MR guidance.

Chapter 1 introduces heat treatment and heating modalities. It also details previous work done with ultrasound devices and discusses the importance of temperature measurement spatial accuracy with MR temperature imaging.

Chapter 2 outlines the biothermal model used to theoretically evaluate novel ultrasound transducer and device designs.

Chapter 3 details the construction, design, and evaluation of multisectored interstitial ultrasound applicators. This work has been previously published in the journal, *Medical Physics*.[61]

Chapter 4 compares the new multisectored interstitial ultrasound devices with a catheter-cooled rotating directional interstitial ultrasound device. The rotating device was also developed and constructed in the course of this research. Parts of this work were presented and published in the proceedings of the conferences, IEEE-SPIE 2004 and IEEE-EMBS 2004.

Chapter 5 discusses the evaluation of multisectored transurethral ultrasound applicators for high-temperature thermal therapy of the prostate. The transurethral devices were constructed and designed for use with real-time MR temperature monitoring and evaluated in three *in vivo* canine prostate glands. This work has been recently submitted for publication in *Medical Physics*.[60]

Chapter 6 gives a brief overview of the ability of the multisectored transurethral applicators developed and discussed in Chapter 5 for hyperthermia treatment. Low maximum temperature studies were conducted in three *in vivo* canine prostates.

Chapter 7 summarizes theoretical evaluation of the transurethral ultrasound applicators in the biothermal model outlined in Chapter 2. Different theoretical treatment, device, tissue, and control system parameters are identified and evaluated in simulated prostate tissue. These studies outline the potential and limitations of multisectored transurethral ultrasound applicators.

Chapter 8 offers conclusions of the research presented in this dissertation and a glimpse of future directions of ultrasound thermal therapy, as monitored by MR temperature monitoring.

Chapter 2

Biothermal Model of Multisectored Ultrasound Applicators

2.1 Introduction

The mechanisms of heat transfer in living tissue have been studied extensively. Accurate models of the biothermal response of tissue to thermal therapy are continually being developed and modified. Mathematical models of heating tissue are based upon Fourier's Law of Heat Conduction, which describes how heat conducts through a material over time. In living tissue, these models are significantly more complicated because of the effects of perfusion, large blood vessels, variable tissue properties, and tissue heterogeneities.

Typically, these mathematical models are solved using computer models and calculations, the two most common being finite difference and finite element methods. These computer models and simulations can be used for developing treatment strategies and, most importantly, for device design evaluation.[108] Biothermal models are often specific to individual device designs, including RF[20,113] and HIFU heating applicators.[42,108] In many cases, a model provides a fast method of testing many different design parameters. In addition, by incorporating simulated dynamic tissue characteristics, many possible treatment conditions can be observed that are difficult to experimentally model.

It is almost impossible to develop an encompassing heat transfer model for living biological tissue. This is because anatomy can vary greatly between patients, as well as significant differences between different types of tissues. In terms of cancer treatment, tumors have very irregular vasculature. Large blood vessels in the target tissue and variable vasculature in tumors can both cool the tissue or redistribute the heat in an unpredictable manner. However, some simple assumptions can be made to create a model that provides excellent insight into expected thermal therapy distributions and heating applicator performance. The most common method of modeling temperature distributions in living biological tissue was developed and published by a physician, H. H. Pennes, in 1948.[88] If one assumes that all heat transfer between the blood flow system and tissue occurs in the capillaries and that capillaries are uniformly distributed throughout the tissue, tissue perfusion can be modeled by a simple heat

convection term. The Pennes bioheat equation is Fourier's Law of Heat Conduction with terms added to incorporate perfusion and metabolism:

$$p_t c_t \frac{\partial T}{\partial t} = \nabla \cdot k \nabla T + \dot{m}_b c_b (T_b - T) + \dot{q}$$

where T is temperature (°C), t is the heating time (s), p_t is tissue density (kg m^{-3}), c_t is the tissue heat capacity (J kg^{-1} °C^{-1}), k is the thermal conductivity of the tissue (W m^{-1} °C^{-1}), m_b is the perfusion mass flow rate (kg m^{-3} s^{-1}), and c_b is the heat capacity of the blood (J kg^{-1} °C^{-1}). The assumption of uniform perfusion in the target tissue leads to a single constant term, T_b, describing the temperature of the blood (°C). Finally, the most important and flexible part of the equation is the heat generation term, q (W m^{-3}). In thermal ablation cases, heat generation from metabolism is typically ignored.

As a thermal dose is delivered to a tissue based on the equation detailed in Chapter 1, tissue properties such as perfusion and attenuation can vary. In the case of perfusion, when a large thermal dose is delivered, the blood vessels are destroyed as well as target tissue. To account for this change in perfusion in a mathematical model, perfusion ceases at $t_{43} > 300$ min.[35,63] As thermal dose accumulates, the properties of the target tissue change. This can include tissue shrinkage or tight tissue coagulation. It has been shown experimentally that the attenuation of tissue with respect to ultrasound changes as thermal dose accumulates.[22] In this work and other ultrasound models,[76,108] the ultrasound attenuation was modeled to increase linearly in proportion to the

$\log_{10}$ of the thermal dose from 10^2 to 10^7.

2.2 2D R-θ Model

A two-dimensional finite difference model in cylindrical coordinates was used to evaluate multisectored tubular ultrasound transducers incorporated into interstitial and transurethral applicators. The model was initially developed and published by P. D. Tyreus.[108] In this work, the model was modified to incorporate multisectored transducers, a bang-bang controller, multiple pilot point temperature controllers, and a manually adjusted power controller. In addition, an R-θ model and an R-Z model were used to evaluate heating in the angular dimension and along the length of applicator, respectively. These models were modified for multisectored ultrasound transducers and different types of control systems. Finally, the basis for a three-dimensional finite difference model was programmed and developed in this work and will be described later in the chapter. All the models were programmed in the Java language.

The 2D R-θ models used to evaluate tubular ultrasound applicators in this work were based on the Pennes bioheat equation in cylindrical coordinates:

$$\rho_t c_t \frac{\partial T}{\partial t} = \frac{1}{r}\frac{\partial}{\partial r}\left(kr\frac{\partial T}{\partial r}\right) + \frac{1}{r^2}\frac{\partial}{\partial \theta}\left(k\frac{\partial T}{\partial \theta}\right) + \frac{\partial}{\partial z}\left(k\frac{\partial T}{\partial z}\right) + \dot{m}_b c_b (T_b - T) + \dot{q}$$

The finite difference method for integration of partial differential equations was

used to solve this equation computationally. With a cylindrical coordinate system, finite differencing provides an advantage because it is straightforward and the coordinate system is not complex. To increase the accuracy of the model without significantly increasing the number of nodes, variable spacing was implemented to maintain the rigid spatial stability constraints that the finite difference method requires by keeping a large number of nodes near the transducer.

Finite difference methods can be solved using either explicit or implicit methods. Explicit methods provide excellent solution accuracy; however, they demand rigid system requirements to achieve numerical stability. Implicit methods are inherently stable; however, they ignore small-scale fluctuations in temperatures, which can then trickle down throughout the model and provide inaccurate solutions. The model used in this work is calculated using a mixed implicit and explicit finite difference method, known as the Crank-Nicholson method.[92] This method takes a simple average of the explicit and implicit estimates to determine the temperature change in tissue, offering better accuracy than an implicit method, while still maintaining stability.

2.2.1 Multisectored Tubular Transducers

Acoustic energy propagates radially away from a tubular (cylindrical) ultrasound source and generates heat in the tissue according to:

$$\ddot{q} = \frac{2\alpha I_s r_o}{r} e^{-2\mu(r-r_o)}$$

where α is the ultrasound absorption coefficient (Np m^{-1}), μ is the ultrasound attenuation coefficient (Np m^{-1}), I_s is the acoustic intensity at the surface of the transducer (W m^{-2}), r_o is the transducer radius (m), and r is radial position (m). The absorption coefficient is given a value equal to 65 % of the acoustic attenuation according to soft tissue heating studies.[22] The surface intensity was determined by the acoustic efficiency of the transducer (v) multiplied by the applied electrical power [P (W)] over the surface area [A (m^2)]. It is assumed in this model that the ultrasound absorption inside the transducer is zero and that the electrical energy that is not converted to acoustic energy (the difference from the acoustic efficiency) is converted to conductive heat within the transducer. In the model, the ultrasound heat generation is defined by:

$$\dot{q} = \begin{cases} 0 & for \quad r \leq r_{inner} \\ (1-v)\dfrac{P}{\pi\left(r_o^2 - r_{inner}^2\right)} & for \quad r_{inner} < r \leq r_o \\ \dfrac{Pv\alpha}{\pi l r} e^{-2\mu(r-r_o)} & for \quad r > r_o \end{cases}$$

where r_{inner} is the inner radius of the tubular transducer (m) and l is the length of the transducer (m). The boundary conditions used for the model for the heat generation term are defined by constant temperature at the model boundary and by a convective cooling term at the applicator surface due to water cooling:

$$\dot{q} = \frac{hA(T-T_w)}{V} \approx \frac{h(T-T_w)}{\Delta r}$$

where the cooling flow device boundary is defined by the surface area [A (m²)] and the flow volume [V (m³)], which can be simplified to the boundary flow thickness [Δr (m)]. T_w represents the temperature of the cooling flow (°C) and h is the convective heat transfer coefficient (W m^{-2} °C^{-1}).

The 2D R-θ model was modified to evaluate multisectored ultrasound transducers incorporated into catheter-cooled (CC) and internally-cooled, direct-coupled (ICDC) interstitial applicators and transurethral applicators. The heat generation term for cylindrical transducers was used to model the multisectored transducers. In this work, multisectored transducers were modeled by tagging each tissue and transducer node according to their radial position. The size of each sector in terms of angular degrees could then be assigned by the user. For example, a three sectored applicator could be split into three 120° sections or 160°, 120°, and 80° sections or any variables assigned by the user. For every tagged radial position, a power scheme was assigned to each node according to the input parameters for the corresponding independent sector. In addition, the model modification accomplished in this work also accounted for the acoustic dead zone that exists at the cuts in the transducers, assigning no direct ultrasound energy to the angular positions corresponding to the dead zones. In this way, the model was programmed to be flexible to any number of transducer segments, all with individual power control.

2.2.2 Applicator Control Systems

An important feature of the biothermal model for evaluating multisectored ultrasound heating applicators was the incorporation of applied power control systems. These systems demonstrate the flexibility of the multisectored applicators to control the shape and size of a heating pattern. A bang-bang style controller and a pilot point control utilize the measured temperature in the tissue as feedback for controlling the amount of power delivered to the applicator during theoretical studies.

2.2.2.1 Bang-Bang

In optimal control problems, often the control is restricted to be between a lower and an upper bound. If the optimal control switches from one extreme to the other at certain times, then it is referred to as bang-bang control. This is an example of a discrete time or digital controller. A bang-bang controller is the simplest type of controller to execute. In this model, the bang-bang controller is set to operate at two bounds: no power applied and maximum power applied as defined by the user. This is also known as an on/off controller. When a set maximum tissue temperature is reached in the simulation, power to the applicator is turned off; when the temperature dips below the maximum, the set power level is reapplied.

The bang-bang controller developed in this model can be customized

according to the user by setting the maximum temperature in the tissue and the controller update time. Typically, the simulations in this work were conducted with a time step of 0.1 s. To maintain controller stability, the controller update time was set at 0.5 s. At these short update times, a bang-bang controller acts as an almost perfect controller for heating in the body due to tissue conduction effects. The controller offers an excellent way to maintain a stable maximum temperature in a tissue for the duration of a simulated heat treatment. These stable maximum temperatures allow the user to explore the capabilities of multisectored applicators, including heating penetration depth, heating pattern shape, and heat treatment duration.

The bang-bang controller was programmed in this work to search for the maximum temperature in the entire simulated tissue at each time step iteration. In the case of multisectored ultrasound transducers, the model was programmed such that the maximum temperature in the area heated by each individual sector was used as feedback for that sector. In other words, each sector was controlled independently based on the directly adjacent maximum temperature. This is displayed in Figure 2.1 for a three sectored ultrasound transducer, where the temperatures T1, T2, and T3 represent the maximum temperature in the different sector areas represented by S1, S2, and S3.

In experimental practice, bang-bang controllers may not be realistic for the control of ultrasound heating applicators because of the monitoring system required to obtain temperature feedback to the applicator control system. If the
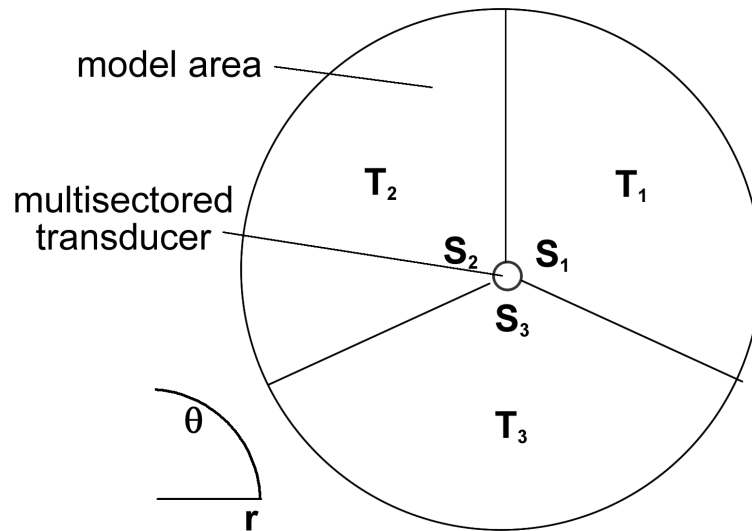
Figure 2.1: Bang-bang control scheme diagram. S_1, S_2, and S_3 represent the individual sector areas, and T1, T2, and T3 represent the maximum temperature feedback in the respective areas

controller temporal resolution becomes more than 1-2 s, then bang-bang control will cause temperature fluctuations in the tissue. Most temperature measurement systems have an update time of 3 s or greater. In the case of MR temperature measurement of heating devices, the temporal resolution is on the order of 5-15 s, making bang-bang controllers mostly obsolete. However, in theoretical models with small, accurate time steps, they provide an optimal control solution.

2.2.2.2 Pilot Point Control

A pilot point control system involves monitoring the temperature at a single predetermined point in the tissue. In this work, this point was positioned at the boundary of the desired thermal lesion. When the temperature reached 52 °C at this point, power to the applicator was turned off. This temperature has been shown in previous studies to correspond to thermal lesion formation with
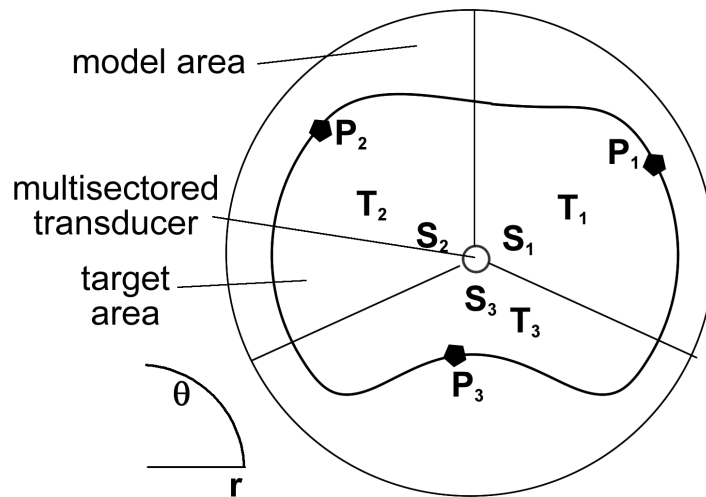
Figure 2.2: Pilot point control scheme coupled with a maximum temperature bang-bang controller. P_1, P_2, and P_3 represent the pilot points for control each respective sector, S_1, S_2, and S_3. The heating target is outlined.

ultrasound applicators.[23,76] For multisectored ultrasound transducers, one pilot point can be assigned for each sector on the transducer. This allows for very flexible control and accurate deposition of the ultrasound energy. By outlining the target area with multiple pilot points, each corresponding sector can be controlled independently to match the thermal lesion to the outlined target as seen in Figure 2.2.

The biothermal model developed in this study allows for pilot point control to be coupled with bang-bang maximum temperature control for each individual sector. This further improves the multisectored applicator control system and offers an excellent method for outlining applicator performance. In experimental practice, the controllers incorporated into the biothermal model cannot be tuned as accurately as in simulations; however, they can be and have been used to control ultrasound heating systems.[75,76]

2.2.2.3 Manual Control

Previous studies with interstitial and transurethral ultrasound applicators overviewed in Chapter 1 have relied on manual control of the applied power. For most feasibility studies, this type of control has provided excellent insight into an applicator's ability to shape a heating pattern. In this work, experiments were controlled manually using either thermocouple or MR-based temperature feedback. To verify the accuracy of the model, a controller was programmed into the model that could simulate previously completed experiments. By changing the applied power levels during the simulation, the simulations could be corresponded directly to experimental data. In tissues without large blood vessels, such as prostate, the biothermal model should correspond very well with experimental results.

2.3 2D R-Z Model

In order to complement simulated applicator performance from the R-θ model, an R-Z model was developed to examine heating pattern along the length of the applicator. The model is based on the same properties as the R-θ and the Pennes bioheat equation in cylindrical coordinates. The R-Z model was programmed using the Crank-Nicholson method of solving a finite difference problem. In addition, the flexibility of the model is the same as that mentioned

previously, as it accounts for changes in attenuation and perfusion with an increase in thermal dose.[108]

The R-Z model geometry represents a plane through the center of the applicator. The applicator is positioned to one side of the model as the heating pattern from a cylindrical ultrasound transducer is assumed to be symmetric. This is not necessarily the case with a multisectored applicator, but in this work it is assumed that this design scheme primarily affects the angular shape of a heating pattern, not the longitudinal shape. Each node in the model is assigned the necessary properties according to its location, and only the nodes directly in line with the transducers receiving any ultrasound energy. The purpose of an R-Z model is to examine the radial heating penetration from cylindrical ultrasound transducers and to evaluate applicators with multiple transducers. The model can investigate the effects of conduction and longitudinal control over the shape of a thermal lesion that is impossible to evaluate from a 2D angular model.

2.3.1 Multielement Control Systems

The bang-bang, pilot point, and manual simulation control schemes discussed earlier in this chapter have been incorporated into the 2D R-Z model. Using a maximum temperature bang-bang controller, heating pattern control in a third dimension can be investigated. As more transducers are added to the length of an applicator, individual pilot points can be incorporated into the model to fit the thermal lesion boundary to a predetermined target area.

Similarly to the 2D R-θ model, the manual controller can be used to verify the model with experimental data. In addition, an R-Z model allows the user to identify the effects of the spacing between transducers on an applicator. Advanced control schemes can also be investigated, such as translating the transducers along the length of the applicator during or between heat treatments or adding more transducers to an applicator array. The 2D R-Z and R-θ models provide a comprehensive evaluation of an applicator's heating potential and performance.

2.4 3D Biothermal Model

Similar to the 2D model described in this chapter, a three dimensional finite difference model based on the Pennes bioheat equation in cylindrical coordinates was developed to evaluate cylindrical ultrasound applicators for thermal therapy. The 3D finite difference model was solved using the Crank-Nicholson mixed implicit-explicit method and incorporated variable node spacing in the R and Z dimensions. In multiple dimensions, each temperature point is a function of every other point in the mesh, making it difficult to simultaneously solve the equations representing each axis. A well established method known as time step splitting can be used to simplify the problem and solve each axis individually. For a 3D model, each time step can be split into three intermediate time steps. In other words, the radial dimension can be solved

using the temperature data from the previous time step. Then, the axial dimension can be solved using the result of the radial dimension calculation; an intermediate temperature solution. Finally, the angular dimension can be solved using the intermediate temperature solutions from the other axes. This method makes the simulation and calculations much simpler and produces an accurate approximation of the result of calculating all three dimensions simultaneously in a single time step. To further improve the accuracy, alternating direction implicit (ADI) methods can be utilized.

A generalized example of the Pennes bioheat equation in three dimensions is:

$$\frac{\partial T}{\partial t} = \frac{\partial}{\partial r}\left(D\frac{\partial T}{\partial r}\right) + \frac{\partial}{\partial z}\left(D\frac{\partial T}{\partial z}\right) + \frac{\partial}{\partial \theta}\left(D\frac{\partial T}{\partial \theta}\right)$$

where D represents a grouping of the complimentary terms. Using finite difference notation of the above equation leads to the creation of the term, β, that encompasses D and its differentiated terms. After imposing the Crank-Nicholson method the equation becomes:

$$\frac{T_{n+1} - T_n}{\Delta t} = \frac{1}{2}(\beta_r + \beta_z + \beta_\theta)(T_{n+1} + T_n)$$

where n represents the current time step and $n+1$ represents the time step being calculated. By splitting this time step into portions, the intermediate temperatures, T^* and T^{**}, were determined during the calculation of the radial and axial dimensions using ADI methods. The temperature at time step $n+1$ is

then finalized in the calculation of angular dimension. The series of the three intermediate time step equations is:

$$\frac{1}{2}\beta_r\left(T^{\bullet}_{n+1}+T_n\right)+\beta_z T_n+\beta_\theta T_n = \frac{T^{\bullet}_{n+1}-T_n}{\Delta t}$$

$$\frac{1}{2}\beta_r\left(T^{\bullet}_{n+1}+T_n\right)+\frac{1}{2}\beta_z\left(T^{\bullet\bullet}_{n+1}+T_n\right)+\beta_\theta T_n = \frac{T^{\bullet\bullet}_{n+1}-T_n}{\Delta t}$$

$$\frac{1}{2}\beta_r\left(T^{\bullet}_{n+1}+T_n\right)+\frac{1}{2}\beta_z\left(T^{\bullet\bullet}_{n+1}+T_n\right)+\frac{1}{2}\beta_\theta\left(T_{n+1}+T_n\right)= \frac{T_{n+1}-T_n}{\Delta t}$$

Most temperature maps from experimental data are in two dimensions. These maps often leave out important information in the third dimension. Many times the heating pattern will be different at the opposite ends of an ultrasound transducer due to blood perfusion, tissue heterogeneities, or acoustic output patterns. The 3D biothermal model developed in this study provides a tool for exploring the entire heating pattern. In this work, the 3D model was developed; however, it was not used on a regular basis to evaluate multisectored applicators. This is because the large number of nodes needed to obtain accurate and stable results requires more memory then is available for a standard desktop computer. For example, a 2D model typically requires ~300 nodes in the radial dimension and ~180 nodes in the angular dimension, or 54,000 total simulation nodes. In the case of the 3D model, to get a similar type of accuracy, you need a similar number of nodes in both the radial and angular dimensions, as well as fine spacing in the axial dimension. This requires >150 nodes in the axial dimension, or >8.1 million total nodes. This number of nodes is not realistic in terms of

computing power, and would also require incredibly long calculation times. The spatial resolution requirement is one of the drawbacks of a finite difference approach. Despite these requirements, future work with the 3D model would include decreasing the memory requirements by optimizing the programming code and determining the minimum number of nodes necessary to maintain calculation stability. Advancements in computer technology would also make this model more practical. With these future advancements, the 3D biothermal model could provide accurate simulation results and would be significantly more useful for treatment planning than 2D models.

Part I

Interstitial Ultrasound Devices for Conformal Thermal Therapy

Chapter 3

Multisectored Interstitial Ultrasound Applicators for Dynamic Angular Control of Thermal Therapy

3.1 Abstract

Dynamic angular control of thermal ablation and hyperthermia therapy with current interstitial heating technology is limited in capability, and often relies upon non-adjustable angular power deposition patterns and/or mechanical manipulation of the heating device. The objective of this study was to investigate the potential of multi-sectored tubular interstitial ultrasound devices

to provide control of the angular heating distribution without device manipulation. Multi-sectored tubular transducers with independent sector power control were incorporated into modified versions of internally-cooled (1.9 mm OD) and catheter-cooled (2.4 mm OD) interstitial ultrasound applicators in this work. The heating capabilities of these multi-sectored devices were evaluated by measurements of acoustic output properties, measurements of thermal lesions produced in *ex vivo* tissue samples, biothermal simulations of thermal ablation and hyperthermia treatments, and MR temperature imaging of *ex vivo* and *in vivo* experiments. Acoustic beam measurements of each applicator type displayed a 35-40º acoustic dead zone between each independent sector, with negligible mechanical or electrical coupling. Thermal lesions produced in *ex vivo* liver tissue with one, two, or three sectors activated ranged from 13-18 mm in radius with contiguous zones of coagulation between active sectors. The simulations demonstrated the degree of angular control possible by using variable power levels applied to each sector, variable duration of applied constant power to individual sectors respectively, or a multi-point temperature controller to vary the power applied to each sector. Despite the acoustic dead zone between sectors, the simulations also showed that the variance from the maximum lesion radius with three elements activated is within 4-13% for tissue perfusions from 1-10 kg m^{-3} s^{-1}. Simulations of hyperthermia with maximum tissue temperatures of 45 and 48 ºC displayed radial penetration up to 2 cm of the 40 ºC steady-state contour. Thermal characterizations of tri-sectored

applicators in *ex vivo* and *in vivo* muscle, using real-time MR thermal imaging, reinforced angular controllability and negligible radial variance of the heating pattern from the applicators, demonstrated effective heating penetration, and displayed MR compatibility. The multi-sectored interstitial ultrasound applicators developed in this study demonstrated a significant degree of dynamic angular control of a heating pattern without device manipulation, while maintaining heat penetration consistent with previously reported results from other interstitial ultrasound applicators.

3.2 Introduction

Thermal treatment of cancer and benign disease has been investigated extensively as an alternative to surgery and as a complement to other treatment modalities. Hyperthermia (41-45 ᵒC) is typically applied as an adjunct to concurrent radiation therapy or chemotherapy.[114,120] Recent randomized, multi-center clinical trials have demonstrated significant clinical benefit of hyperthermia in sites such as cervix,[115] recurrent breast cancer,[101] melanoma,[85] and head and neck tumors.[104] Thermal ablation or high-temperature thermal therapy (>50 ᵒC, lethal thermal dose) can destroy tumor tissue and is an alternative to invasive surgery in sites such as prostate,[70,102] breast,[1] and liver.[40] Many different types of interstitial devices have been explored for treating tissue with heat, including radio-frequency currents,

microwaves, laser, and ultrasound.[37,100] While many modalities and applicator systems have proven useful for different types of disease, ultrasound has inherent advantages that provide favorable control of temperature and thermal dose distributions delivered to a target area. Increasingly, non-invasive magnetic resonance (MR) temperature monitoring has been used as a tool for performance characterization of heating applicators and, more recently, to guide clinical thermal therapy treatments.[93] Non-invasive temperature monitoring and minimally invasive interstitial ultrasound devices with dynamic heating control could significantly improve the delivery of thermal therapy.

Interstitial ultrasound applicators offer greater penetration and spatial control of hyperthermia[34,72] and thermal ablation[15,66,81] than other types of interstitial heating devices. Different ultrasound transducer geometries can focus or shape an acoustic energy deposition and produce a directional heating distribution with deep temperature penetration and high power deposition for thermal ablation. Interstitial devices (1.5-2.4 mm outer diameter (OD)) incorporating tubular ultrasound transducers sectored or cut into a single active sector (e.g. 90°, 180°) can generate directional thermal lesions 3-5 cm in diameter within 5-15 min.[26,27,109] Also, multiple elements along the length of an applicator can control the axial temperature distribution.[81] Planar ultrasound transducers inserted into larger diameter catheters (>3.8 mm OD) can provide narrow directional heating patterns from an interstitial heating applicator.[18,68]

Directional tubular or planar ultrasound transducers that are sequentially

rotated within a catheter during treatment can selectively ablate or heat a target area with greater spatial control in the angular dimension.[18,68,82] Real-time MR temperature imaging can be used to monitor heating with interstitial ultrasound applicators and control applied power or applicator positioning to compensate for tissue changes during treatment.[18,58,82] However, MR temperature monitoring is very susceptible to errors from any movement during imaging. Mechanically rotating a device during treatment may cause motion of the tissue or the device, which will cause an error in the MR temperature images. Cylindrical phased array applicators have been developed to control the angular shape of a heating distribution in an MR scanner without rotating the device.[65,79] This approach can provide good spatial control of a temperature distribution, however, the diameter (>10 mm) of the device is not practical for minimally-invasive interstitial approaches.[65] A small diameter (<2.5 mm) interstitial ultrasound device with dynamic angular control of typical heating patterns for hyperthermia or thermal ablation that required no mechanical manipulation during treatment would be desirable, especially for MR guided procedures.

The objective of this study was to develop MR compatible, small diameter interstitial ultrasound applicators that can dynamically control hyperthermia and thermal ablation treatments in the angular dimension without requiring any mechanical applicator movement. Applicators were constructed in both internally-cooled[27] and catheter-cooled[34] configurations (1.9 mm – 2.4 mm

OD), each containing a tubular ultrasound transducer with three individually controlled sectors. These multi-sectored ultrasound devices were characterized and evaluated by acoustic beam plots, biothermal simulations, and *ex vivo* and *in vivo* heating studies. Experiments were performed using MR temperature monitoring to evaluate the applicators' heating characteristics and determine their MR compatibility. The capabilities of these multi-sectored applicators to improve the spatial control of thermal treatments and further the use of real-time MR temperature monitoring to guide interstitial ultrasound thermal ablation is presented in this work.

3.3 Methods

3.3.1 Applicator Design and Construction

Two types of tri-sectored angularly directive (TriAD) interstitial ultrasound applicators were fabricated in this study. An internally-cooled, direct coupled interstitial ultrasound applicator (TriAD/DC) for thermal treatment was constructed with a 1.8 mm OD and 10 mm long tri-sectored transducer (Boston Piezo Optics, Bellingham, MA). The transducer was sectored into three 120° partitions by cutting a small notch in the outer electrode and part of the ceramic (Figure 3.1[a]) using a computer controlled silicon wafer saw (Automatic Dicing Saw DAD-2H/6, Disco Abrasive Systems, Tokyo, Japan). The silicon wafer saw allowed for small accurate cuts less than 0.7 mm in width, with less than 1 % of

the total surface area of the transducer being removed. Also, to achieve electrical and acoustic isolation between individual sectors, the depth of each cut was more than 50 % of the transducer thickness. Each sector of the transducer had a separate power lead soldered to the outer surface with a common return power lead soldered to the inner surface electrode, enabling each transducer partition to be powered individually at independent frequencies and power levels.

Cooling water flow was delivered by two small pieces of polyimide tubing on the inner surface of the applicator, with an additional piece of polyimide tubing to provide structural support. The transducer was mounted directly over the polyimide tubing inner lumen (Figure 3.1[a]). The return water cooling flow follows the inner surface of the transducer, convectively cooling it from the inside out.[27] The outer surface of the transducer is covered with a thin layer of epoxy and polyester for biocompatibility and electrical isolation. The applicator (1.9 mm OD) is designed to be placed directly into the tissue (Figure 3.1[b]). The tri-sectored, catheter-cooled interstitial ultrasound applicator (TriAD/CC) consisted of a 1.5 mm OD, 10 mm long tri-sectored ultrasound transducer inserted into a 2.4 mm OD, 10 cm long catheter (Figure 3.1[c]). Water cooling flow enters through a single piece of polyimide tubing on which the transducer is mounted and returns through the catheter over the outer surface of the transducer.[34,81] The transducer was sectored into three 120° partitions, each attached to separate power leads, as described above.
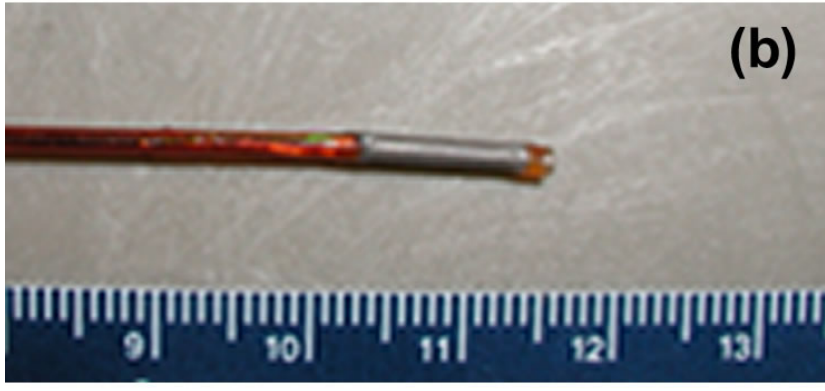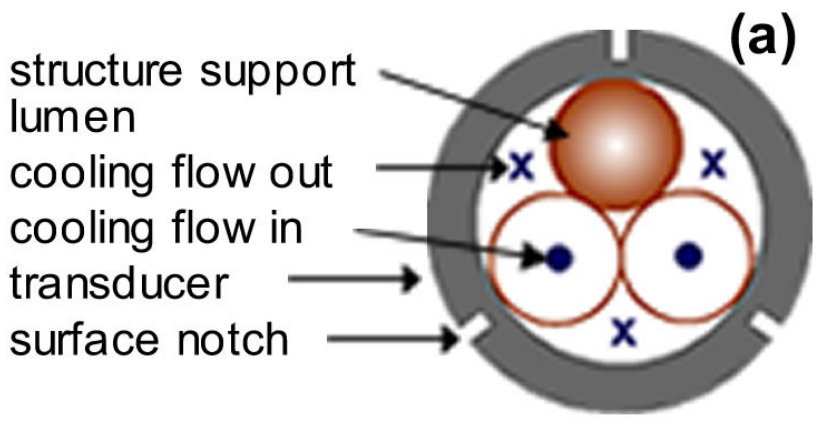
Figure 3.1: (a) Schematic drawing of a tri-sectored tubular ultrasound transducer with internal water-cooling. Pictures of (b) TriAD/DC and (c) TriAD/CC applicators constructed with polyimide tubing.

3.3.2 Acoustic Evaluation

A force balance technique for cylindrical ultrasound sources measured the acoustic efficiency of the power output from each applicator.[54] The measurements were done over a small frequency range at net applied electrical powers of 3 and 7 W for each individual sector on a transducer. The force balance technique also determined the optimal driving frequency as defined by the frequency with maximum measured efficiency.

The acoustic beam profiles of the TriAD/DC and TriAD/CC applicators were measured using a scanning hydrophone (NTR Systems, Seattle, WA) in a tank of degassed, deionized water. The beam profiles were measured to determine the amount of acoustic dead zone between individual sectors on a transducer and whether the sectors were electrically and mechanically isolated from another. Rotational beam plots were performed by scanning the needle hydrophone axially at a fixed radial distance of 8 mm from the transducer while the applicator was rotated in 2.5° steps.[36] The applicators were scanned with active water cooling flow (30 ml min^{-1}) and each sector was individually rotationally scanned. Also, 360° rotational plots of the acoustic output were created with all three sectors active concurrently.

3.3.3 Biothermal Simulations

A two-dimensional finite difference acoustic and biothermal model was

used to evaluate the performance of both types of multi-sectored interstitial ultrasound applicators in simulated, perfused tissue; in particular, the ability to create contiguous heating distributions without apparent cold zones between sectors and the ability to control the angular shape of a thermal lesion with and without temperature feedback control. The capability of multi-sectored interstitial ultrasound devices to create continuous heating distributions with no heating distribution cold zone between sectors and to control the angular shape of a thermal lesion with and without temperature feedback control was evaluated with the biothermal model. A two-dimensional finite difference acoustic and biothermal model was used to evaluate the theoretical performance of both types of applicators. The model was based on the Pennes bioheat equation in cylindrical coordinates, incorporating dynamic changes in attenuation and perfusion as a function of temperature and thermal dose.[108] Thermal dose was calculated from transient temperatures using the iso-effect thermal dose equation. Thermal dose is a descriptive term commonly used for predicting thermal damage from the temperature and duration of thermal exposure.[30] The accrual of thermal dose has been shown to increase exponentially as a function of temperature elevation and linearly with respect to time. A thermal dose threshold of 200 min at 43 ^{o}C was used in our study for describing tissue destruction, where t_{43} values of ~50-240 min have been verified *in vivo* to correlate to thermal damage in different tissue types.[32] Acoustic attenuation was modeled to vary linearly with the log of thermal dose from 10^2

to 10^7 equivalent minutes at 43 °C (EM$_{43°C}$), following experimental data.[22] Perfusion in the simulated tissue was homogeneous and once the tissue reached a thermal dose of 300 EM$_{43°C}$ there was no perfusion because the tissue was considered necrosed.[10]

The temperature distributions were calculated numerically using the Crank-Nicholson method, a mixed implicit and explicit integration technique, which improved simulation speed and stability of fine spatial grid spacing.[92] Further details of the model development, including *in vivo* verification were described by Tyreus and Diederich.[108] Applicator beam profiles were modeled from the measured acoustic characteristics of the TriAD applicators by approximating the acoustic output of each independent sector as uniform in the angular dimension.

Many different model parameters were varied in the biothermal model to evaluate the TriAD applicators. Variable node spacing was employed in the radial dimension following a continuous smooth sigmoidal function from 0.01 mm near the transducer to 1 mm at the model boundary. The angular node spacing was fixed at 2°. Simulations were solved with a 0.1 s time step and a multi-point maximum temperature controller (bang-bang) with fast update times (0.5 s) was selected for temperature based power control in the simulations. The automatic controller utilized multiple temperature points along the heating radius extending from the center of each sector in the simulations. This type of controller was easy to implement and, at fast simulation update times, performs

equivalent to a well-tuned PID controller. The simulations were performed in generic normal tissue similar to brain and prostate tissue (0.53 W m^{-1} K^{-1} thermal conductivity, 6.7 Np m^{-1} MHz^{-1} acoustic attenuation). Heating distributions were simulated at different perfusions (1, 4, 7, 10 kg m^{-3} s^{-1}), treatment times (5, 10, 15, 20 min), and maximum temperatures in the tissue (55, 65, 75, 85 °C) with the internally-cooled (TriAD/DC, 2700 W m^{-1} K^{-1} convective cooling coefficient) and catheter-cooled applicators (TriAD/CC, 3000 W m^{-1} K^{-1} convective cooling coefficient). The minimum and maximum radius of a thermal lesion, defined as the outer boundary of a thermal dose equivalent to 200 EM$_{43°C}$, was measured after simulated heats with the TriAD applicators. Hyperthermia simulations were performed at low maximum temperatures (45, 48 °C). The 40 °C temperature contour outlined the effective hyperthermia treatment region at steady-state.

3.3.4 *Ex Vivo* Tissue Studies

The heating performance of the TriAD applicators was evaluated in *ex vivo* freshly butchered, degassed beef liver at a baseline temperature of 37 °C in a saline water bath. The applicators were inserted directly into the tissue and were connected to a closed water-cooling flow loop (22°C). A multiple channel radio frequency amplifier system (Advanced Surgical Systems, Tucson, AZ) powered the devices. Heating experiments were conducted with both types of TriAD applicators with one, two, or three sectors active on the applicator at different

cooling flow rates (25-35 ml min^{-1}) and power levels (5-10 W) for 10 min.

3.3.5 MR Compatibility

The compatibility of TriAD devices with MR temperature monitoring was evaluated by measurements of the MR image artifact patterns. The applicators were filled with water, placed in a beef muscle tissue phantom, and imaged in an interventional 0.5 T MR scanner (Signa SP, GE Medical Systems, Milwaukee, WI) and a 1.5 T whole body scanner (Signa EXCITE, GE Medical Systems). The applicators were aligned parallel to the magnetic field and evaluated at excitation sequences commonly used for MR temperature monitoring based on the proton resonance frequency (PRF) shift method. The applicators were also aligned perpendicular to the magnetic field to determine the effect of the orientation of the applicators on their MR susceptibility. An in-house five inch surface coil was used as the receive coil in the experiment in the 0.5 T with a fast spoiled gradient echo sequence (TE = 14.3 msec, TR = 150 msec, flip angle = 60°, bandwidth = 12.5 kHz, FOV = 21 cm).[14,96] In the 1.5 T scanner (TE = 20.45 msec, TR = 41 msec, flip angle = 30°, bandwidth = 3.52 kHz, FOV = 19 cm)[78], fast spoiled gradient echo sequences were used with a standard knee receive coil.

3.3.6 Tissue Studies under MR Temperature Monitoring

3.3.6.1 MR Temperature Monitoring

MR temperature monitoring during the treatment was accomplished using the proton resonance frequency (PRF) shift method.[14,58,93] PRF is a phase subtraction method where an image is subtracted from a baseline pre-treatment image to create a temperature map. The PRF of water varies linearly with an increase of temperature, and can be measured using phase images. The applied imaging parameters (TE = 14.3/28.6 msec, TR = 190 msec, flip angle = 60°, bandwidth = 6.95 kHz, FOV = 20 cm) allowed the temperature map to be updated about every 15 s. Three transverse slices (thickness 5 mm) in the target region, orthogonal to the applicator and centered in the middle of the transducer, were monitored and displayed continuously.

3.3.6.2 Applicator Hardware

The multiple channel radio frequency amplifier system was located directly outside the MR suite and supplied power to the applicator. Coaxial cables from the amplifier were connected to the applicator through a shielded access panel. In-line, high-power, 0-11 MHz low-pass 60 dB filters (Werlatone, Brewster, NY) were used to reduce RF noise from the amplifier cables and prevent degradation of the MR images. Room temperature, degassed cooling water was provided to the applicator (30 ml min^{-1}) from a peristaltic pump positioned outside the MR suite. The in-house surface coil was used as the receive coil in experiments with the TriAD/CC devices and an endorectal receive only coil was used in experiments with the TriAD/DC applicators.

3.3.6.3 *Ex Vivo*

The heating effectiveness and the ability of TriAD/DC and TriAD/CC applicators to dynamically control the angular shape of a heating pattern was examined in *ex vivo* beef muscle tissue at room temperature. The heating studies were done under MR temperature monitoring in the 0.5 T interventional scanner with the in-house surface receive coil. In each experiment, the applicator was placed in the center of the beef and 6 to 8 W of power were applied to each individual sector for 5 min. Each applicator heated with one, two, or three sectors active and had a convective water-cooling flow of 30 ml min^{-1}.

3.3.6.4 *In Vivo*

The heating distribution of a TriAD/CC applicator was evaluated within *in vivo* canine thigh muscle using MR temperature monitoring during the procedure. Animal experiments were reviewed and approved by Institutional Animal Use and Care Committee at Stanford University in accordance with the Guide for the Care and Use of Laboratory Animals. The animal was anesthetized with subcutaneous atropine (0.05 mg kg^{-1}), followed by ketamine (0.5 mg kg^{-1}) and valium (10 mg kg^{-1}) given together intravenously. The dog was intubated and maintained on isoflurane gas inhalation anesthesia for the duration of the procedure. Prior to the study, the animal received nothing by mouth (NPO) for 24 h. The animal was positioned supine, headfirst into the 0.5 T interventional

scanner and its vital signs were continuously monitored. The applicator was inserted directly into the thigh muscle.

3.4 Results

3.4.1 Acoustic Evaluation

The acoustic output characteristics of each TriAD applicator were evaluated using measurements of acoustic efficiency and beam distributions. The TriAD/DC applicator transducer sectors had an acoustic efficiency between 30-40 %. Similarly, the sectors of the TriAD/CC transducers had acoustic efficiencies of 35-50 %, which was reduced to 20-35 % within a catheter. At a higher power applied of 7 W, the acoustic efficiencies were similar to the efficiencies measured at 3 W, and the values were within the reported range. The operating frequency of each sector was determined by the frequency with the maximum acoustic efficiency and visual inspection of the ultrasound beam in water. The operating frequencies of each sector varied slightly within the wall thickness tolerance of the transducers or +/- 0.1 MHz.

Rotational beam profiles of the applicators displayed an active acoustic sector of about 85° from a 120° sector as defined by 10 % of the peak intensity (Figure 3.2). Individual 360° scans of each sector's acoustic output displayed that the active acoustic zone was isolated to an area directly in front of the sector. A 360° scan with all three sectors simultaneously active correlated directly to a plot
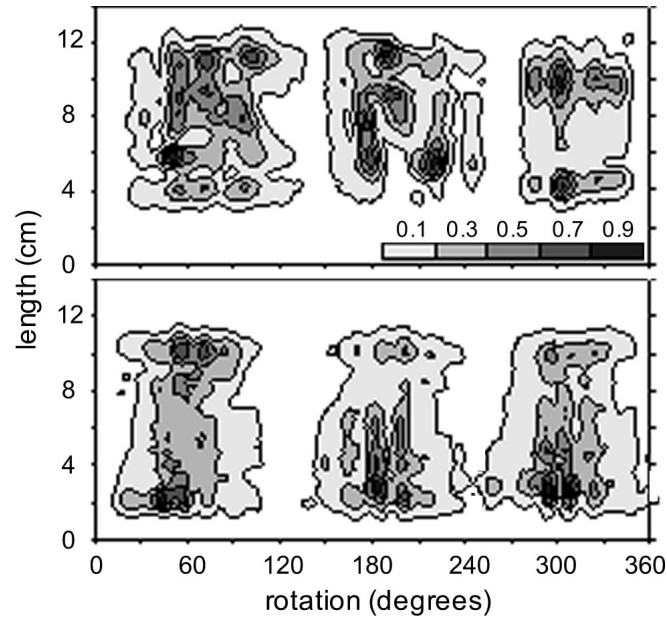
Figure 3.2: Rotational beam plots of a (top) TriCC applicator and (bottom) TriAD applicator at 8 mm radial distance. The figure represents the normalized intensity of the ultrasound beam profile of a transducer with all three elements active, measured at a radial depth of 8 mm. Each sectored element had an active surface area of ~85°.

merging the individually scanned sectors' beam profiles. There was a clear

acoustic dead zone between each sector in Figure 3.2 and visual inspection of the

beam profile displayed that the sectors were individually isolated. Also, beam

profiles measured with a hydrophone and visual inspections of the ultrasound

beam displayed that as increased power was delivered to one sector on the

transducer, it did not affect the beam profiles of the other sectors. The sectors

were electrically and mechanically isolated from each another.

3.4.2 Biothermal Simulations

The biothermal model was used to analyze the radial penetration and

continuity of the angular heating pattern as a function of applicator operating parameters and tissue characteristics. Different methods of controlling the angular shape of a thermal lesion from a TriAD applicator were simulated at a moderate tissue perfusion (2 kg m^{-3} s^{-1}) in Figure 3.3. These methods included delivering power simultaneously to all elements at different applied power levels (9, 6, and 3 W) (Figure 3.3[a]) and delivering the same amount of applied power (10 W) to each sector for different durations (200, 400, and 600 s) (Figure 3.3[b]). Also, the angular dimension of a thermal lesion was controlled by individually activating two sectors (Figure 3.3[c]) or one sector (Figure 3.3[d]).

A multi-point maximum temperature controller was used to dynamically control the penetration and angular shape of a heating distribution from a TriAD applicator (Figure 3.4). The maximum temperature in a region directly in front of each sector was used to control the applied power to the individual sectors. All three sectors of the TriAD/CC (Figure 3.4[a]) and TriAD/DC (Figure 3.4[b]) applicators were controlled to a maximum temperature of 85 °C in perfused tissue (4 kg m^{-3} s^{-1}), demonstrating similar shapes and slightly greater radial penetration with the TriAD/CC applicator. Also, in 2 kg m^{-3} s^{-1} perfused tissue, the sectors of a TriAD/CC applicator were controlled to maximum temperatures of 85, 70, and 70 °C (Figure 3.4[c]) and 85, 75, and 65 °C (Figure 3.4[d]) to demonstrate the ability of the applicators to vary the angular shape of a heating pattern.
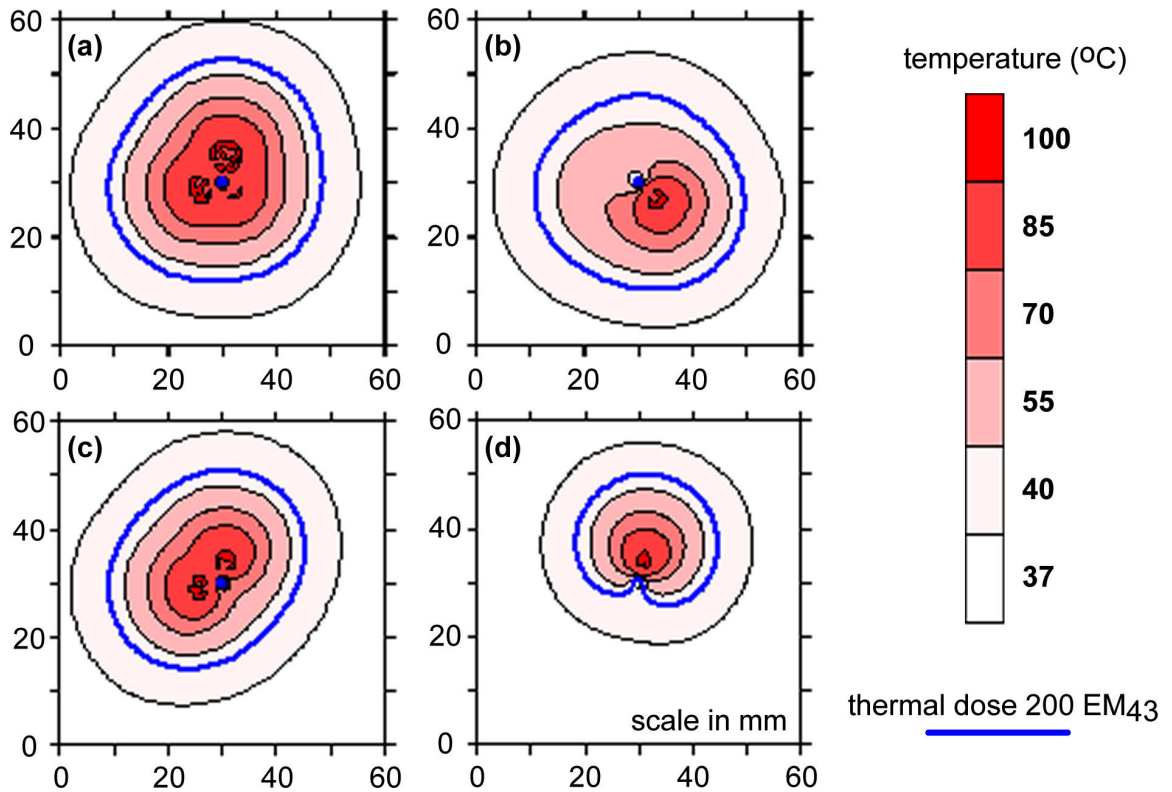
Figure 3.3: Simulated temperature distributions and thermal lesions created by a TriAD/DC applicator. (a) Different applied powers (9, 6, 3 W) for 600s were used for each sector. (b) 10 W was applied to each sector for different activation times (200, 400, 600 s) to control the angular shape of a thermal lesion. (c) Two sectors and (d) one sector active for 600s with 10 W applied power.
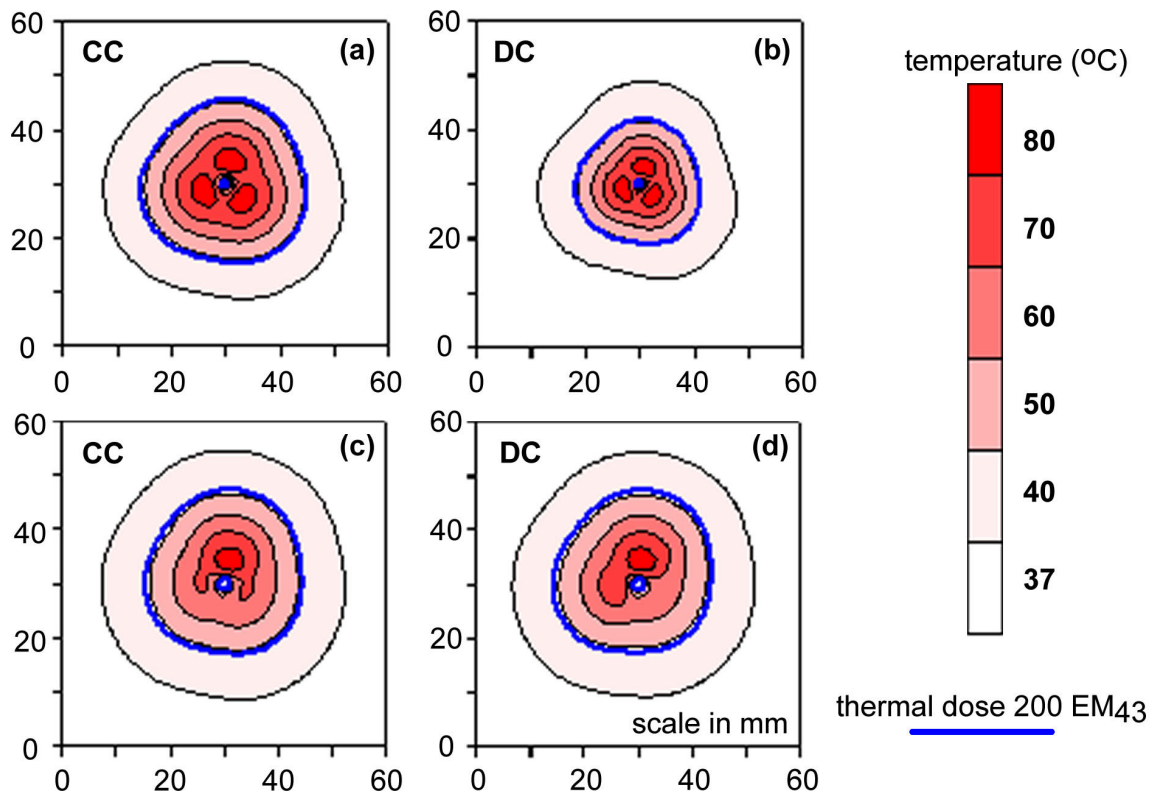
Figure 3.4: A maximum temperature controller was used to control the angular shape of simulated thermal lesions with TriAD/DC and TriAD/CC applicators. All three sectors were independently controlled to maximum temperatures of (a,b) 85 °C, (c) 85, 70, and 70 °C, or (d) 85, 75, and 65 °C to demonstrate real-time temperature feedback control for shaping a heating pattern. The simulations in the top half of the figure (a,b) was conducted in 4 kg m^{-3} s^{-1} perfused tissue and in the bottom half of the figure (c,d), the perfusion rate was 2 kg m^{-3} s^{-1}.

A series of simulations with both TriAD applicators with three sectors controlled to the same maximum temperature (similar to Figure 3.4[a,b]) examined the continuity of the thermal lesion borders at different maximum temperatures, tissue perfusions, and treatment times (Figure 3.5). These simulations were also conducted to display that the heating pattern did not have a discernable cold zone between transducer sectors or clover leaf shape, but rather, was continuous along the border. The minimum and maximum radial penetration of the resulting thermal lesions and the difference from the median radius were presented as error bars in Figure 3.5, reflective of the shape at the lesion boundary. The thermal lesion was defined by the 200 $EM_{43°C}$ thermal dose contour. The heating distribution was more circular at higher control temperatures (85, 75 °C) than at lower temperatures (65, 55 °C). However, in both the high and low temperature cases, a consistent lesion shape was observed with minimum heating loss between sectors. In the simulations shown in Figure 3.5, the TriAD/DC applicator created slightly smaller lesions than the TriAD/CC applicator, but created a pattern with greater continuity of the lesion boundary. At a maximum control temperature of 85 °C in mildly perfused tissue (1 kg m^{-3} s^{-1}) and 10 min treatment duration, both TriAD designs achieved a maximum thermal lesion diameter of at least 3.5 cm with the radius differing from the median by no more than 5 %. The lesion boundary became increasingly more continuous at longer treatment times and increased perfusion reduces radial penetration. Homogeneous perfusion primarily affected the size of the median
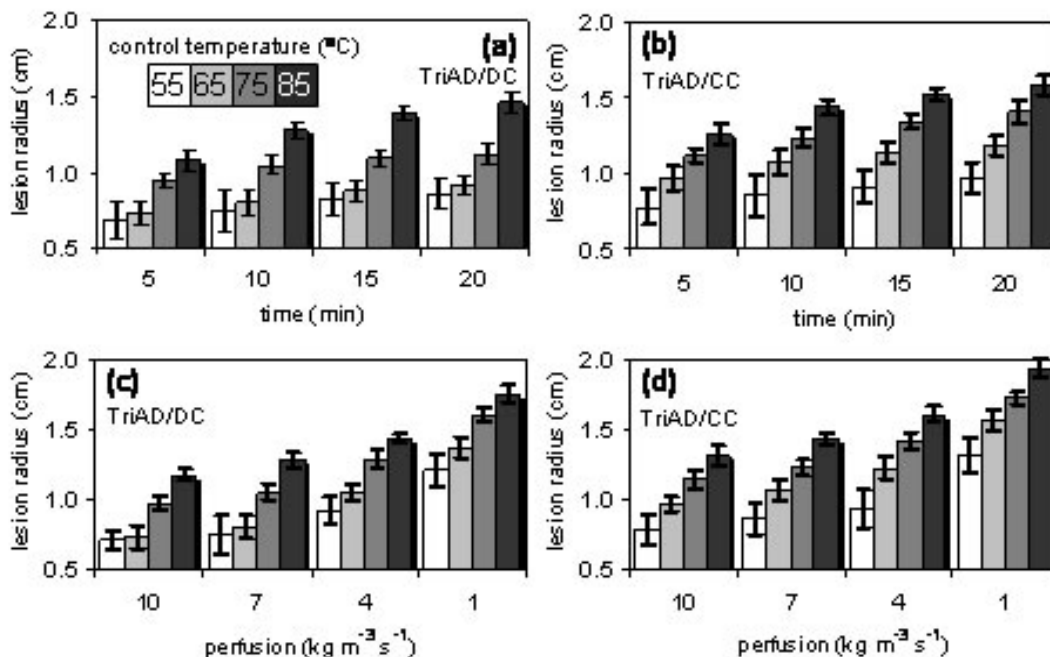
Figure 3.5: Radial measurements of simulated thermal lesions at different maximum control temperatures, treatment times, and tissue perfusions. The median radius of a lesion is plotted with the error bars representing the variation of the radius for each thermal lesion. (a,b) Simulated thermal lesion radius at moderate tissue perfusion (4 kg m^{-3} s^{-1}). (c,d) Power applied of 10 W to all three sectors of a tri-sectored interstitial ultrasound applicator for 10 min.

lesion radius and had little effect on the shape of the thermal lesions at thermal ablation temperatures.

The penetration and angular continuity of a heating pattern from TriAD/DC and TriAD/CC applicators were also evaluated for delivering hyperthermia temperatures. Low maximum temperature simulations were run in the same simulated tissue as the thermal therapy simulations (Table 3.1). At a control temperature of 45 °C, the 40 °C contour of the heating pattern created by the TriAD/DC and TriAD/CC applicators had a maximum radius of 1.83 and 1.96 cm, respectively. At a higher tissue perfusion (10 kg m^{-3} s^{-1}), a clover leaf

Maximum tissue temperature (°C)	Simulated tissue perfusion (kg m^{-3} s^{-1})	TriAD Applicator	40 °C contour maximum radial depth (cm)	40 °C contour minimum radial depth (cm)
45	2	DC	1.83	1.58
		CC	1.96	1.66
	10	DC	1.16	0.88
		CC	1.36	0.89
48	2	DC	1.92	1.74
		CC	2.07	1.81
	10	DC	1.21	0.98
		CC	1.29	1.05

Table 3.1: Simulated thermal heating distribution from the TriAD/DC and TriAD/CC applicators at a maximum tissue temperatures suitable for hyperthermia. The radius of the 40 °C contour line was measured with all three sectors active for 30 min.

shape at the periphery of the heating distribution between sectors was slightly more pronounced than at the lower perfusion (2 kg m^{-3} s^{-1}) at hyperthermia temperatures. At a maximum control temperature of 48 °C, the 40 °C contour from a TriAD/DC had a maximum and minimum radius of 1.92 and 1.74 cm from the applicator. The higher maximum temperature in the tissue appeared to increase overall border continuity.

3.4.3 *Ex Vivo* Tissue Studies

The radial depths of thermal lesions created by the TriAD applicators in *ex vivo* liver tissue are shown in Table 3.2. A thermal lesion was defined as tissue that changed color or lightened. Lesion radii varied from 13 to 18 mm at different applicator flow rates and power levels. The maximum radius from a TriAD/DC applicator was 18 mm with two sectors active at 7 W of applied power. The

Applicator	Active sectors	Cooling flow rate (ml min-1)	Applied power per sector (W)	Maximum lesion radius (mm)
TriAD/DC	3	30	5	16
	2	30	7	18
	1	30	7	14
TriAD/CC	3	35	7	16
	2	35	7	14
	1	35	7	13
	3	25	10	18

Table 3.2: Maximum thermal lesion radius produced by tri-sectored interstitial ultrasound applicators in 37 °C *ex vivo* beef liver tissue. Power was applied to the applicators for 10 min.

TriAD/CC applicator created a lesion with a maximum radius of 18 mm with all three elements active on the transducer at 10 W of applied power.

The radial distances of the *ex vivo* lesions created were similar to the simulated thermal lesions controlled to a maximum temperature of 75 °C or greater with a maximum applied power of 10 W. Both in simulations and in *ex vivo* tissue, the applicators were able to create lesions greater than 3.0 cm in diameter. These radial depths of the lesions created by the TriAD applicators in *ex vivo* beef liver were similar in size to lesions created by other interstitial ultrasound sources. Interstitial ultrasound applicators with similar transducer diameters (1.5–3.0 mm OD) created lesions of 2–3.5 cm in diameter in *ex vivo* beef muscle.[18,81,109] The applicators developed in this study were able to maintain the radial depths and control of similar interstitial ultrasound devices, while adding a significant amount of angular control of the shape of the thermal lesions.
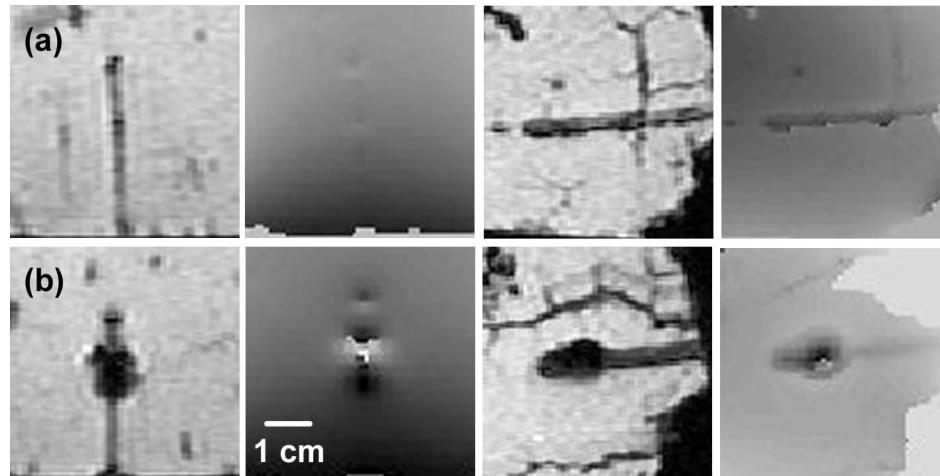
Figure 3.6: Magnitude and phase images of tri-sectored interstitial ultrasound applicators inserted into beef muscle tissue in a 1.5 T MR scanner. (a) Images of an applicator with negligible MR susceptibility artifact and (b) the maximum applicator susceptibility artifact seen in this study of about 3 mm in radius.

3.4.4 MR Susceptibility Artifact

The MR temperature compatibility of the two types of applicator configurations was examined at different magnetic field strengths (0.5, 1.5 T). The image artifact from the devices was measured with the applicators aligned both parallel and perpendicular to the magnetic field. In Figure 3.6, magnitude and phase images were used to determine the susceptibility artifact of both types of applicators in this study in a 1.5 T scanner. Artifact in the phase images minimally increased with a change in orientation and the applicators were determined to be suitable for MR temperature procedures. An example of an applicator with negligible susceptibility artifact was seen in Figure 3.6(a). The image artifact associated with the TriAD/CC applicator in Figure 3.6(b) represents a worst-case artifact, which was not present on all devices that are

properly screened and fabricated. The presence of this artifact was not ideal and extended to 8 mm in diameter. However, devices with artifact were still be suitable for use in MR guided thermal ablation procedures as long as the critical zone of temperature monitoring (e.g., outer boundary of the treatment) was beyond the artifact.[82] This experiment was also conducted in the 0.5 T interventional scanner with very similar results (not shown).

3.4.5 Tissue Studies under MR Temperature Guidance

3.4.5.1 *Ex Vivo*

Each of the TriAD applicators was tested in beef muscle with non-invasive MR temperature monitoring. MR temperature maps created by a TriAD/CC applicator with one, two, and three active elements with 8 W of applied power for 5 min displayed little to no clover leaf shape of the heating pattern (Figure 3.7). Similarly, Figure 3.8 displayed a time sequence of the heating pattern in beef muscle of a TriAD/DC applicator with 7 W applied power for 10 min to all three elements demonstrating the continuity of the heating boundary in the angular dimension throughout the treatment.

3.4.5.2 *In Vivo*

Evaluation of the heating from tri-sectored interstitial ultrasound applicators were performed in *in vivo* canine thigh muscle under MR temperature imaging in the 0.5 T interventional scanner. Both the TriAD/DC and
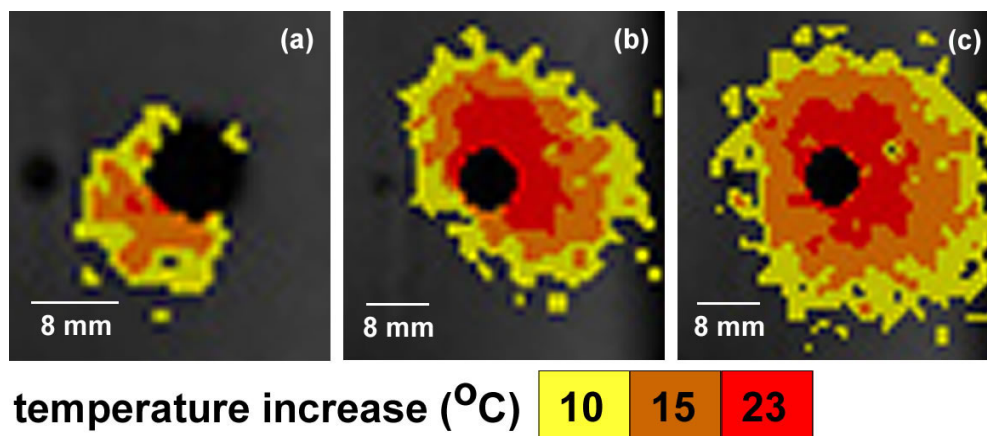
Figure 3.7: MR thermal images of a TriAD/CC temperature distribution in a beef muscle sample. (a) One, (b) two, (c) or three elements were activated with an applied power of 10 W per sector for 5 min.

Figure 3.8: Time sequence of a heat with a TriAD/DC applicator in room temperature beef muscle with MR temperature monitoring in the 0.5 T interventional MR. The blank spot in the top right of the heating pattern is due to a strip of fat running through the tissue.

TriAD/CC applicators were able to create thermal lesions more than 10 mm in radius in less than 10 min. The applied power to each sector was manually controlled during the experiments with visual feedback from the MR temperature measurements. The *in vivo* studies also showed that despite perfusion in the tissue, there is no heating dead zone between sectors of the transducers and they created thermal lesions with continuous borders. The *in vivo* results corresponded well with the *ex vivo* experiments and biothermal simulations.

When 10 W was applied to two sectors of a TriAD/CC applicator for 5 min, a temperature increase of 10-15 ^{o}C, from the baseline temperature of 34 ^{o}C, was observed 12-14 mm radially from the applicator (Figure 3.9). The temperature artifact at the top of the image was due to movement of the skin and adjacent tissue as there was an observable shift in the tissue position during treatment and the temperature artifact remained throughout the sequence of images after the shift was observed. Variable low levels of noise were seen in the MR temperature measurements during some of the experiments, but this noise was eliminated or reduced by RF filtering and shielding the effects on the MR images. A TriAD/DC heating sequence with all three sectors active on the transducer was illustrated in Figure 3.10. The 15 ^{o}C temperature increase contour corresponded closely to the to the thermal dose distribution in the tissue. The sequence displays no heating dead zone between the sectors and radial heat penetration of about 10-15 mm. The heating patterns in the images supported the
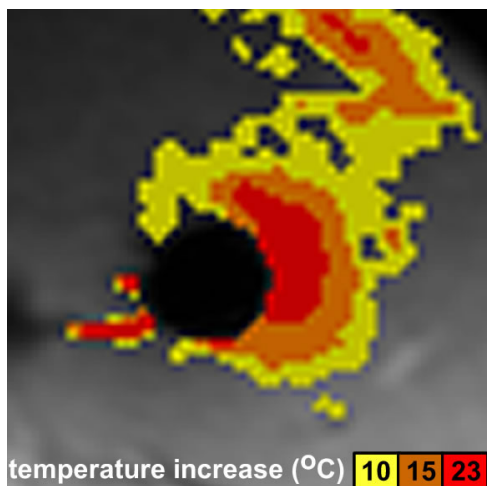
Figure 3.9: TriAD/CC heating pattern in *in vivo* canine thigh muscle with two active sectors. The temperature distribution displayed no unheated area between sectors and effective radial penetration. The color seen at the top of the image is due to motion of the skin and adjacent tissue during the procedure.

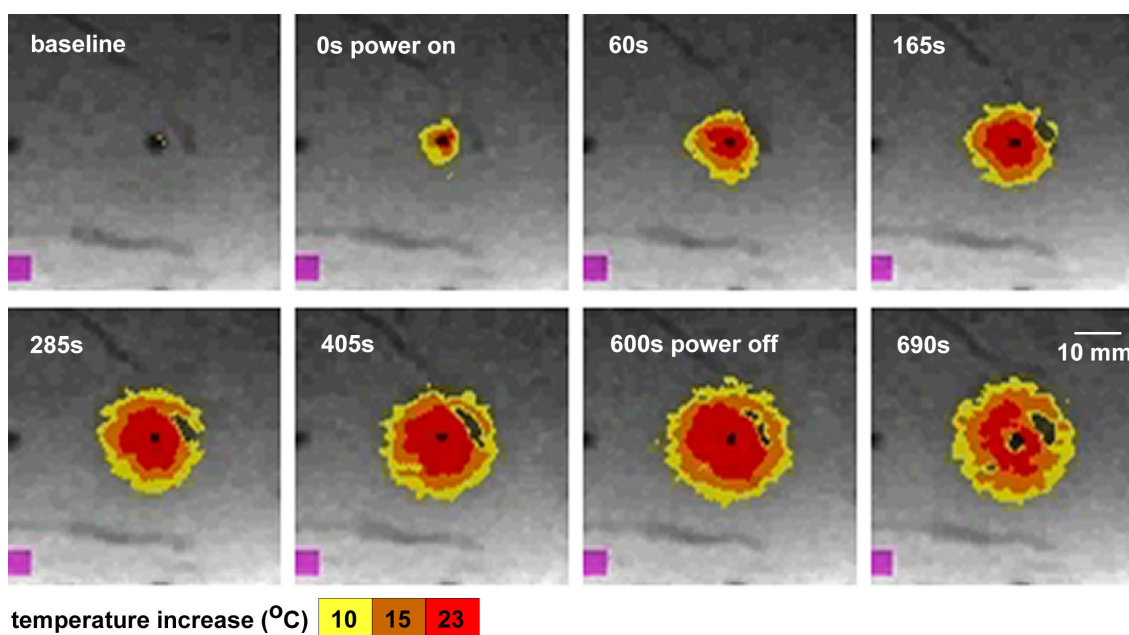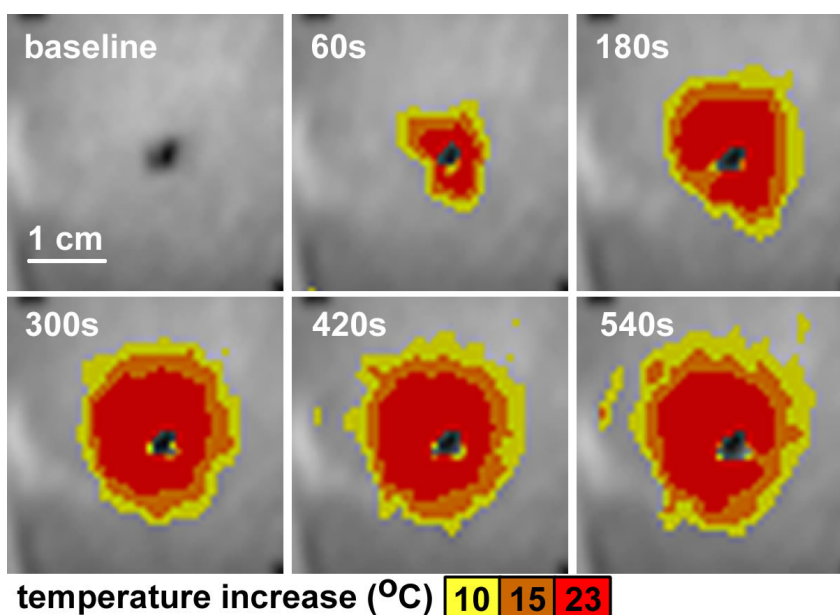Figure 3.10: Time sequence of a heat with a TriAD/DC applicator in *in vivo* canine thigh muscle with MR temperature monitoring in the 0.5 T interventional MR. The 15°C temperature increase contour (orange) corresponds closely with the thermal dose delivered.

simulation and *ex vivo* results of this study and displayed that heating with TriAD applicators under MR temperature monitoring is possible.

3.5 Discussion

In tissues with deep-seated, localized tumors, interstitial heating devices can be inserted directly into the target tissue and may be a more effective way of delivering localized thermal therapy in areas that may be difficult to treat with external thermal therapy or other approaches. Ultrasound devices have distinct advantages over other interstitial thermal therapy devices including offering increased radial penetration from a single heating source. Applicators utilizing planar and single-sectored tubular ultrasound transducers have been shown to provide good spatial control and penetration of a thermal treatment.[37] Tubular transducers sectored into one directional element (e.g. 90°, 180°) are able to control both the radial penetration and directionality of a thermal treatment. These applicators have a fixed heating pattern and cannot vary the angular spatial control during treatment without mechanical manipulation.[26] MR temperature monitoring technology provides real-time temperature feedback for controlling heating devices. The PRF MR temperature monitoring method may be sensitive to errors created by movement of any objects in an image, including rotating or translating thermal therapy devices. Thus, the objective of this study is to investigate an interstitial thermal therapy device that can dynamically

control the angular shape of a heating distribution during treatment without requiring applicator manipulation, and maintain the axial and radial control advantages of interstitial ultrasound.

Interstitial ultrasound applicators (1.9–2.4 mm OD) with multi-sectored tubular transducers were developed and evaluated in this study to demonstrate dynamic angular spatial heating control can be achieved without mechanical movement and coagulate tissue to radial depths of at least 1-2 cm (Figures 3.5, 3.8, 3.9, 3.10). Temperature distributions and thermal lesion dimensions are similar to interstitial ultrasound applicators with fixed-directional, small tubular ultrasound transducers.[27,64] In this study, the ultrasound transducers are sectored into three sectors due to the small dimensions and the experimental aim of testing feasibility. This represents a practical test configuration for demonstrating angular control while maintaining small applicator diameters, which are adequate for minimally invasive thermal treatment.

One of the experimental aims in this study is to determine that TriAD applicators can create continuous thermal lesions without obtaining a clover leaf heating pattern between sectors. The biothermal simulations and *ex vivo* and *in vivo* tissue studies show thermal redistribution filled in potential dead spots of ultrasound energy from the sectoring of the surface of the transducer (Figure 3.5). The simulations also provide insight into the use of a tri-sectored applicator design for creating modified thermal lesions. A simple multi-point maximum temperature controller has been used in many of the simulations with a separate

control point in the tissue in front of each sector to allow for control of heating distributions from multi-sectored interstitial ultrasound applicators (Figure 3.4). In *in vivo* canine thigh muscle both the TriAD/DC and TriAD/CC applicators can create thermal lesions more than 10 mm in radius in less than 10 minutes (Figures 3.9, 3.10). The *in vivo* studies also show that despite perfusion in the tissue, the temperatures are continuous between the sectors of the transducers and they can create thermal lesions with continuous borders. This work corresponds well with the *ex vivo* experiments and biothermal simulations.

A feedback controller may be used with the TriAD applicators using real-time MR temperature measurements to more accurately treat a target tissue volume. In this study, the update time of the temperature imaging is 15 s. Treating a large area all at once in 5–15 min means the MR temperature imaging does not need to be as fast as with external high intensity focused ultrasound devices that heat in short times. The 15 s sampling time is currently inherent to the 0.5 T MR scanner for the heat treatments discussed in this work. The MR temperature monitoring software used in this study is currently under active development, hence the slight differences in the temperature monitoring sequences used in this study. Additional research is being done to improve the MR temperature accuracy and the speed of image acquisition in the 0.5 T interventional scanner to allow for real-time applicator feedback control. The increased angular control offered by a multi-sectored applicator and MR temperature monitoring could allow thermal targeting to a specific

predetermined volume and reduces the chance of heating healthy tissue.

The applicators created in this study are non-ferrous and MR temperature monitoring compatible. Image susceptibility artifact, as seen for a TriAD/CC applicator in Figure 3.6, is dependent upon contaminates obtained by a device during the construction of the ultrasound transducers or the applicator itself. This study shows that the applicator MR susceptibility artifact at different magnetic strengths (0.5, 1.5 T) ranges from negligible to a maximum case of ~3 mm in radius from the applicator. This could be due to differences in the thickness of the electrical plating on the surface of the transducers or possible contamination during construction. Previous studies have shown that this artifact is not dependent on the direct-coupled or catheter-cooled designs.[58] Although the maximum artifact case is not ideal, applicators with this amount of susceptibility artifact are still suitable for thermal ablation MR procedures where the boundary of heating is the primary concern. More careful transducer manufacturing, screening of materials, and applicator construction should eliminate most MR compatibility issues. The cooling water flow did not disturb the MR images and RF power can be applied to the applicators and adjusted with minimal disturbance of the MR temperature images without requiring the power delivered to be turned off during image acquisition.[38,82]

The two TriAD applicator designs evaluated in this study provide very similar angular thermal lesion control and radial penetration. The internally cooled applicator (TriAD/DC) was smaller in total diameter (1.9 mm) and

contains a larger diameter transducer (1.8 mm) than the catheter-cooled applicator (TriAD/CC) (1.5 mm OD transducer, 2.4 mm OD catheter). When using a maximum temperature controller, the TriAD/CC offers better radial temperature penetration than the TriAD/DC applicator due to more effective water-cooling. However, because the maximum temperature of a treatment is farther into the tissue, thermal lesion border continuity is slightly less than the lesions created by the TriAD/DC applicator, which maintains the maximum tissue temperature closer to the applicator due to less effective tissue cooling.

Hyperthermia temperatures often increase the efficacy of chemotherapy and radiotherapy by increasing cell oxygenation and tumor blood flow.[120] The applicators developed in this study may also be able to increase the accuracy of heating a specific tissue at lower temperatures. The results in Table 3.1 suggest a TriAD applicator with a low control temperature can control the angular shape of a heating distribution. The simulated 40 ^{o}C contour extends as far as 2 cm into the tissue at moderate tissue perfusions (2 kg m^{-3} s^{-1}). For single applicator implant hyperthermia treatments, a larger applicator may improve heating border continuity because the percentage of transducer surface area lost to cutting the transducer is much smaller than with the small diameter applicators. However, simulations of the applicators in this study provide evidence that a TriAD applicator could be effective in delivering a hyperthermia dose to a target area.

Angular control of a heating distribution during treatment has been

explored with numerous types of ultrasound applicators. One method for achieving angular control of these distributions is heating with a fixed-directional applicator that rotates or sweeps during treatment. Rotating sectored tubular and planar ultrasound applicators have been shown to improve the angular control of a heating distribution from an interstitial or intracavitary ultrasound applicator.[18,64,96] These applicators can create precise lesions from thermal treatments in longer treatment times (>30 min). These larger diameter (>4 mm OD) applicators can also treat large areas accurately, such as the entire prostate gland, and can be controlled with MR temperature monitoring.[16,97] A cylindrical, intracavitary ultrasound phased array applicator is a sophisticated approach that does not require applicator movement during treatment and has also been shown to provide very good angular control of a thermal lesion.[79,80] An electronic beam rotation of a plane wave beam is used instead of mechanical rotation of a planar transducer to selectively heat discrete regions.[65] Theses devices have been effectively demonstrated for intracavitary applications in the esophagus and rectum, but due to size constraints this technology may not be practical for interstitial applications where devices smaller than 2.5 mm OD are desired.

The multi-sectored ultrasound heating configurations developed in this work require no mechanical manipulation during treatment, maintain good angular spatial control, and offer a simpler approach for dynamically tailoring thermal therapy in the angular dimension. They also should be able to heat a

large area in a shorter time (<15 min) than rotating devices and do not require control over an additional parameter, rotation rate. Multi-sectored ultrasound devices are also small in diameter for practicality for minimally invasive interstitial procedures, while providing heating penetration that is similar to more complex rotating and phased array approaches. Another notable difference is that rotating phased arrays and planar transducer devices require multiple shots of heat treatment, whereas the multi-sectored interstitial ultrasound applicators heat the treatment volume in a single heat, with simultaneous angular control. Devices with multiple transducers along the length of the applicator could provide longitudinal control in addition to angular control of thermal therapy. Multi-sectored device configurations overcome some of the difficulty faced by rotating applicators, including MR temperature movement sensitivity and potentially longer treatment times for achieving an adequate thermal dose over a large area. Furthermore, the diameters (1.9–2.4 mm) of the TriAD applicators are significantly smaller than interstitial applicators with a rotating, planar transducer (>3.8 mm OD).[17] These smaller applicators create lesions in *ex vivo* liver tissue with very similar radial depths (up to 15 mm, Table 3.2) to lesions created by larger, rotating interstitial ultrasound applicators.[18]

In summary, this study outlines the capability of small, multi-sectored interstitial ultrasound applicators with dynamic angular heating control to create adaptable and targeted thermal lesions without requiring mechanical manipulation of the device during treatment. Furthermore, incorporating multi-

sectored interstitial ultrasound applicators with real-time MR temperature feedback may provide a treatment method that allows quick, adjustable heating in the angular and radial dimensions without requiring movement of the applicator. This could better account for tissue boundaries, irregularities in tissues, blood vessels and perfusion, and other factors that often complicate heating. These applicators have the potential to greatly improve the conformability of a thermal treatment delivered to a predetermined target region in tissue sites with deep-seated tumors inaccessible to surgery and external heating methods.

Chapter 4

Comparison of Rotating Sectored and Stationary Multisectored Tubular Interstitial Ultrasound Applicators

4.1 Abstract

Hyperthermia and high temperature thermal therapy are currently used in the clinical treatment of a variety of cancers. Despite the increasing use of thermal therapies, heat treatments have not gained large-scale clinical acceptance, due in part to inconsistencies in controlling heat deposition *in vivo* and the lack of precise temperature measurement. Interstitial ultrasound

applicators provide superior spatial control over power deposition and heating patterns compared to other interstitial techniques. Real-time MR temperature imaging provides thermal therapies with an accurate, non-invasive method for measuring temperature within the body during treatment. In this study, three MR-compatible water-cooled interstitial ultrasound applicator designs were developed and evaluated for dynamic angular control of the thermal dose to a target area. Two of the applicator designs utilize an ultrasound transducer separated into three individually powered sectors allowing the user to control heating deposition without manipulating the device. The third design utilizes a 90° sectored transducer that can be rotated to target the thermal treatment to a specified area. A tri-sectored water-cooled applicator (TriAD) and a rotating catheter water-cooled applicator (RIUS) angularly controlled thermal dose to a target area. Both devices were small in diameter (1.8-2.4 mm), making them clinically feasible for minimally invasive treatment in size-sensitive tissues. Comparisons and predictions of the *in vivo* performance of all applicators was examined by biothermal model simulations and in *ex vivo* tissue experiments. The biothermal model incorporated changes in acoustic attenuation and perfusion as a function of thermal dose. *Ex vivo* experiments with real-time MR temperature monitoring correlated well with results from the biothermal model. The results of this study bracketed the feasibility and potential in vivo performance of the applicator designs for minimally invasive cancer treatment with MR guidance.

4.2 Introduction

Thermal treatment of cancer and benign disease has achieved been slow to be accepted in the clinic due to uncontrollable temperature distributions. The major successes in the field have typically been achieved through the development of devices that are able to accurately distribute a thermal dose to a target area. This device development coupled with major improvements in temperature monitoring within the body may provide the future of thermal therapy. Different modalities for treating tissue with heat have been thoroughly explored, including radio-frequency,[51] microwave,[104] laser,[107] and ultrasound.[37] While all modalities have proven useful for different types of disease, ultrasound has some inherent advantages regarding control of the thermal dose delivered to a target area. Ultrasound has a small wavelength that allows for favorable penetration and control of energy deposition, thus it offers an inherent advantage in controlling the amount of heat deposited in the tissue. Varying the frequency and power of the ultrasound energy can control the radial penetration depth. By placing a small ultrasound transducer on the tip of a small catheter or needle, the energy source can be directly inserted into a tumor. Interstitial ultrasound applicators have been demonstrated to maintain a high degree of control of the radial penetration depth and axial location of heating energy.[18,65,83]

Different sectoring sizes of a tubular ultrasound transducer allow for control of the shape and size of a lesion in a certain direction. Recent studies involve rotating a sectored ultrasound applicator to effectively 'paint' a target region with a thermal dose.[96] These studies offer good control of the angular dimension of a thermal lesion; however, the applicator designs become significantly more complicated and require manipulation of the device during treatment. Rotating applicators also increase the total treatment times needed to thermally ablate a large area of tissue, perhaps up to two hours. However, at the current time, rotating ultrasound applicators provide the most control of a thermal lesion in the angular dimension.

High temperature thermal therapy (>50 °C) can selectively destroy regions of tissue. Thermally coagulating a selected area of tissue has been used as a minimally invasive treatment option for recurrent malignancies and benign prostate tumors. Thermal therapy has not become a widely accepted treatment option for many diseases because of inherent difficulties in heating physiological tissue sites. Dynamic and heterogeneous tissue thermal properties and heat transport properties of blood and blood vessels create a major obstacle in accurately modeling and predicting the thermal dose in living tissue. Thus, accurate real-time temperature monitoring is needed to understand temperature distributions *in vivo*. MR temperature imaging has recently provided thermal therapy with an accurate (±2 °C) and precise (±1 mm) non-invasive method of monitoring temperatures during treatment.[93] This technology has excited new

interest and investigation into thermal therapy treatments and sparked research towards the development of thermal therapy devices for accurate delivery of heat to a prescribed area.

The majority of MR thermal monitoring utilizes the PRF phase shift which varies linearly with increases in temperature. This method is a phase subtraction method, where each successive image is subtracted from a baseline image to determine the total phase shift and in turn, temperature rise. PRF phase subtraction is very sensitive to motion and any slight shifts in tissue position can disrupt images or lead to false measurements.

In this study, two applicator designs with multiple individually controlled sectors on a single tubular ultrasound transducer and an applicator design with a rotating 90° sectored transducer were evaluated in biothermal model simulations and *ex vivo* heating studies with MR temperature imaging. This study displays the feasibility of both types of applicators for clinical use and their anticipated performance *in vivo*. This chapter emphasizes the rotating interstitial device. Interstitial ultrasound coupled with real-time MR temperature imaging offers a promising approach for thermally treating cancerous tissue.

4.3 Applicator Construction and Characterization

A tri-sectored angularly directive applicator design consisting of a single
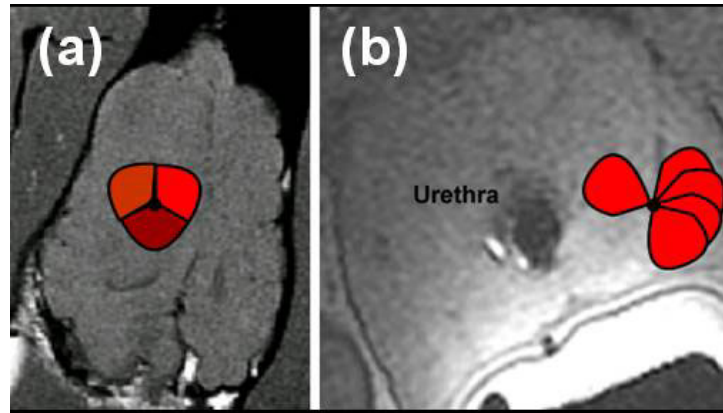
Figure 4.1: Heating schema for (a) a tri-sectored tubular ultrasound applicator and (b) a rotating 90° sectored tubular ultrasound applicator. The rotating applicator can be a single heating shot (left) or rotating the applicator and heating in steps.

ultrasound transducer mounted on polyimide tubing was developed in this study. The transducer was sectored into three individually controlled 120° active elements by a silicon wafer dicing saw. Power leads were soldered to each element allowing for separate power control to each sector. Two different catheter designs were created using the tri-sectored ultrasound transducer as described in Chapter 3. One applicator was developed with internal water cooling (TriAD/DC) and the other applicator (TriAD/CC) was convectively cooled on the outside of the transducer using a catheter-cooled design.[81]

A rotating interstitial ultrasound applicator (RIUS) was developed for controlling the angular shape of a thermal lesion. It consisted of a 90°-sectored 1.5 mm OD transducer (7.2 MHz) inserted into a 2.4 mm OD Celcon catheter. The RIUS applicator had a built-in rotating hub, which allows the transducer assembly to rotate freely within the catheter.

The RIUS applicator design was constructed similarly to the TriAD/CC
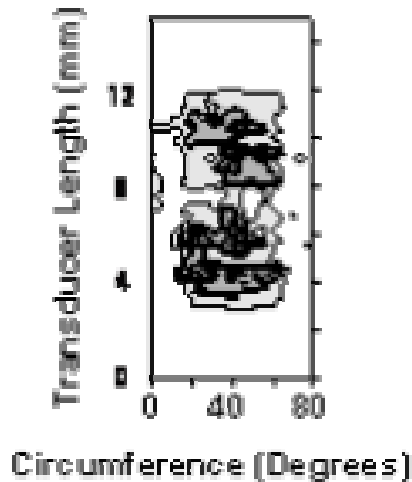
Figure 4.2: Rotational beam profile of a 1 cm long, 90° sectored tubular ultrasound transducer that can be incorporated into a rotating interstitial applicator.

applicator. Figure 4.1 shows general heating schema for both the tri-sectored applicators and the RIUS. The RIUS applicator can be used as a single shot or rotated to conformally treat an area. All the applicators used in this study were characterized with acoustic beam plots. The RIUS applicator beam profile showed a single 60° acoustic output zone as seen in Figure 4.2. The acoustic output zones of the transducers are smaller than the actual electrode surface possibly due to mechanical damage from cutting a transducer, diffraction effects, and clamping the edge of the transducer.

A force balance technique for cylindrical ultrasound sources measured the acoustic power output of each applicator.[54] The goal of the experiments was to determine the acoustic efficiency of each individual sector and the frequency at which powering the sector would result in the most acoustic energy deposited in the tissue. Tests were done at a net applied electrical power of 3 W to determine

the acoustic efficiency of each individual sector on the transducer over a small frequency range. The TriAD applicator achieved acoustic efficiencies of 30-40 %, while the catheter cooled applicators achieved acoustic efficiencies of 40-50 % outside of the catheter and 20-30 % within the catheter. The differences between the two applicator designs may explain the differences in the measurement of acoustic power output seen in these experiments. The internally cooled applicator design may decrease the acoustic efficiency of the transducer due to the cooling flow structures on the inside of the transducer. Also, the catheter in which the catheter cooled applicators are inserted clearly reflects or absorbs some of the ultrasound energy aimed at the tissue.

4.4 Biothermal Model Simulation Results

A finite difference biothermal model based on the Pennes bioheat equation was used to evaluate the theoretical heating performance of each applicator at different blood perfusions, attenuations, and heating times. The 2D model accounts for changes in attenuation and perfusion as a function of thermal dose.[108] A multi-point bang-bang controller was used in the model to control the maximum temperature in simulated *in vivo* tissue. Simulations were done using a maximum temperature of 65, 75, and 85 °C to evaluate the size and shape of the lesions created by all the applicator designs. Other parameters including tissue perfusion and duration of treatment were also modified to display

increased performance of the applicators. The shape of the acoustic power distribution obtained from the acoustic beam plots was approximated in the model.

The model showed controlled continuous lesions could be made by the TriAD and RIUS applicators at nominal values of attenuation and perfusion in brain (6.7 Np MHz^{-1} attenuation, 7.0 kg m^{-3} s^{-1} blood perfusion) and prostate (7.0 Np MHz^{-1} attenuation, 5.0 kg m^{-3} s^{-1} blood perfusion) tissue. Simulated results in normal tissue with the TriAD and RIUS applicators are shown in Figure 4.3. The RIUS applicator was rotated stepwise in the simulations to dynamically control the angular shape. The results of these *in vivo* simulations indicate the feasibility of controlling the size and shape of thermal lesions in the clinic.

4.5 *Ex Vivo* Tissue Experiments

Thermal lesions were created using both types of applicators in *ex vivo* tissue. The experiments were conducted in a water bath at 37 ^{o}C. Thermal dose contours from the biothermal model correlated very well with the coagulated zones in the tissues. All the experiments were done in fresh beef liver (harvested the same day.) All the applicators created relatively large lesions in the tissue up to 2 cm in radius. Room temperature cooling at a flow rate of 35 ml min^{-1} cooled all the applicators during the experiments. The RIUS applicator was rotated using an ultrasound motor connected to the rotating hub. These experiments
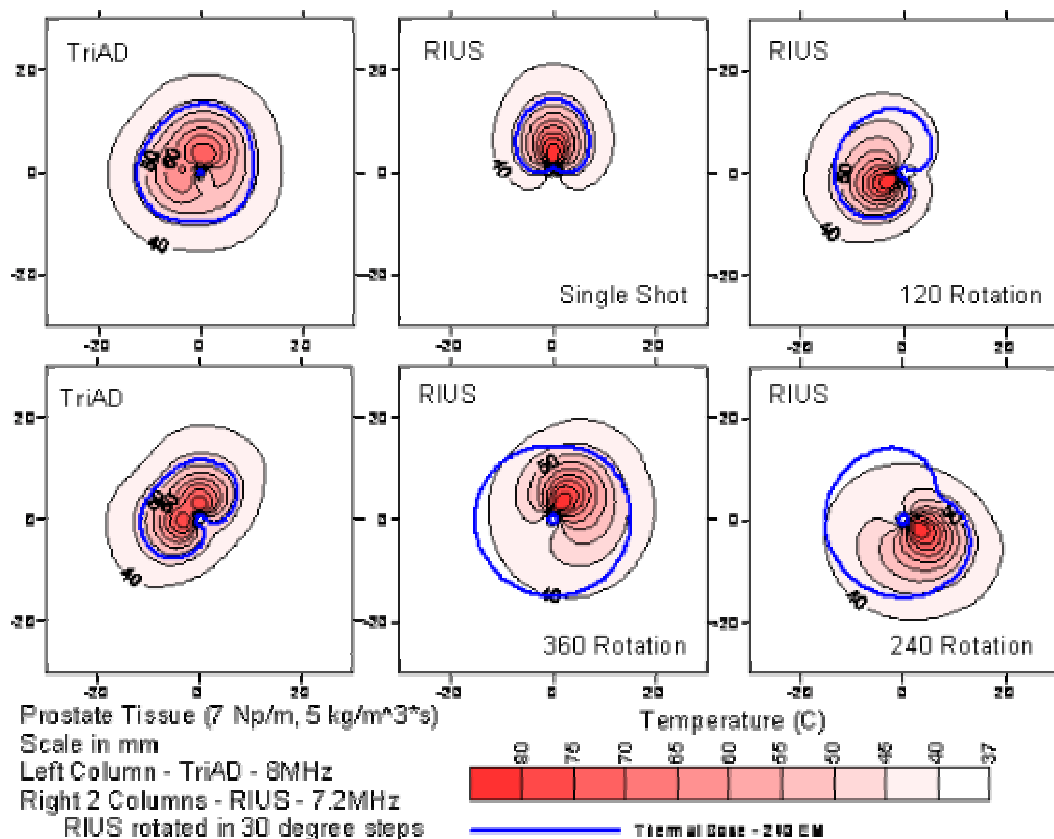
Figure 4.3: Simulated thermal lesions in prostate tissue. The top left figure is a TriAD applicator with three active sectors individually controlled to maximum temperatures of 85, 75, and 65 °C. All other lesions were created by controlling the maximum temperature to 85 °C. The lesion on the bottom right was created by a TriAD with two active elements. The four lesions on the right are simulated RIUS lesions rotated stepwise 30° every two minutes to create conformal angularly controlled lesions.

provide good correlation to the biothermal model simulations and display the

ability of interstitial ultrasound applicators to create large controllable thermal

lesions in the angular dimension. Lesions created by the tri-sectored applicators

are shown in Figure 4.4.

The TriAD and RIUS applicators were also evaluated in beef muscle tissue

under MR temperature imaging in a GE 0.5 T interventional scanner. The PRF
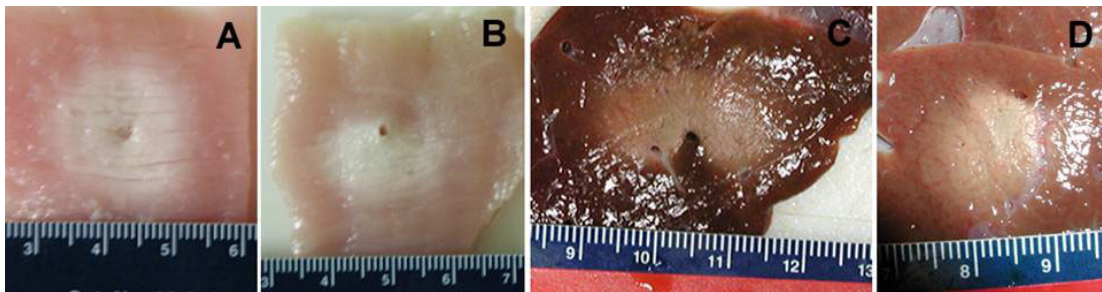
Figure 4.4: Thermal lesions in *ex vivo* turkey breast tissue with (A) 3 active sectors and (B) 2 active sectors with a TriAD/DC applicators. Thermal lesions in *ex vivo* beef liver with a RIUS applicator (C) rotated and (D) a single shot treatment.

MR temperature imaging method is sensitive to movement in the tissue because it is a phase subtraction method. The TriAD applicator required no manipulation or movement of the applicator during the treatment to achieve dynamic angular control. A RIUS applicator heated the beef muscle similarly to the TriAD applicator under MR temperature guidance. It was rotated in 30° steps with a MR compatible ultrasound driving motor every two minutes to demonstrate the control of the angular shape of the heating pattern of the applicator. The applicator heated in a single shot toward the top of the image, then it was rotated 120° and power was applied continuously as the device rotated 30° every 2 min thereafter to display the angular control of the rotating interstitial applicator. The sequence of MR temperature images is shown in Figure 4.5. The cumulative temperature map from a treatment is shown in Figure 4.6. The stepwise rotation of the RIUS applicator allows for a higher degree of control of the lesion shape and size than the TriAD. The RIUS applicator requires manipulation within the catheter during treatment and could affect temperature measurements in real-
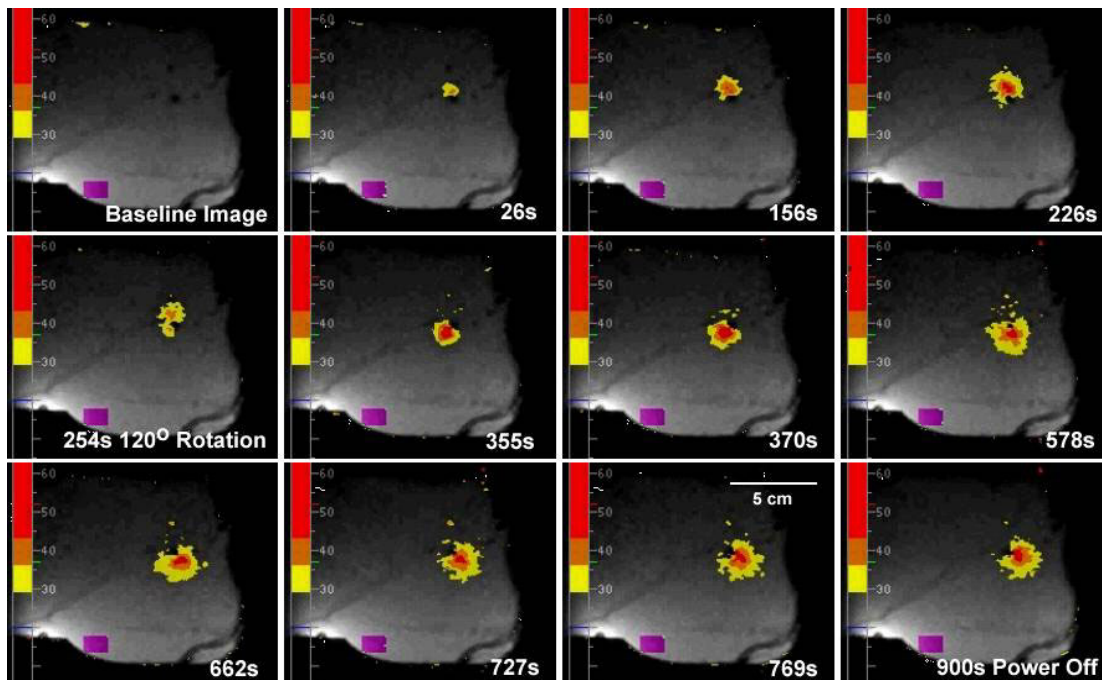
Figure 4.5: Time sequence of MR temperature images during heating in beef muscle with RIUS applicator (8.9 W applied power.) Applicator was rotated 120º at 250 s and 30º every 120 s thereafter.
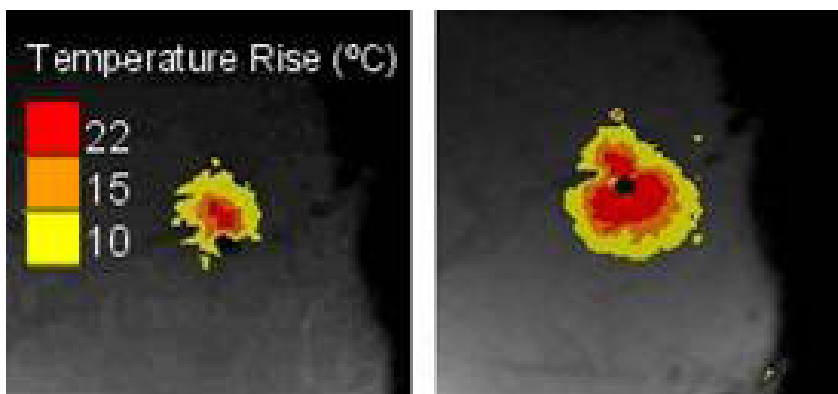
Figure 4.6: MR temperature images of a RIUS applicator. Image on left is a single shot heating pattern. The image on the right shows the cumulative maximum temperature distribution achieved during the experiment in beef muscle sequenced in Figure 4.5.

time. The internal rotation of the transducer within the catheter did not affect the temperature measurements in this study. The RIUS applicator was able to accurately treat a prescribed area under MR temperature imaging guidance. The heating patterns of both applicator designs corresponded very well to the biothermal model simulations.

The *ex vivo* tissue experiments conducted in this study outline the potential *in vivo* performance of the tri-sectored applicator design and the rotating interstitial design. The rotating applicator can provide a more accurate thermal dose than the tri-sectored applicator; however, in this study and previous studies, the treatment time is substantially longer, up to 1 hour, and the applicator requires movement during treatment which could create inaccuracies in measuring temperatures with the motion-sensitive PRF MR temperature imaging method.

4.6 Discussion

The TriAD and RIUS interstitial ultrasound applicators created and evaluated in this study allow for the control of the angular shape and radial size of a thermal lesion. Each applicator has different advantages for tailoring a treatment to a prescribed area. The TriAD applicators are smaller in size and do no require external movement, allowing for shorter treatment times and less perturbation during MR temperature imaging. The devices also incorporate

internal water cooling, directly coupling the ultrasound energy to the target tissue. The TriAD/CC applicator has similar advantages to the TriAD/DC; however, due to the catheter water cooling system, ultrasound energy is deposited the farther into the tissue, creating slightly larger lesions as seen in the simulation charts. The RIUS applicator and the use of a rotating ultrasound driving motor allow for very precise control of power deposition into a tissue and the creation of accurate, conformal thermal lesions. As mentioned above, the RIUS applicator had significantly longer treatment duration in this study and requires manipulation during treatment.

Interstitial ultrasound applicators provide superior spatial control of power deposition and heating patterns compared to other interstitial techniques. Real-time MR temperature imaging provides thermal therapies with an accurate, non-invasive method for measuring temperature within the body during treatment. The combination of these technologies and improvements to the existing technology, such as the applicator designs evaluated in this study, could lead to improved thermal treatments for cancerous and benign tumors. *In vivo* evaluation needs to be conducted for the RIUS design, but the *ex vivo* experiments and biothermal model simulations at different perfusions bracket their anticipated performance in living tissue. These applicators in conjunction with MR temperature imaging provide a promising, practical approach to the thermal ablation of tumors.

Part II

Transurethral Ultrasound Devices for Conformal Thermal Therapy of the Prostate under MR Temperature Guidance

Chapter 5

Transurethral Ultrasound Applicators for Dynamic 3D Control of Prostate Thermal Therapy under MR Guidance

5.1   Abstract

Thermal therapy can be used as a minimally-invasive alternative to surgical methods for the treatment of localized prostate cancer and benign prostate hyperplasia (BPH). In this study, transurethral ultrasound applicators incorporating a linear array of two multisectored tubular transducers (7.8-8.4 MHz, 3 mm OD, 6 mm length) were evaluated *in vivo* in three canine prostate glands under MR temperature guidance. The

transurethral catheter provided water flow cooling to the applicator (100 ml min^{-1}) and consisted of an expandable urethral cooling balloon (10 mm diameter). Also included was an integrated positioning hub for accurate targeting of the thermal therapy by rotating and translating the transducer assembly within the catheter. The transducers consisted of three independently powered sectors that emitted a 90-100° acoustic pattern from the 120° partition characterized by rotational acoustic beam plots. In the *in vivo* experiments, these devices created large contiguous thermal lesions that extended to border of the prostate (>13 mm) in a single short heat treatment (<10 min). Also, by adjusting individual applied power levels to each sector on both transducers, the radial, angular, and longitudinal dimensions of the heating pattern were effectively controlled to treat a target area in the prostates. MR temperature guidance was used to monitor the treatments in the axial and coronal imaging planes, and provided real-time visual feedback for manually adjusting the power delivered to the applicators (8-16 W). The MR temperature measurements were used to track the 52 ^{o}C iso-contour during treatment and calculate the delivered thermal dose, which corresponded well to gross histology of the canine prostates. Other studies with MR controlled, rotating transurethral ultrasound devices have shown good control of the angular shape of the thermal lesion, but required monitoring in the axial imaging plane, longer treatment times (>30 min), and mechanical movement during treatment. The multisectored transurethral applicators designed and evaluated in this study offered fast, conformal therapy of the prostate in three dimensions, without requiring mechanical manipulation of the device. In addition, these devices could be monitored and controlled with MR temperature imaging in both the axial and coronal imaging planes, possibly making them more suitable and practical for thermal therapy of

the prostate under MR temperature guidance. In this study, multisectored transurethral ultrasound applicators created contiguous, conformal thermal lesions in three dimensions under MR temperature guidance, which demonstrated the potential of these devices for treating targeted prostate volumes for BPH and cancer therapy.

5.2   Introduction

High-temperature thermal therapy devices have been developed and utilized for treatment of benign and malignant prostate disease. Many modalities of heating have been used for prostate thermal therapy, including radio-frequency (RF),[11] microwaves,[4,69,102] and ultrasound.[12,110] In most cases, prostate heat treatments are being used and studied as an alternative to surgical procedures, and are often delivered with transurethral or transrectal devices. For benign prostate hyperplasia (BPH) therapy, recent reviews and studies have suggested similar results with transurethral microwave therapy (TUMT) devices compared to transurethral resection of the prostate (TURP) surgeries, but with less major complications when using TUMT.[4,25] In addition, studies have been conducted that indicate higher temperatures produced from high-energy TUMT devices may improve post-procedure symptom scores.[24,59] Transurethral thermal therapy appears to be an effective option for treating BPH, but the evidence suggests that increased spatial control of the temperatures and more accurate targeting of the anterior/lateral lobes of the prostate may further improve treatment.[50,71] For treating prostate cancer, thermal therapy is

typically used as an alternative to radical prostatectomy in high risk patients who are not surgical candidates and for treatment of local recurrence after external beam radiotherapy.[6,12] Cancer treatments require accurate targeted thermal dose delivery to assure destruction of the cancerous tissue, while avoiding damage to surrounding tissues (rectum, prostatic sphincters, neurovascular bundles). Transrectal high-intensity focused ultrasound (HIFU) devices offer a high degree of control over the creation of a thermal lesion in the prostate,[7,43,110] and recent advancements in ultrasound imaging-based treatment monitoring may further improve treatment results.[56] However, transrectal HIFU devices require significant treatment times to ablate large volumes and face difficulties targeting the anterior portion of the gland.[110]

Magnetic resonance (MR) imaging techniques are being investigated for non-invasive monitoring of thermal therapy.[93] MR temperature monitoring offers the potential to guide the delivery of thermal treatments and improve the accuracy of delivering target thermal doses. Recently, MR guided thermal therapy with HIFU devices has become commercially available for the treatment of uterine fibroids.[77,106] Non-invasive MR monitoring of thermal treatment of prostate tissue has been applied in canine models[49,89] and humans.[13] Prostate thermal therapy devices with a greater degree of spatial control during treatment can take advantage of real-time MR temperature measurement feedback and offer a more accurate way to target and verify thermal treatment.

Transurethral ultrasound devices are currently under pre-clinical

evaluation as an alternative technique for thermal treatment of BPH and cancer.[38] Directional planar,[16,67,96] curvilinear,[97] and single-sectored tubular[33,39] ultrasound transducers have been incorporated into transurethral heating applicators. By rotating the transducer assembly or applicator during treatment, heating can be conformed to a target boundary, accurately treating a predetermined region of prostate.[16,96] These applicator configurations have been studied both in simulations and preliminary canine prostate studies. Planar ultrasound applicators appear to provide good penetration and control of thermal lesions, however, due to narrow acoustic beam width (~4 mm), they require many rotations and significant treatment times (>30 min) to ablate a large area of the prostate.[96,97] Mechanical manipulation of the applicators during treatment can create problems and inaccuracies with proton resonance frequency (PRF) based MR temperature imaging because phase subtraction methods are very sensitive to movement in a series of images. As the number of rotations and heat treatment durations increase, the more likely it is that applicator movement, tissue movement, image phase drift, or a change in prostate dimensions will create significant inaccuracies in temperature measurement. A device that does not require mechanical manipulation during heating and can accurately treat a target volume in a relatively short period of time should further decrease temperature monitoring errors. Similar advantages have recently been demonstrated with interstitial ultrasound applicators, consisting of small multisectored tubular ultrasound transducers [<1.8 mm outer diameter (OD)],

which are able to conform heat treatment in the angular dimension without requiring applicator movement during treatment.[61] A stationary, larger multisectored transducer configuration incorporated into a transurethral catheter could offer a practical solution for prostate thermal therapy with MR guidance.

The objectives of this study were to design, develop, and evaluate multisectored transurethral ultrasound applicators for three-dimensional dynamic control of prostate thermal therapy under MR guidance. A linear array of multisectored transducers, with independent power control to each sector, could be adjusted to control both the angular and axial heating pattern without requiring mechanical movement of the device during treatment. This design concept was validated in this study using bench top acoustic measurements and *in vivo* canine prostate heating experiments under MR guidance. In the experiments, real-time MR temperature maps, thermal dose calculations, and visual inspection of thermal lesions demonstrated the flexibility of angular and longitudinal control of thermal treatment with these devices.

5.3 Materials and Methods

5.3.1 Design and Characterization of Multisectored Applicators

The transurethral heating applicators designed in this study incorporated two high-frequency tubular ultrasound transducers (7.8-8.4 MHz, 3 mm OD, 6 mm length) sectored into three independent 120° partitions with a silicon wafer

dicing saw (Automatic Dicing Saw DAD-2H/6, Disco Abrasive Systems, Tokyo, Japan). Each sector was individually powered through small diameter (0.1 mm) silver wire (California Fine Wire, Grover Beach, CA) leads soldered to the outer transducer electrode, with a common ground soldered to the inner electrode. The wires were then connected to miniature coaxial cables (0.69 mm OD, Temp-Flex Cable, South Grafton, MA) that were fed to a 6-pin quick connect (REDEL, Alpine Electronics, San Jose, CA) on the back end of the applicator. To construct an applicator, the two transducers were aligned with the same orientation and mounted onto an inner polyimide tubing lumen with a silicone adhesive (NuSil, Carpinteria, CA). This inner lumen would also provide input of water flow cooling to the delivery catheter and urethral cooling balloon described later. The outer surface of the transducer assembly was coated with a thin layer of mineral oil and covered with thin-walled (0.025 mm) PET tubing (Advanced Polymers, Salem, NH). Another polyimide tube was placed over the inner polyimide lumen to protect the lead wires from damage and applicator cooling flow. A plastic Y-connector (Qosina, Edgewood, NY) at the proximal end of the applicator isolated the input water cooling flow from the miniature coaxial cables.

The catheter was designed in this study to contain the applicator and provide return water cooling flow through a urethral cooling balloon. The main portion of the catheter consisted of TPAX tubing (4.3 mm OD) secured to a large bore, Touhy-Borst hub at the proximal end. The distal portion of the catheter consisted of a PET urethral cooling balloon (10 mm OD, 40 mm length,
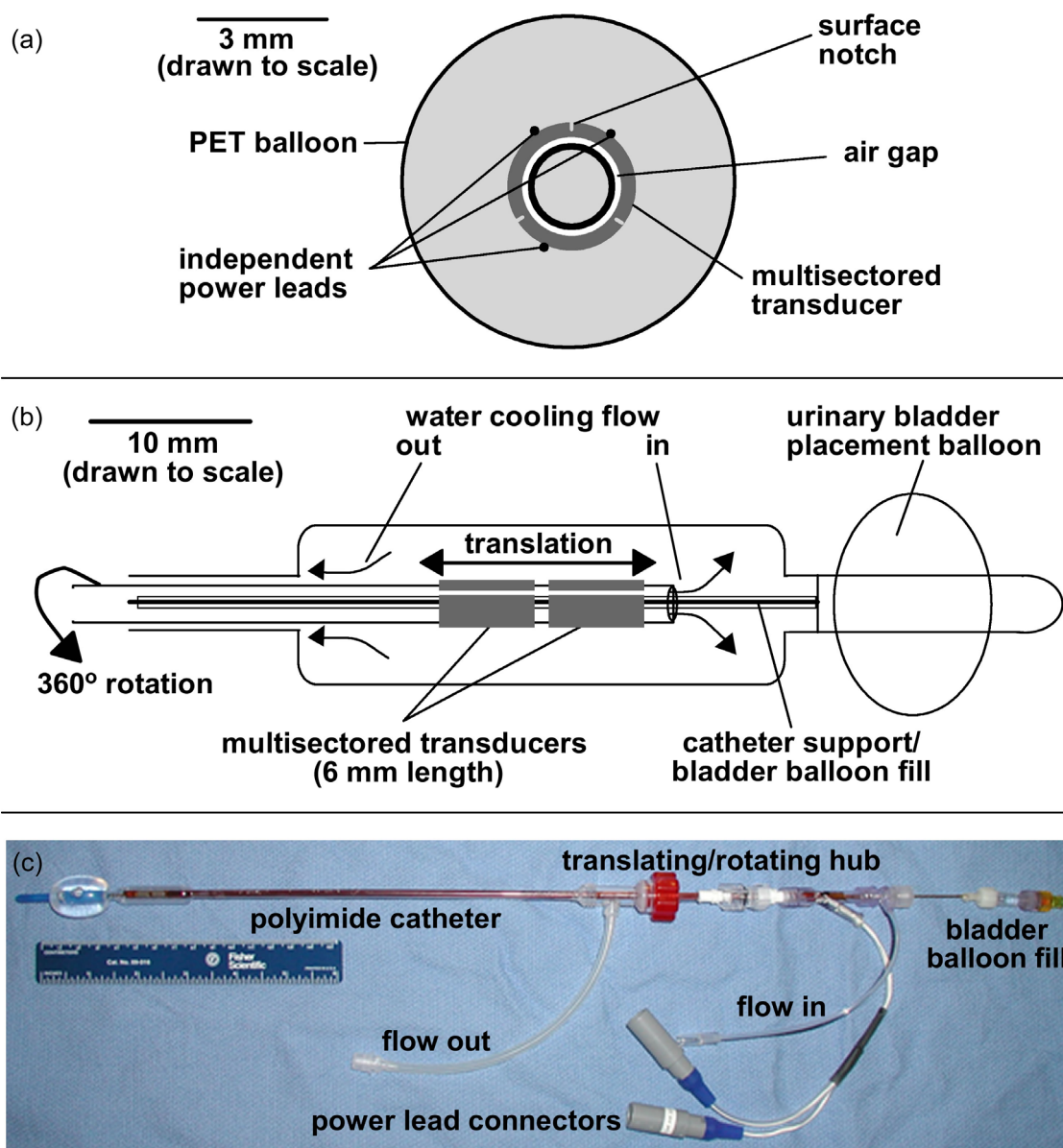
Figure 5.1: (a) Schematic diagram of the interior of the transurethral catheter and incorporated multisectored transducer. (b) Diagram of the tip of the multisectored transurethral ultrasound applicator with concentric water flow cooling, urethral cooling balloon, and urinary bladder placement balloon. (c) Photograph of the applicators used in this study with a translating and rotating hub for accurate positioning of the transducer assembly.

Advanced Polymers) secured to a PEBAX tip (4 mm OD, Danforth Biomedical, Santa Clara, CA). A polyimide tubing lumen ran the down the center of the catheter to provide a filling system for a C-Flex urinary bladder balloon (Extrusioneering, Placentia, CA) that was secured to the PEBAX tip. An MR-compatible titanium rod (0.71 mm OD) was inserted within the center polyimide tubing lumen to provide structural support to the catheter. The multisectored applicator was placed within the transurethral catheter, allowing for concentric water cooling flow through the inner lumen of the applicator assembly and out through the catheter and positioning hub. The water flow through the urethral balloon provided acoustic coupling of the ultrasound energy to the tissue and cooled both the applicator and adjacent tissue. The hub at the proximal end of the catheter enabled both rotation and translation of the applicator within the catheter for accurate positioning before heating. Manganin wire (0.025 mm OD, California Fine Wire) was wrapped around the catheter near the proximal end of the urethral cooling balloon to act as a fiducial marker in MR images. A generalized design scheme of the applicator design is shown in Figure 5.1, along with a photograph of one of the constructed devices.

The force balance technique for cylindrical ultrasound sources[54] measured the acoustic output power and acoustic efficiency, the percentage of RF power converted to ultrasound, of the multisectored transducers. For each sector on each transducer, the optimal operating frequency, as defined by maximum efficiency, was determined by conducting measurements at net

applied powers of 3 and 7 W for every 0.1 MHz step between 7.6-8.5 MHz. The acoustic output pattern was determined by obtaining rotational beam plots[33] of the normalized pressure-squared as measured from a computer-controlled scanning needle hydrophone (NTR Systems, Seattle, WA). The applicators were scanned within the catheter with the urethral balloon (10 mm OD) inflated by active water cooling flow (100 ml min^{-1}). The hydrophone was scanned 10 mm axially in 0.2 mm steps at a fixed radial distance, 4 mm from the outer surface of the urethral balloon, while the applicator was rotated 360° in 2.5° steps. These rotational acoustic beam plots were used to characterize the angular acoustic output pattern of each multisectored transducer, the acoustic dead zone between individual sectors, and whether the sectors were electrically and mechanically isolated from another.

5.3.2 MR Temperature Monitoring

MR temperature imaging was used to monitor and evaluate the heating performance of the multisectored applicators during *in vivo* experiments. The temperature images were based on the proton resonance frequency (PRF) phase subtraction method[93] and acquired with a receive-only prototype endorectal coil 0.5T interventional scanner (Signa SP, GE Healthcare, Milwaukee, WI). The endorectal coil was fitted with a water cooling flow jacket to protect the rectum during heat treatments. The specific imaging parameters for each *in vivo* canine experiment are listed in Table 5.1. Three echo times were acquired in 1 or 2

MR parameters	Canine 1	Canine 2	Canine 3
Echo time (TE) TE1/TE2/TE3 (ms)	14.3/21.5/28.6	14.3/21.5/28.6	14.3/21.5/28.6
Acquisitions	2	1	2
Relaxation time (TR) (ms)	170	160	190
Flip angle (FA) (deg)	60	60	60
Field of view (FOV) (cm)	18x12.5	16x16	18x12.5
Acquired resolution (pixels)	256x72	96x96	192x72
Reconstructed temperature map resolution (pixels)	96x72	96x96	96x72
Bandwidth (kHz)	15.6	12.5	12.5
Slice thickness (mm)	5	5	5

Table 5.1: MR imaging parameters used for the *in vivo* canine prostate experiments.

acquistions and averaged to increase the signal-to-noise ratio (SNR) and improve the accuracy of the temperature measurements in post-processing. During the real-time monitoring, one of these echo times was used to display the temperature maps. The reconstructed temperature resolution was used for both real-time monitoring and post-processing.[91] The temporal resolution of the temperature monitoring was 12-15 s in the experiments. Three imaging slices (5 mm thick with 1 mm spacing), centered in the middle of the transducer assembly, were used for real-time monitoring. The baseline temperatures used for the MR thermal imaging were determined immediately prior to heating using invasive measurements of core body temperature as described later. Custom software displayed the temperature maps in all three image slices during

treatment and allowed the user to set three different temperature thresholds (e.g. 48, 52, and 60 ºC) for monitoring the temperature in real-time. The software also had the capability of monitoring cumulative temperature and thermal dose.

The cumulative thermal dose, measured in equivalent minutes at 43 ºC, was calculated from the post-processed MR temperature data, where the SNR was improved by averaging all the echo times. The calculation was performed using the Sapareto-Dewey isoeffect thermal dose equation as a function of temperature and time:[30,99]

$$t_{43} = \sum_{t=0}^{t_{final}} \Delta t \bullet R^{(T-43)}$$

where $R = 2$ for $T \geq 43$ ºC, $R = 4$ for $T > 43$ ºC, T is measured temperature (ºC), Δt is the time between temperature measurements, and t_{final} is the total heating time. R is a constant that is empirically derived from Arrenhius analysis of thermal cell killing and protein denaturation.[30] A thermal dose of $t_{43} = 240$ min was used to define the thermal lesion boundary, based on previous studies of the temperatures and thermal dose that caused thermal necrosis in soft tissue,[32] including prostate tissue.[70,89]

5.3.3 *In Vivo* Canine Prostate Experiments

The heating performance of the multisectored transurethral applicators was tested in three separate *in vivo* canine prostate glands following procedures approved by the Institutional Animal Use and Care Committee at Stanford

University. The animals were anaesthetized and intubated for the duration of the procedure, and their vital signs were continuously monitored. Due to differences between human and canine anatomy, an urethrostomy was performed to access the urethra, and a 20 French introducer sheath was inserted into the urethra. The animals were positioned supine, headfirst into the 0.5 T interventional scanner and the bottom part of the abdomen was secured to minimize movement due to breathing. The multisectored transurethral applicator being tested was inserted into the introducer sheath, which was subsequently removed. The bladder placement balloon was then filled with 8-10 ml of a 4% gadolinium solution and the applicator was gently retracted until firmly seated within the bladder neck. The endorectal imaging coil with a water cooling jacket was inserted within the rectum and positioned adjacent to the prostate. Based upon pre-treatment MR images and integrated fiducial markers that marked the position of the applicator, the transducer assembly was rotated and translated within the catheter for positioning in relation to the predetermined target region. Once positioned, the applicator was locked into place and the urethral cooling balloon was expanded with degassed water. A screen captured MR image (resolution 256 x 128 pixels, FOV 20 x 20 cm, TE/TR 13/150 ms, flip angle 60°, bandwidth 6.94 kHz) of the setup of the applicator in the prostatic urethra is labeled and displayed in Figure 5.2.

Immediately prior to applying power to the applicator, ambient
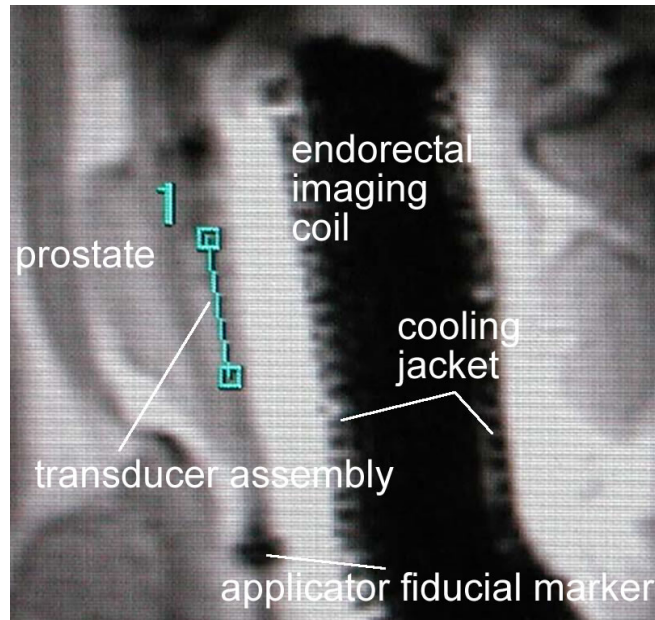
Figure 5.2: Screen captured MR image of the applicator setup in the prostatic urethra. The applicator, endorectal coil, and prostate are labeled on the image.

temperature water flow cooling was provided by peristaltic pumps outside the MR suite to the endrorectal jacket (60 ml min^{-1}) and applicator (100 ml min^{-1}). RF power was applied to the applicator by two custom, four channel RF amplifiers (Advanced Surgical Systems, Tucson, AZ) located outside the suite. Coaxial cables from the amplifier were connected to the applicator through a shielded access panel. RF noise at the Larmor frequency of the 0.5 T scanner was reduced by in-line, high power, 0-11 MHz low-pass filters with 60 dB attenuation at 20 MHz (Werlatone, Brewster, NY) to prevent degradation of the MR images. The core body temperature of the animal was measured by a deep nasal thermocouple probe before each heating trial to establish the baseline temperature for MR temperature imaging.

        After treatment, the animals were removed from the scanner and

sacrificed ~60-90 min later. The prostate was removed and cut into ~5 mm serial slices, which were immediately placed into a 2% triphenyl tetrazolium chloride (TTC) stain for 15-20 min. TTC is a redox indicator that is reduced by enzymes in viable tissues, and stains those tissues red. It can be used to distinguish viable and non-viable cells and clearly mark the border of thermal coagulative necrosis.[14]

Each of the canine prostate experiments was performed under MR guidance to evaluate the heating performance of multisectored transurethral applicators and establish compatibility within the MR suite. In Canine 1, the transducer assembly was positioned toward the base of the prostate and rotated to direct two active sectors (S1, S2) toward the ventral portion of the gland and the remaining inactive sector toward the rectum. Different power levels were applied to the active sectors on each transducer (T1, T2) [Figure 5.3(a)] and adjusted during treatment to contour the lethal thermal exposure towards the outer boundary of the prostate, according to the MR temperature measurements. Temperature was continuously monitored in three MR axial imaging slices. The central slice was positioned through the center of the transducer assembly, serving as the primary images for monitoring treatment progression and controlling the applicator power levels. Temperature thresholds and thermal dose calculations from the MR temperature measurements determined the extent of thermal damage and were correlated with the acute TTC stained tissue.

In Canine 2, the transducer assembly was positioned mid-gland with all
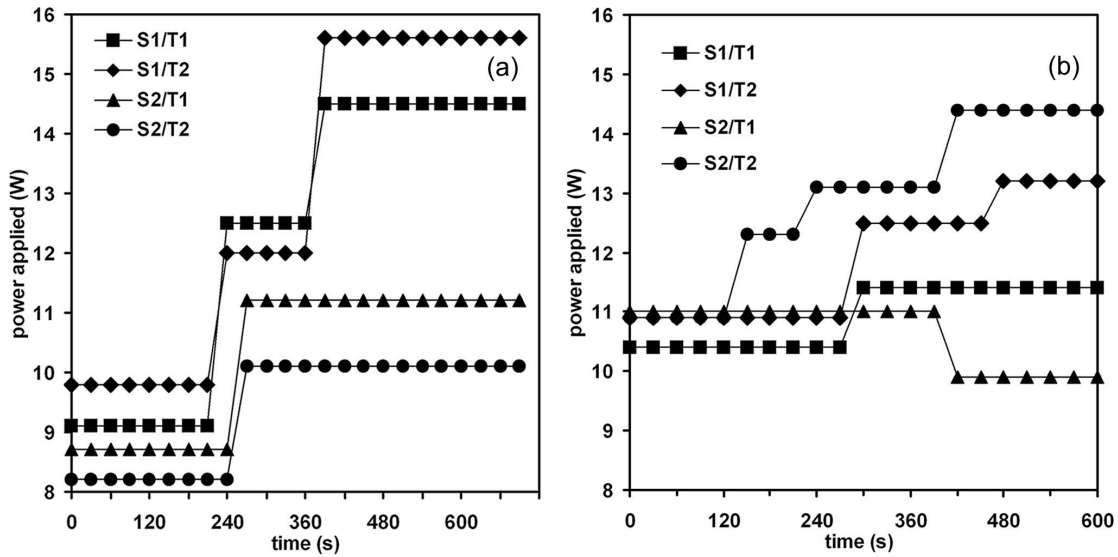
Figure 5.3: Power delivered to 2 active sectors (S1, S2) on both transducers on an applicator (T1, T2) in (a) Canine 1 and (b) Canine 3, as adjusted by hand using visual MR temperature feedback.

three sectors active to target the whole angular cross-section area of the prostate. The transducers were rotated to position sector 1 (S1) on both transducers (T1, T2) ventrally and sectors 2 and 3 (S2, S3) dorsally, with the acoustic dead zone between S2 and S3 directed toward the rectum. The applied RF power levels delivered to all elements (~11 W/sector) remained constant for the duration of the treatment (15 min). The MR temperature images were obtained in three axial slices as described for Canine 1.

In Canine 3, the transducer assembly was translated and positioned toward the proximal end of the urethral cooling balloon to target the apex of the prostate. The applicator was rotated and positioned to target the ventral portion of the gland, as described for Canine 1. Three coronal MR imaging slices were used to monitor temperature during treatment, with the central slice in plane

with the applicator. The applied RF power to each sector (S1, S2) on each transducer (T1, T2) was adjusted [Figure 5.3(b)] to fit the 52 $^{\circ}$C temperature contour to the border of the prostate, according to visual feedback from the MR temperature measurements in the center imaging slice (slice 1).

5.4 Results

Prior to the animal experiments, the multisectored transurethral applicators were characterized by measurements of acoustic power output efficiency and beam distributions. The peak acoustic efficiencies, at the optimal drive frequencies of each sector, ranged from 41-53 %, within a frequency range of 7.8-8.4 MHz. Rotational beam plots demonstrated 90-100° active acoustic patterns associated with each 120° partition with no apparent cross-coupling between sectors (Figure 5.4). Measurements were made with both two and three sectors active on the transducer. In consideration of experiments performed in an MR suite, separate RF electrical power measurements indicated ~30 % of the RF power delivered by the amplifier to the applicator was lost in the ~15 m coaxial cable and low-pass RF filters. The initial driving power of each sector in three *in vivo* canine experiments was adjusted according to the measurements of acoustic efficiency and transmission loss in the coaxial cable sets.

The ability of the multisectored applicators to control the angular shape and radial depth of clinically relevant heating patterns was examined in three *in*

(a)

(b)

2 active sectors
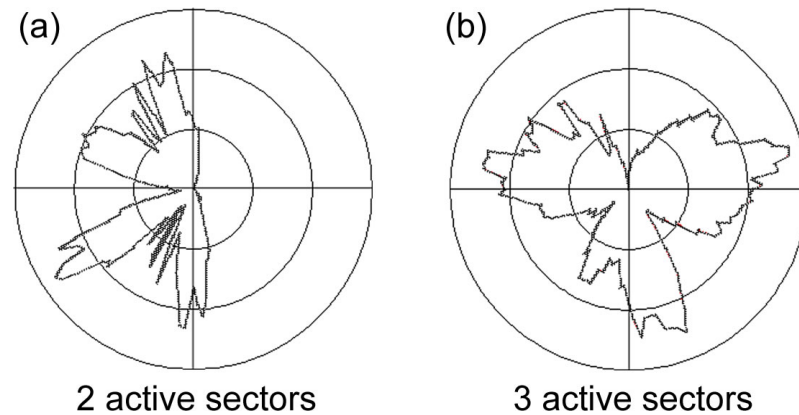
3 active sectors

Figure 5.4: Rotational beam plots of a three-sectored transurethral ultrasound transducers (3 mm OD, 6 mm length) with (a) 2 and (b) 3 sectors concurrently active.

vivo canine prostate glands. These experiments were carried out under MR temperature imaging guidance to assess the controllability of the devices using either axial or coronal imaging planes. In Canine 1, two sectors were active and the third sector was inactive, to ablate a large ventral portion of the gland, while directing heat away from the rectum. Figure 5.3(a) displays the power levels applied to sectors S1 and S2 on each transducer (T1, T2) over the course of the treatment. Higher power levels were delivered to S1 on T1 and T2 than to S2 in order to evaluate the heating patterns attainable with different maximum temperatures from each sector and demonstrate the effectiveness of independent power control. The 52 °C contours were displayed continuously during treatment with MR temperature monitoring and were used to control applied power levels during the treatment. The radial progression of the 52 °C contour during the procedure is displayed in Figure 5.5(a) for different time points (80, 180, 355, 505 s). The radial temperature profiles extending from the center of S1

and S2 [corresponding to the linear track denoted by arrow in Figure 5.5(a)] are shown in Figures 5.5(b,c) for the four time points. The temperature profiles increased quickly as a function of radial distance within 1-2 mm of the urethral cooling balloon and gradually decreased after reaching a peak temperature 3-4 mm from the applicator, as expected due to the urethral cooling. At 505 s, the 52 °C contour had penetrated to the prostate boundary. The lower power delivered to S2 translated into a lower peak temperature in the tissue adjacent to this sector and slightly less radial penetration of the 52 °C contour. Thermal redistribution and conduction filled in any gaps in ultrasound energy that was seen in the acoustic pressure profiles and created a contiguous 52 °C boundary, predictive of the thermal destruction. These results demonstrate the potential of multisectored transurethral ultrasound applicators to produce conformal, contiguous heating patterns in the angular dimension through differential power level control to each sector.

Figure 5.5(d) shows the contours of lethal thermal dose threshold (t_{43} = 240 min) as calculated from the MR temperature measurements at the same time points during treatment (80, 180, 355, and 505 s). An aberration in the thermal dose contour at 505 s was noted outside the ventral portion of the prostate gland and was most likely caused by temperature measurement artifact in one of the MR images. The MR image SNR, which determines the accuracy of the temperature measurement, decreases rapidly with increasing distance from the endorectal coil. Therefore, temperature measurement artifacts are more likely to

occur where image SNR is low. Furthermore, the cumulative thermal dose distribution, based upon calculations that are nonlinear with respect to temperature rise, was calculated without temporal filtering and was very susceptible to artifacts and small transient errors in MR temperature measurement. Figure 5.5(e) displays the TTC-stained prostate section obtained after thermal treatment and demonstrates a clear contiguous thermal lesion in the targeted portion of the gland, while the red-stained viable tissue indicates the dorsal portion of the prostate toward the rectum was protected from thermal damage. The lethal thermal dose contour and final 52 ^{o}C contour [Figure 5.5(a)] appeared to correspond very closely to the outer boundary of thermal destruction identified from the histological analysis.

In Canine 2, fast, complete thermal bulk ablation of the prostate was performed. The experiment was conducted with all sectors active on each transducer at constant applied power levels. The progression of the 52 ^{o}C contour, as monitored in central MR imaging slice during treatment, is shown in Figure 5.6(a) at selected treatment times (150, 240, 360, and 450 s). The corresponding cumulative lethal thermal dose contours (t_{43} = 240 min) at the different treatment time points are shown in Figure 5.6(b). Within 4 min, thermal redistribution filled any gaps in the heating pattern and created a contiguous lesion shape. The radial temperature profiles as a function of time in front of each sector are shown in Figures 5.6(c-e) corresponding to the arrows (S1, S2, S3) in Figure 5.6(a), respectively. The peak temperature was 4-5 mm from the urethra
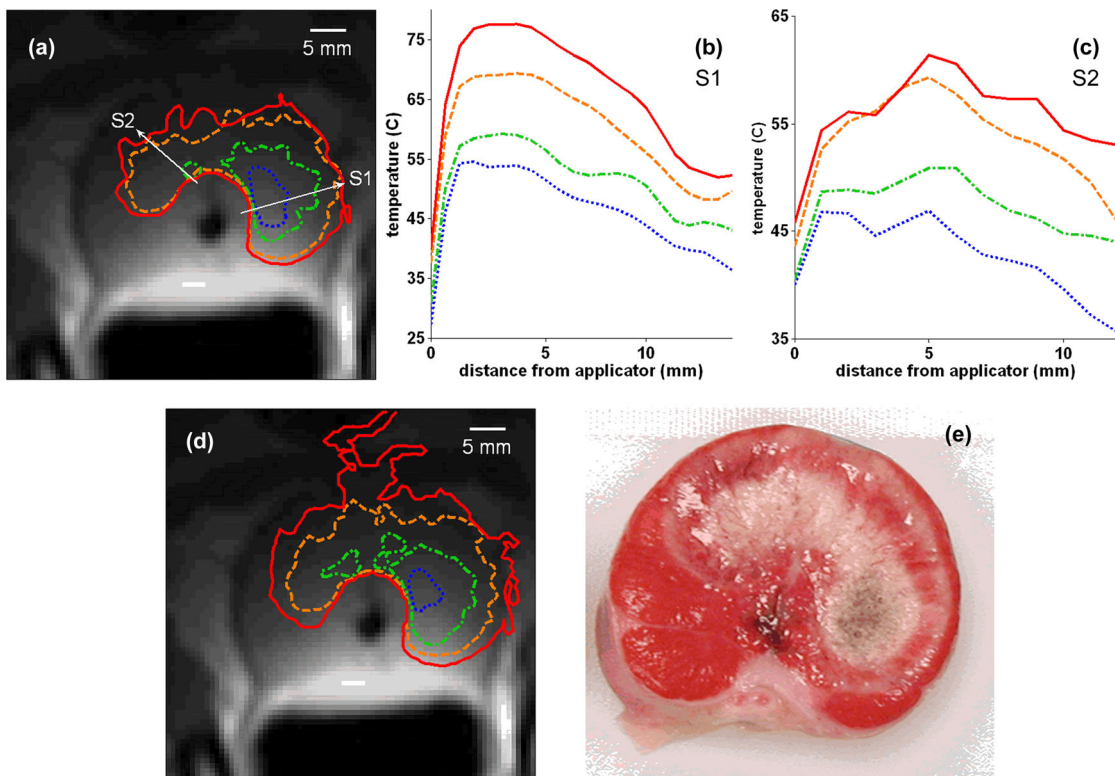
Figure 5.5: MR temperature and thermal dose measurements of a 2 active sector (S1, S2) heat from a multisectored transurethral ultrasound applicator at 80 s (•••), 180 s (•—•), 355 s (— —), and 505 s (solid). The 52 °C contour throughout time (a) and the radial profile of the heating along the white arrows (S1, S2) (b,c) are shown. The thermal dose (t_{43} = 240 min) at the different times (d) was calculated from the MR temperature measurements and corresponded with acute gross histology of the thermal lesion (e).

and the 52 °C contour reached the edge of the prostate (>10 mm radial) in less than 8 min.

Experiments in Canine 3 evaluated the ability to use multiple coronal MR imaging planes to monitor and adjust the heating pattern. The transducer assembly was translated to the proximal portion of the urethral cooling and rotated for positioning to selectively direct heating to the ventral portion of the apical region of the prostate. The power levels applied during treatment were
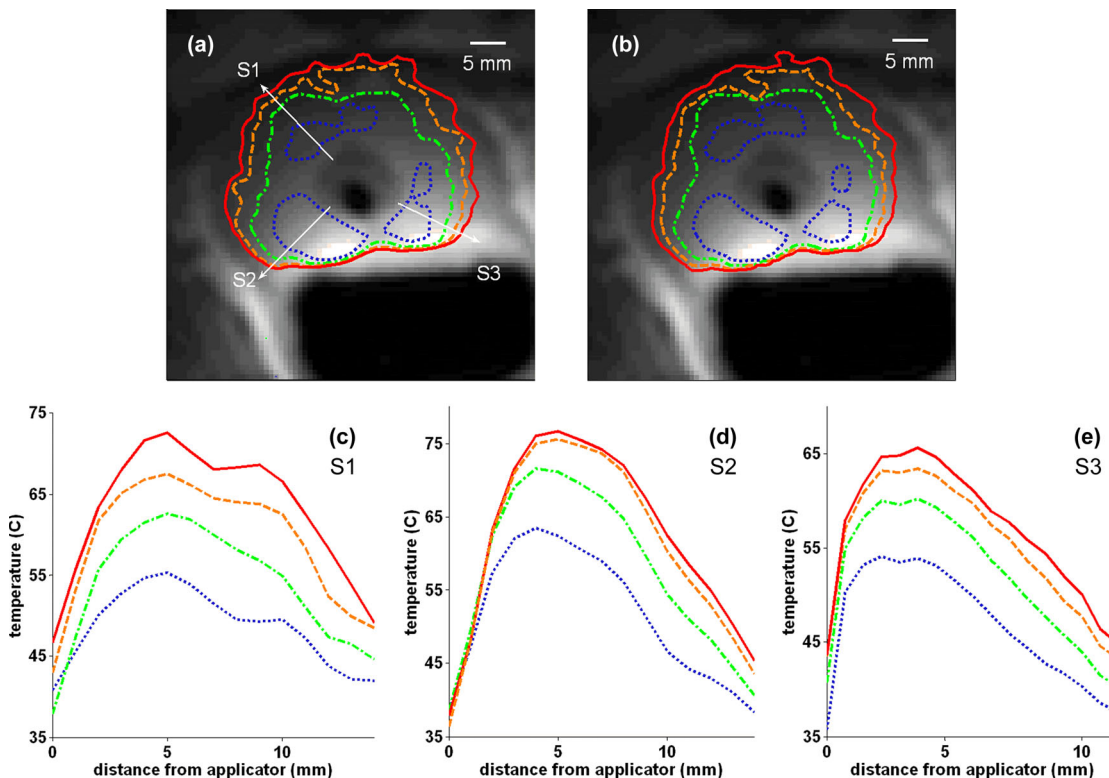
Figure 5.6: MR temperature and thermal dose measurements of a 3 active sector (S1, S2, S3) bulk ablation of a canine prostate with a multisectored transurethral ultrasound applicator at 150 s (•••), 240 s (•—•), 360 s (— —), and 450 s (solid). The 52 °C temperature contours (a) expanded throughout the treatment and thermal conduction filled in the heating pattern at 240 s. The thermal dose contours (t_{43} = 240 min) (b) fit closely to the 52 °C contour at the different time points and showed bulk ablation of the prostate in less than 7 min. The peak temperatures of the heating distribution from S1 (c), S2 (d), and S3 (e) were about 5 mm from the urethral cooling balloon.

manually adjusted [Figure 5.3(b)] using visual feedback from the MR temperature monitoring to extend the 52 °C contour to the outer edge of the prostate. In this experiment, the temperature was monitored in three imaging slices, but the power levels were based upon the measurements in the center slice (slice 1). Figure 5.7(a) displays the MR temperature map in slice 1 at the end of the thermal treatment where the 52 °C contour has reached targeted boundary of
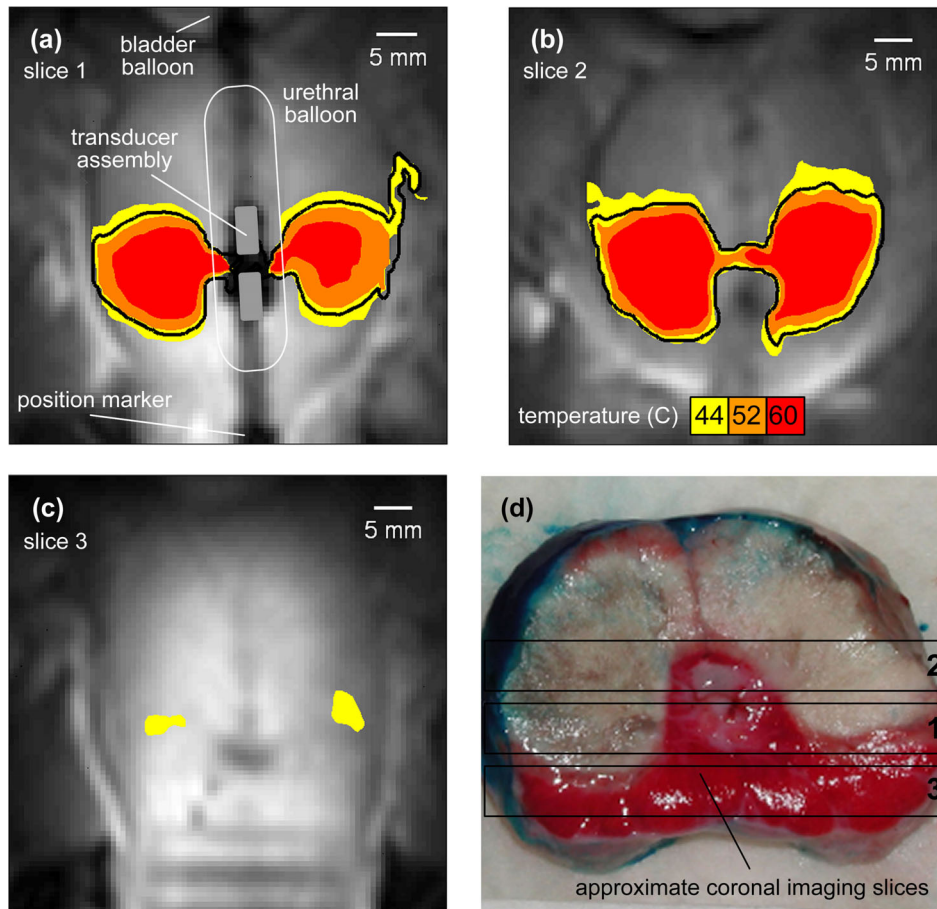
Figure 5.7: Three coronal MR temperature images at the end of a 10 min heat treatment and gross histology of the resulting thermal lesion from a multisectored transurethral applicator with two active transducer elements. (a) The 52 °C contour was manually fitted to the border of the prostate according to visual MR temperature feedback. The thermal dose contour (t_{43} = 240 min) (solid line) was calculated from the MR temperature measurements. A schematic of the approximate applicator and transducer position is overlaid on the image. The imaging slices directly above (b) and below (c) the applicator displayed the large thermal dose delivered to the ventral portion of the gland and the protection of the tissue in the dorsal gland, respectively. (d) TTC stain of the thermal lesion and the approximate location of the monitored coronal imaging slices.

the prostate. The cumulative lethal thermal dose contour (t_{43} = 240 min) calculated from the MR temperature images is overlaid as a solid line on the temperature map and reaches the target boundary. In addition, the approximate position of the applicator and transducer assembly is displayed on the temperature image. The ventral prostate tissue experienced higher temperatures (slice 2) [Figure 5.7(b)] due to the angular position of the applicator. Slice 3 in Figure 5.7(c) demonstrates that the prostate tissue below the applicator did not experience high temperatures and inferred that the rectum was protected. Along the length of the applicator, two transducers (6 mm length, 2 mm spaced) created a thermal lesion 15-18 mm in length and 13-16 mm in radius from the urethra during a short 10 min treatment. The 52 °C contours were contiguous and displayed the ability of multiple transducer arrays to control heat delivery along the length of the applicator. The TTC-stained prostate, sliced axially, reinforced the temperature and thermal dose data acquired in the MR [Figure 5.7(d)] and corresponded to the 52 °C and thermal dose contours in slices 1 and 2 [Figures 5.7(a,b)]. The setup of MR imaging slices used to monitor the treatment is shown on Figure 5.7(d), but the true locations of the imaging may be slightly different from those displayed due to differences with the slicing of the prostate for histological analysis.

5.5 Discussion

Multisectored transurethral ultrasound applicators were developed and evaluated to determine their potential for delivering conformal thermal ablation to targeted regions of prostate tissue in conjunction with MR guidance and temperature monitoring. Furthering a design strategy first discussed for interstitial ultrasound technology,[61] the transurethral applicator developed in this study was constructed with a linear array of larger diameter tubular radiators, each with three independently powered 120° sectors, for dynamically tailoring heat treatments in angle and length without requiring mechanical manipulation during treatment. The transducer assembly incorporated into the devices was capable of rotation and translation within the catheter for accurate positioning and selective targeting of thermal treatment. In a series of three *in vivo* experiments within canine prostate glands, these devices proved to be capable of conforming heat treatments to large target volumes in a relatively short treatment times. The treatment times and radial heating penetration were consistent throughout the three canine prostate experiments. By adjusting applied power levels to each sector on multiple transducers, the heating pattern could be effectively directed and controlled in the radial, angular, and longitudinal dimensions under MR temperature guidance.

The experiments performed in Canines 1 and 3 used two active sectors on each transducer, directed ventrally, to produce a well-defined thermal lesion that extended toward the outer boundary of the prostate, with no energy or heating directed toward the rectum (Figures 5.5, 5.7). The active cooling within the

urethral cooling balloon provided a protective effect extending 1-2 mm from the urethra [Figures 5.5(e), 5.7(d)]. Angular control over the heating penetration was possible by applying different powers to each set of independent sectors (S1, S2) and controlling treatment duration (Figure 5.3), according to MR temperature monitoring of the 52 °C contour. In the Canine 2 experiments, the transducer assembly was rotated and positioned with a sector notch and inherent acoustic dead zone directed toward the rectum. All three sectors on each transducer segment were activated to produce fast thermal ablation conforming to the whole prostate gland axial imaging cross-section, with reduced maximum temperatures directly toward the rectum. Together these three *in vivo* experiments consistently demonstrated these applicators are capable of fast thermal ablation (7.5-10 min) extending 12-15 mm from the applicator to the prostate boundary, with the ability to shape the angular heating pattern by appropriate sector activation and positioning. The power handling capabilities and penetration depths of these multisectored transurethral applicators are similar to previously reported values for fixed, single-sectored directional tubular transurethral devices,[39,96] but with the significant advantage of dynamic angular control.

An additional objective of this study was to determine the effect, if any, of the acoustic dead zone that exists between sectors has on the angular heating distribution in prostate with multisectored transurethral ultrasound applicators. The loss of acoustic output at the edge of the transducer sector of a tubular

source is documented and can be attributed to physical loss of material during cutting, de-poling of material adjacent to the notch, and near-field diffraction patterns.[33,61] Recent investigations have demonstrated that the presence of acoustic dead zones on small diameter multisectored tubular transducers (<1.8 mm OD) for interstitial applications did not significantly impact angular control of heating.[61] The larger diameter transurethral transducers (3 mm OD) used in this study displayed a 90-100° active acoustic zone from a 120° sector as measured outside the urethral cooling balloon (Figure 5.4). In this study during power application with two or three sectors active, discontinuity in the 52°C contour due to the acoustic dead zone was noted during the initial phase of power application, but by 4 min the effects were negligible as higher temperatures were achieved and thermal redistribution filled in the heating pattern. Additionally, as demonstrated in Figure 5.5, the 52 °C contour and resulting thermal lesion remained contiguous despite driving sectors at different power levels and creating different maximum temperatures adjacent to each sector.

Heating control along the length of the applicator was accomplished using a linear array of two short transducers (6 mm). A linear array of ultrasound transducers has been shown to provide adaptable lesion control along the length of a heating applicator,[39] however, as more transducers are added to the array, the power control and driving systems become significantly more complicated. The transducer assembly designed in this study could be translated into a

designated heating position without moving the catheter, allowing for heating one area in the prostate and then moving to a different area. Heating in multiple steps with two transducer arrays may be practical with multisectored transurethral ultrasound applicators because of the short treatment time to ablate a large tissue area. In addition, heating the entire prostate in multiple steps should simplify the applicator power delivery system and setup and provide an alternative to large transducer arrays.

Currently, the methods available for heat treatment of prostate cancer with ultrasound are external and transrectal HIFU devices that typically involve rapid thermal damage (<10 s) to multiple small volumes of tissue.[47,110] MR verification of the delivered temperatures from HIFU devices has been recently approved for the treatment of uterine fibroids.[77] For prostate cancer, ultrasound imaging has recently been suggested and used as a non-invasive temperature monitoring system for improving treatment heating patterns with HIFU devices by adjusting the treatment parameters between pulses.[56] Regardless of the method used to monitor and control HIFU prostate thermal therapy, the heating requires significantly long treatment times for prostate cancer (169 min average).[110] When monitoring the temperature with MR, the cost and resources involved can become significant with this long treatment. In comparison, an important benefit of multisectored transurethral ultrasound applicators for treating prostate cancer and BPH is their ability to ablate a large volume in a short period of time, while controlling the shape of a thermal lesion

in the angular dimension. In this study, bulk ablation of the prostate area was accomplished in a short treatment duration (<10 min) (Figure 5.6) under MR temperature monitoring.

Transurethral ultrasound applicators are currently under pre-clinical evaluation as an alternative to HIFU for high-temperature ultrasound thermal therapy. Transurethral devices heat larger volumes in a single treatment and offer less severe thermal gradients at the boundaries of heating than HIFU devices. The slower growth of the thermal lesion boundary and shorter overall treatment times possibly make the transurethral devices more practical for use with MR temperature feedback.[19,49,96] The multisectored transurethral ultrasound applicators developed in this study were evaluated in a 0.5 T interventional magnet because of the ease of access to the canine during experimental setup. A recent study explored the optimal spatial and temporal resolutions in the 0.5 T scanner to balance image and temperature map resolution with higher SNR.[91]

Rotating transurethral applicators with planar or curvilinear transducers can thermally ablate narrow zones of prostate tissue extending 15-20 mm towards the boundary of the gland in around 60 s.[16,96,97] In order to treat larger target volumes, many mechanical rotations are required to sweep out and contour a composite ablative region while using MR temperature imaging as feedback with these devices, which can significant increase overall treatment duration. Previous studies with directional tubular transurethral ultrasound

applicators (180° sector) were able to ablate a large tissue volume in a short treatment, but these devices lacked the flexibility to more carefully control the angular dimension of the thermal lesion during treatment.[33,38] With a very directional sectored transducer (90°), angular control was accomplished by rotating the transducer during treatment;[96] however, this extended the overall treatment time and introduced mechanical movement during treatment. Although these rotating transurethral devices are very controllable, the requirement to rotate or sweep during therapy delivery can induce movement artifact or errors in PRF-based MR temperature monitoring, due to the sensitivity of the measurements to any motion with respect to the initial baseline image. In addition, the longer treatment duration associated with rotating transurethral heating applicators could also introduce temperature measurement errors associated with image phase drift or a change in prostate dimensions due to heating. When controlling rotating transurethral applicators with MR temperature feedback, the treatments must be monitored in the axial imaging plane. As seen in Figure 5.5, multisectored transurethral applicators can be monitored in the other imaging planes (coronal, sagittal), because the device power control does not have to depend on the temperature maps in the axial imaging plane. When compared to rotating transurethral ultrasound applicators, multisectored devices offer less angular control of heating patterns, however, the multisectored devices allow much simpler heating control with MR temperature feedback and do not require any device manipulation during treatment. These

factors and the short treatment times to ablate a large volume of tissue, as found in this study, contribute to multisectored transurethral ultrasound applicators possibly being more suitable and practical for prostate heat treatments with MR temperature monitoring.

This study has demonstrated the feasibility and clinical potential of this design concept for prostate thermal therapy. The multisectored tubular ultrasound device configuration could be useful for thermal ablative treatment of BPH, which typically targets the anterior/lateral lobes of the human prostate to reduce obstructive hyperplasic tissue.[24,59,122] Compared to TUMT devices, these multisectored transurethral ultrasound applicators offer increased spatial heating control both in positioning toward the bladder neck and in directing the energy into the anterior/lateral portion of the gland. This improved control, coupled with faster treatment times and greater heating penetration, may improve overall clinical efficacy and durability.[38] Other multisectored transducer configurations (e.g. number of sector and angles, intentional dead zones) may be applicable or tailored to BPH treatment. Although not required for treating BPH, using MR temperature guidance with these ultrasound devices would allow more precise and thorough targeting of the obstructive tissue and patient specific therapy. In contrast, cancer treatment would require MR temperature monitoring to ensure that the targeted cancer region receives a prescribed thermal dose, while avoiding damaging the rectum, sphincters, or neurovascular bundles. Additional studies are warranted to optimize applicator

design, including the number of sectors and transducers, and develop disease specific treatment strategies to ensure adequate target destruction and protection of non-targeted tissues.

In conclusion, multisectored transurethral ultrasound devices offer dynamic angular and longitudinal control over the creation of contiguous thermal lesions conforming to prescribed target regions within the prostate. Fast treatment times (10-12 min), radial heating penetration (12-15 mm), and formation of contiguous thermal lesions (180-360°) were consistently achieved in the three *in vivo* canine prostate experiments. The multisectored transurethral ultrasound applicators were designed to be practical for controlled heating in conjunction with MR temperature guidance. These devices and MR temperature monitoring provided real-time angular and longitudinal control over heating distributions without introducing any device motion during treatment. Treatment times were dramatically reduced by the ability to simultaneously apply and control power to all required sectors. Multisectored transurethral ultrasound heating devices coupled with MR thermal monitoring are useful for conforming a thermal dose to either discrete target volumes or the entire gland for cancer treatment or reducing obstructive symptoms of BPH.

Chapter 6

Hyperthermia of the Prostate with Multisectored Transurethral Ultrasound Applicators

6.1 Abstract

Transurethral multisectored ultrasound applicators have been shown to provide excellent heating penetration and control of prostate high temperature thermal therapy in canine studies. These applicators have an acoustic dead zone between the sectors due to surface cuts. Thermal effects and smearing allow for the creation of contiguous thermal lesions with high maximum temperatures in

the tissue. In the case of hyperthermia (<48 ^{o}C), this study showed that despite the lower maximum temperature than the thermal ablation studies, thermal effects still created a contiguous therapeutic heating pattern in three canine prostates. Also, when low power levels were applied to the ultrasound applicators (<3 W), the temperature in the tissue was maintained at non-lethal hyperthermia temperatures for up to 20 min. In all three *in vivo* canine prostate experiments, the heating pattern reached the prostate boundary in a single heat treatment. This study and the study in Chapter 5 displayed the flexibility of multisectored transurethral ultrasound applicators to deliver both high-temperature thermal therapy and hyperthermia with a minimally-invasive approach.

6.2 Introduction

Quality of life is a major concern for treating prostate cancer. Many men do not suffer from the symptoms of the disease at the time of diagnosis, but as it progresses they can potentially enter into years of therapy. Short term side effects of treatments become a major factor affecting the quality of life. When treating the prostate with radiation, a number of patients suffer from treatment failure. As an adjunct to radiation therapy, hyperthermia can be administered to improve the overall efficacy of treatment. In general, the late-stage clinical results

from this method have shown a significant improvement in the efficacy of therapy when compared to stand-alone radiation therapy.[3,116,118]

Different heating methods have been used to deliver hyperthermia to the prostate including transurethral and transrectal ultrasound devices.[45,53] As detailed in the previous chapter, transrectal ultrasound can have limitations, including long treatment times. A transurethral device that can accurately deliver hyperthermia temperatures (<48 ^{o}C) may be a simpler way to deliver treatment. However, to be used for prostate cancer treatment, the device needs to be able to treat up to the capsule of the gland. In addition, a device that could heat discrete target volumes of the prostate could further improve treatment by limiting side effects like incontinence.

In this study, multisectored transurethral ultrasound applicators were used to deliver standard hyperthermia temperatures in three *in vivo* canine prostates. The treatment was monitored with MR temperature imaging for verification and control of the heating. The purpose was to test the ability of the multisectored transurethral devices to deliver hyperthermia temperatures and determine the shape and effect of the heating pattern from the applicators.

6.3 Experimental Methods

The multisectored transurethral ultrasound applicators designed, characterized, and described in Chapter 5 of this work were used to provide non-

MR parameters	Canine 1	Canine 2	Canine 3
Echo time (TE) TE1/TE2/TE3 (ms)	14.3/21.5/28.6	14.3/21.5/28.6	14.3/21.4/28.6
Acquisitions	2	2	2
Relaxation time (TR) (ms)	170	190	150
Flip angle (FA) (deg)	60	60	60
Field of view (FOV) (cm)	18 x 12.5	18 x 12.5	16 x 12
Acquired resolution (pixels)	256 x 72	192 x 72	256 x 72
reconstructed temperature resolution	96 x 72	96 x 72	96 x 72
Bandwidth (kHz)	15.6	12.5	12.5
Slice thickness (mm)	5	5	5

Table 6.1: MR temperature monitoring imaging parameters for the *in vivo* canine hyperthermia experiments

lethal hyperthermia tissue temperatures to canine prostate glands *in vivo* (n = 3). The animals were prepared and the applicators inserted into the prostates in the same manner as those described in Chapter 5. The experiments were conducted in a 0.5 T interventional MR suite. The MR imaging was done in a similar manner to the high temperature *in vivo* canine experiments in Chapter 5, with multiple echoes being used to acquire the images to improve the signal-to-noise ratio (SNR) in post-processing. The temperature imaging for all the animals was done with three axial imaging slices using the custom software that allowed for three temperature contours to be monitored continuously. The imaging parameters are shown in Table 6.1. The prototype receive-only endorectal coil was covered with a jacket for water cooling flow (60 ml min^{-1}) to protect the rectum. The MR temperature images were used to adjust the power levels to the applicators and

monitor the treatments. Urethral water cooling flow (60 ml min^{-1}) was turned on to the applicator immediately before treatment. Because the baseline temperatures of the animals were lower than normal body temperatures (37 ^{o}C), the goals of the hyperthermia treatments were to elevate the temperature 2 ^{o}C above baseline in a contiguous area of the prostate, while keeping the maximum temperature <10 ^{o}C above baseline, for a period of at least 10 min. In all of the experiments, all three sectors were active on both multisectored transducers, and low powers levels were applied to each sector independently.

In Canine 1, the multisectored transurethral applicator was positioned with one sector aimed directly toward the rectum and the other two sectors aimed toward the ventral portion of the prostate gland. All three sectors on the applicator were active for 10 min. The power levels applied to the two ventrally aimed sectors were 2.9-3.3 W, while the applied power to the third sector was 0.4-0.6 W. The baseline temperature in Canine 1 was 33 ^{o}C and the temperature thresholds used to evaluate the treatment were 35, 38, and 41 ^{o}C.

The applicator was positioned in Canine 2 with one sector aimed ventrally, while the other two sectors aimed toward the dorsal/lateral lobes of the prostate. All sectors were activated for 20 min and the applied power levels (1.9-3.0 W) to the ventrally aimed sector was adjusted according to the MR temperature measurements to accomplish the treatment goals. The power levels delivered (1.0-2.0 W) to the other two sectors were adjusted in a similar manner, while remaining slightly lower to avoid heating the rectal tissue. In Canine 2, the

baseline temperature of the animal was 32 ºC and the temperature contours used to evaluate the treatment were 34, 37, and 40 ºC.

In Canine 3, the multisectored applicator was aimed in a similar fashion to the experiment in Canine 2, with one sector aimed ventrally. All sectors were active for a 10 min treatment, during which the applied power levels were adjusted according to the treatment goals and MR temperature measurements. The sector aimed ventrally had power applied at 2.1-2.9 W, while the other two sectors, which treated near the rectum, received applied powers of 1.4-1.5 W. The baseline temperature was 30 ºC and the evaluation temperature contours were 32, 35, and 38 ºC.

6.4   Results and Discussion

Hyperthermia of the prostate requires a device that can deliver a consistent temperature distribution throughout the gland. In Canine 1, one of the primary goals of the treatment was to avoid high temperatures in the tissue near the rectum. A higher thermal dose to the rectum can result in serious complications after treatment. However, hyperthermia temperatures should not be lethal, so heating near the rectum is of slightly less concern than with high temperature thermal ablation treatments. By positioning one of the three sectors directly toward the rectum and only delivering a very low amount of power, a lower maximum temperature was attained in the posterior portion of the gland.
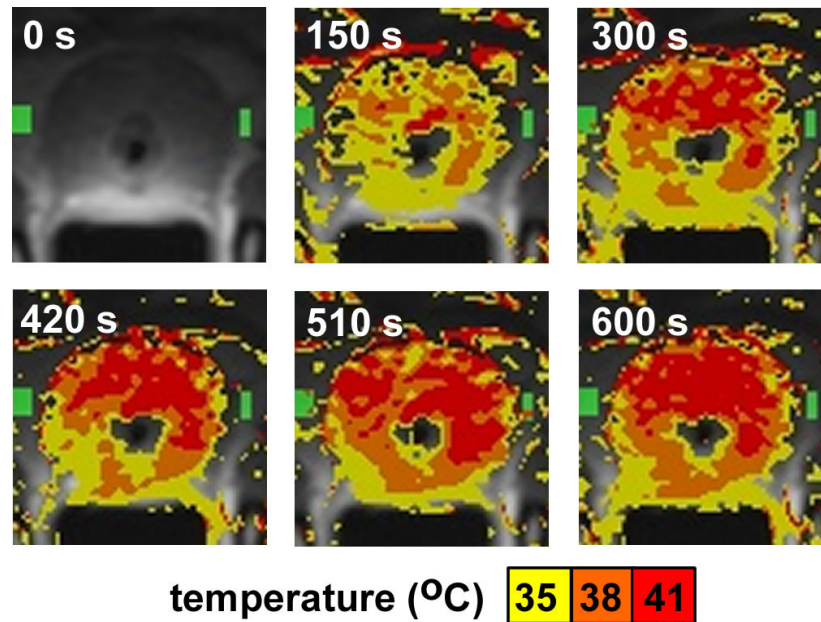
temperature (°C) 35 38 41

Figure 6.1: MR temperature images of a hyperthermia treatment in canine prostate. The heating was accomplished with a multisectored transurethral ultrasound applicator with all three sectors active. The sector aimed towards the rectum was delivered lower power than the other two sectors.

In the anterior portion of the gland, the temperature rose to ~10 °C above the baseline, similar to a standard hyperthermia treatment. In traditional hyperthermia treatments, an elevated temperature is maintained for 30-60 min. Figure 6.1 shows that after 7 min of heating, the temperature was consistent throughout the gland and was maintained at very similar levels for the final 3 min of experimental treatment time. In addition, the flexibility of a multisectored applicator for delivering low temperature heat treatments was observed, as the area of the prostate near the rectum, where more sensitive structures exist (as outlined in Chapter 5,) was maintained at 3 °C less than in the anterior portion of the gland. Finally, this experiment also demonstrated the ability of a single

minimally-invasive transurethral ultrasound applicator to heat to the boundary of the prostate in a single treatment.

In Canine 2, the applicator was positioned to examine another method of treatment setup. In this experiment, the heat treatment was monitored in two axial slices along the length of the applicator as seen in Figure 6.2. This gives a better picture of the volume of the thermal lesion and displays the ability of MR temperature imaging to monitor the target volumes. In addition, the heating was carried out for 20 min and the multisectored devices were again able to maintain consistent hyperthermia temperatures for an extended period of time. The applicator was positioned in a similar fashion in the experiment in Canine 3 (Figure 6.3) and supported the results from Canine 2.

One of the concerns with hyperthermia heat treatments is thermal redistribution from perfusion. The heating experiments in this chapter do not seem to show major effects of thermal redistribution. There are no major blood vessels in the prostate, which is one reason that the prostate is an excellent candidate for thermal therapy. In addition to perfusion concerns, multisectored tubular ultrasound transducers have an acoustic dead zone in their energy output pattern due to the cuts in the surface. A possible concern with delivering low temperature heat treatments with these types of transurethral applicators was whether the heating pattern would become contiguous because of thermal conduction and smearing. In this study, thermal effects filled in the heating pattern as seen in Figure 6.1, and did not require a significant increase in the

Figure 6.2: Hyperthermia treatment in canine prostate with a multisectored transurethral ultrasound applicator active for 20 min.

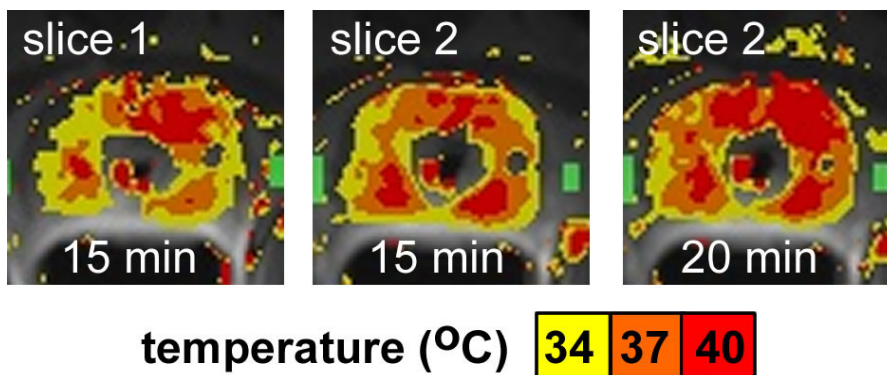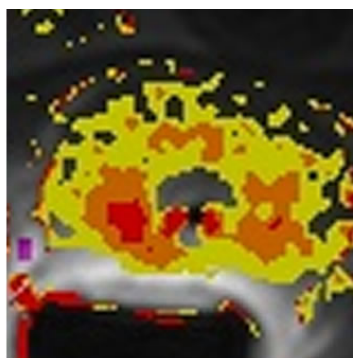Figure 6.3: Hyperthermia treatment in canine prostate with a multisectored transurethral ultrasound applicator active for 10 min.

maximum temperature in the tissue. An additional concern for hyperthermia treatments is heating the entire prostate gland. In all the experiments, therapeutic temperatures reached the edge of the prostate gland using the transurethral multisectored ultrasound devices.

6.5 Conclusions

Hyperthermia has been shown to be an effective adjuvant to radiotherapy. In order to gain widespread clinical acceptance, prostate hyperthermia needs to be able to treat the entire prostate gland in a reasonable treatment time (~30-60 min) using an approach that is minimally-invasive and simple to set up. Radiotherapy treatments can be very successful in a cancerous prostate if the disease is at a fairly early stage. Combining radiotherapy with hyperthermia has been shown to increase the efficacy of treatment[3,52] and may offer the possibility of delivering lower radiation doses to the target tissue, which would help protect healthy surrounding tissue. A transrectal HIFU device can provide accurate heat deposition, but is probably more suited for thermal surgery than hyperthermia treatments because of the large amount of time required to set up and deliver heat to the entire gland. Interstitial heating devices would require many invasive implants into the tissue, which increases set up time and the possibility of set up errors. An exception to this would be in the case of brachytherapy, where interstitial heating devices can be inserted into the radiotherapy implant catheters that are already in place.[Sneed 1998] This approach has many benefits, but adjusting the power deposition from multiple applicators can be difficult. TUMT devices offer excellent minimally-invasive access to the prostate, but they may not be suitable for cancer treatments because the radial heating penetration depth is limited. The transurethral multisectored

ultrasound applicators studied in this work maintain many of the qualities of transrectal HIFU devices in terms of heating control, while offering shorter treatment times. In addition, as seen in the experiments in this study, these devices can deliver therapeutic temperatures to the capsule of the prostate for cancer treatment.

Chapter 7

Biothermal Modeling of Multisectored Transurethral Ultrasound Heating Applicators

7.1 Abstract

Mathematical models of human body systems are difficult to formulate and solve because of the complexity of living tissue. A biothermal model based on the Pennes bioheat equation relies on simple assumptions in tissue without large blood vessels. The most important of these assumptions is the convective heat transfer in these tissues occurs at the capillary level and that the capillaries

are evenly distributed throughout the tissue. In this work, 2D and 3D cylindrical models based on the bioheat equation were created and modified for the evaluation of multisectored transurethral ultrasound applicators. Using bang-bang and pilot point control systems, the heating capabilities and flexibility of this applicator configuration could be examined. In studies with a 2D R-θ model, three and four sectored applicators were able to conform a thermal dose to predetermined target area in simulations. In order to evaluate the 3D control offered by multielement, multisectored transurethral applicators, a 2D R-Z model was used to evaluate the heating pattern and heating strategies of adding multiple transducers of varying size along the length of the applicator. In addition, this study shows the results of using a two transducer array to treat a large area along the length of the applicator by heating in two separate steps with translation of the assembly within the catheter in between the steps. These studies show the ability to control thermal lesion shape along the length of the applicators with multiple transducers or with translation of the transducer assembly. A 3D model was also developed to further the understanding of ultrasound tissue heating and could offer excellent insight in the future. The biothermal model simulations in this study outline some of the potential for conformal thermal lesion creation with temperature feedback controllers.

7.2 Introduction

Computer-aided mathematical modeling of complex systems is important for understanding situations and nuances that cannot be easily experimentally replicated. In the case of thermal therapy, a biothermal model that accounts for tissue changes and blood perfusion becomes increasingly complex and difficult to solve. Very intricate tissue and patient specific models may be necessary to create a model that is accurate enough for treatment planning.[112] In Chapter 2, a finite difference biothermal model based on the Pennes bioheat equation in cylindrical coordinates was created and modified to evaluate ultrasound heating devices. An important role of thermal therapy models is evaluating design parameters and treatment strategies. In this work, multisectored transurethral ultrasound applicators have been designed and developed in Chapter 5 and the model described in Chapter 2 has been a very important tool in evaluating their performance. The model can be modified for many different applicator design parameters including: applicator type, applicator diameter, applicator length, transducer diameter, transducer length, multisectored transducers, acoustic efficiency, transducer frequency, applied power, applied power control systems, applicator cooling flow, applicator cooling temperature, and applicator rotation. Tissue properties are also very important for evaluating applicator heating performance. Many tissue properties can be adjusted by the user including: type, density, specific heat, acoustic absorption and attenuation, perfusion, and thermal conductivity.
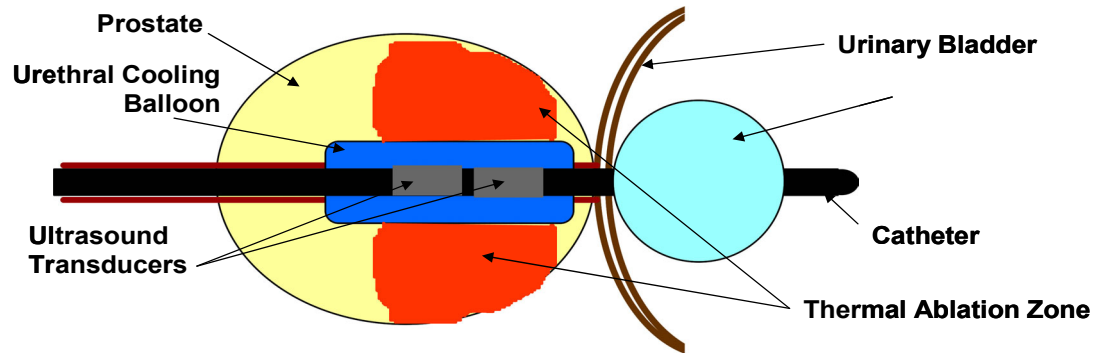
Figure 7.1: Experimental heating schema and setup in a canine prostate along the length of a transurethral ultrasound applicator
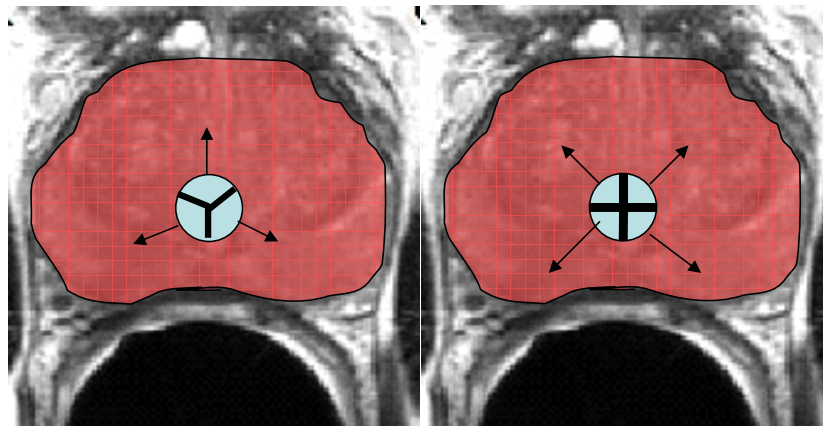
Figure 7.2: Experimental heating schema for three-sectored and four-sectored multisectored transurethral ultrasound applicators.

7.3 Simulations

7.3.1 Applicator Configuration

The multisectored ultrasound applicators were modeled as modified tubular ultrasound transducers as detailed in Chapter 2. The experimental applicator setup and heating schemes in the R-θ (Figure 7.1) and the R-Z (Figure 7.2) planes needed to be modeled accurately. The R-θ model was modified to incorporate the acoustic dead zone (ADZ) between sectors on a multisectored

transducer. The energy delivered (q) from the different sectors was independent in the model and programmed into the mesh as seen in Figure 7.3. In the R-Z model, the applicator was assumed to have symmetric power deposition for tubular transducers. As elements are added along the length of the model, they can be adjusted to be different sizes and have independent control of energy deposition (Q). The R-Z model setup for multielement tubular transurethral applicators is shown in Figure 7.4.

7.3.2 2D R-θ Model

Utilizing the bang-bang and pilot point control systems incorporated into the model, the heating pattern from a multisectored transurethral ultrasound applicator can be controlled to fit a target area. In the case of treating benign prostate hyperplasia (BPH), only the anterior/lateral lobes of the prostate are targeted. By placing pilot points at the edge of the outlined treatment boundary, the multisectored applicators have the ability to conform treatment to a target area because of their independent sector control. The pilot points turn off the applied power to their controlled sector when the tissue temperature reaches 52 ^{o}C at those points. When coupled with a bang-bang maximum temperature controller, the simulations show that these applicators can create contiguous and conformal thermal lesions. In Figure 7.5, a three-sectored transurethral ultrasound applicator was simulated for BPH treatment. A pilot point was placed on a predetermined target boundary for each active sector and the
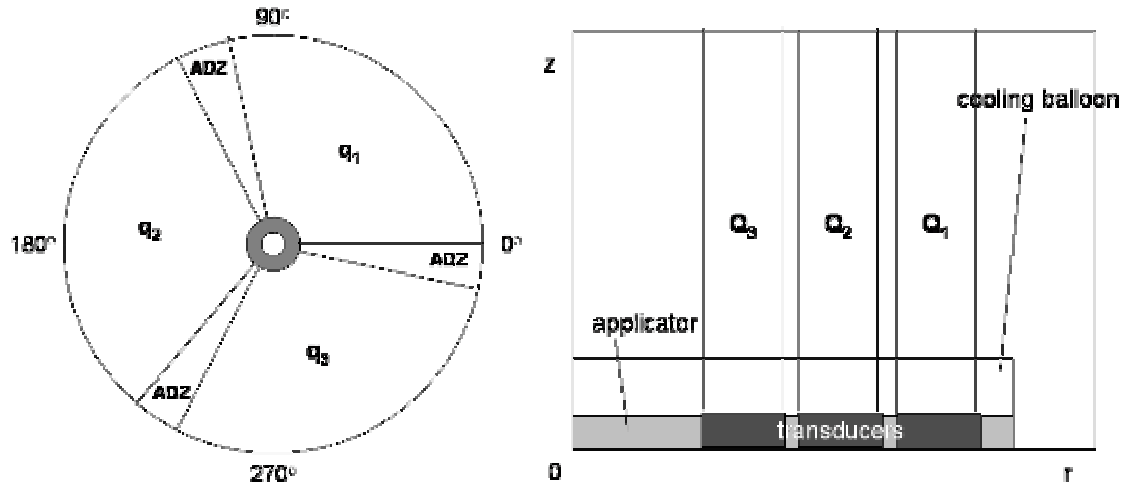
Figure 7.3: Biothermal modeling schema of the acoustic output from a three-sectored multisectored transurethral ultrasound applicator. q_1, q_2, and q_3 represent the heat generation terms from each individual sector on the transducer in the 2D R-θ model. The acoustic dead zone (ADZ) does not see any ultrasound energy during simulations.

Figure 7.4: 2D R-Z model schema of modeling tubular ultrasound transducers along the length of a heating applicator. Q_1, Q_2, and Q_3 represent the areas that receive heat generation from the individual transducers.

simulation shows conformal thermal treatment was achieved in less than 10 min.

Another important feature is that the model in this work was adjustable according to the number of sectors incorporated onto a tubular transducer and the angular size of the sectors. While the experiments in Chapters 5 and 6 were conducted with three-sectored applicators, the biothermal model allows for exploration of the heating patterns from two-, four-, and five-sectored transducers as well. This is an excellent example of the utility of a model to evaluate heating strategy and applicator design parameters. In Figure 7.6, a four-sectored (90º sectors, 70º active area) applicator simulated treatment is shown to treat a large area of the prostate. Each sector still had independent bang-bang
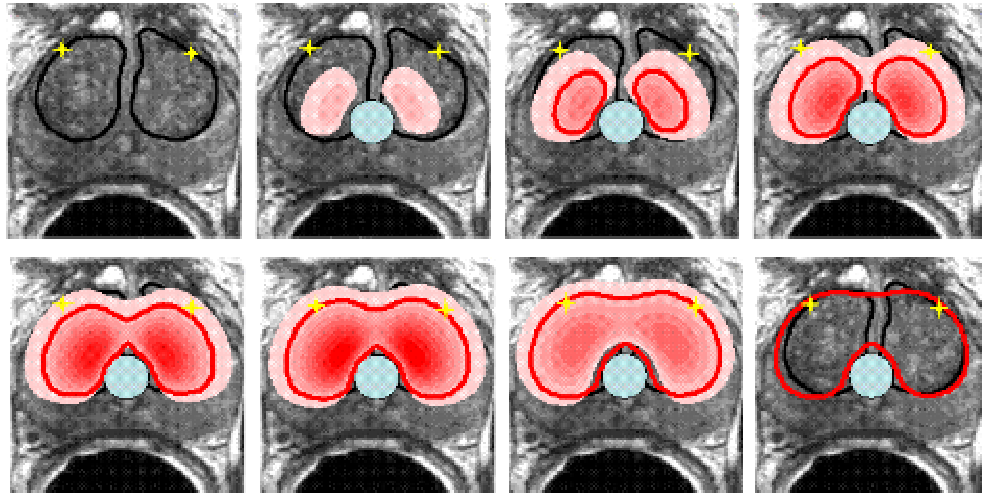
Figure 7.5: Conformal heating simulation with a three sectored transducer. The target was outlined before treatment simulation (black line) and pilot point control was implemented for each sector (stars). The maximum temperature was controlled with a bang-bang controller to 85 °C. Each image represents 60 s of heating time.
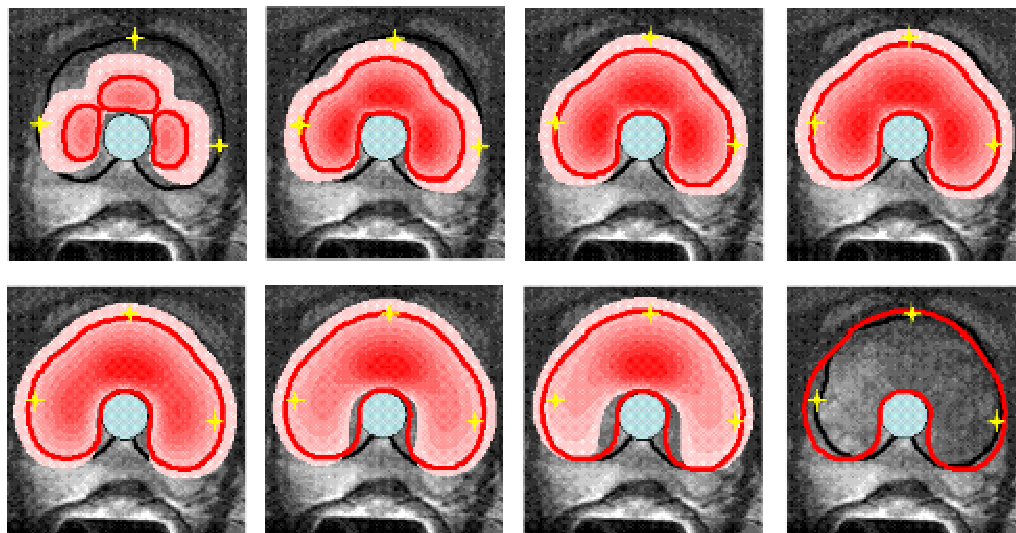
Figure 7.6: Conformal heating simulation with a four sectored transducer. The target was outlined before treatment simulation (black line) and pilot point control was implemented for each sector (stars). The maximum temperature was controlled with a bang-bang controller to 85 °C. Each image represents 60 s of heating time. The pilot point controller turned off the power to the lateral sectors, while the anterior sector continued heating to create a conformal lesion.
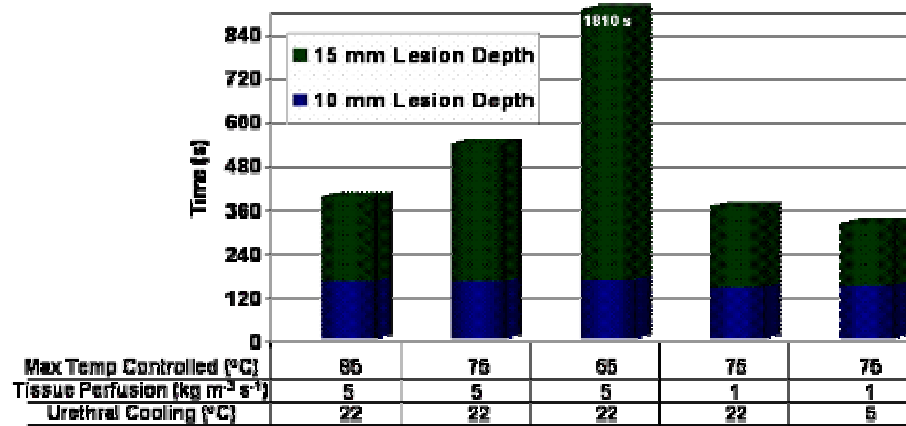
Figure 7.7: Heating pattern radial penetration depth and time from a multisectored transurethral ultrasound applicator with varying applicator and tissue parameters.

maximum temperature control as well as independent pilot points. In this case, the anterior sector needed the heat to reach farther into the tissue than the lateral two sectors. As seen in the time steps of the simulations in Figure 7.6, the power was turned off to the lateral sectors, while it continued to heat toward the anterior portion. This is an example of independent sector control for creating conformal thermal lesions.

The effects of perfusion and other tissue properties can change the shape and size of thermal lesions produced by multisectored ultrasound applicators. These applicators can account for tissue and heating pattern changes by adjusting treatment during heating. In Figure 7.7, the radial penetration of the heating pattern from tubular transurethral ultrasound applicators was simulated and quantified according to differences in maximum tissue temperature, tissue perfusion, and urethral balloon cooling temperature.

7.3.3 2D R-Z Model

The 2D R-Z model can be used to evaluate ultrasound heating along the length of the applicator. In this work, the model was programmed to be adjustable to user inputs of the number of transducers and transducer length. This is an important design consideration for controlling a thermal treatment in three dimensions. In Figure 7.8, the heating patterns from applicators with one (1 cm long,) two (1 cm long,) and four (6 mm long) transducers along the length of the applicator are examined. They show excellent radial penetration of the heating pattern and also display the effects of the tissue properties on the edges and shapes of the thermal lesion.

The applicators developed in this work and described in Chapter 5 have a unique hub that allows for translation of the transducer assembly within the catheter. Currently, most MR temperature monitoring image slices are 3-5 mm thick [Chopra, Rieke], which makes it difficult to understand and control multiple transducers along the length of the applicator when monitoring in the angular dimension. As more transducers are added, more and smaller imaging slices will be needed. This can tax the parameter limitations of non-invasive MR temperature monitoring. When using multisectored transducers and multiple transducers, the number of elements driven with independent applied power can become significant (>10). As the number of channels increases, RF noise in the MR suite increases and device construction and applicator control systems
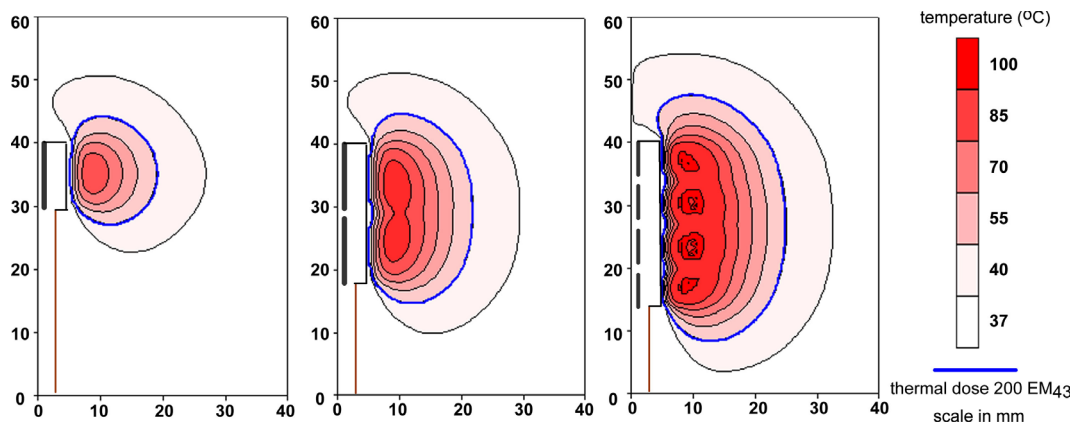
Figure 7.8: Simulated heating patterns along the length of a transurethral applicator. In the two images on the left, the applicator consists of 10 mm long transducers. The righthand image shows an applicator with four 6 mm long transducers.

Figure 7.9: Simulations with 6 mm long transducers along the length of a transurethral applicator. The results on the left represent the maximum temperature obtained from a two transducer array that heated in two separate steps and was translated between treatments. The right figure represents the heating pattern from a five transducer array heating simultaneously. The thick black line represents a thermal dose of t_{43} = 240 min.

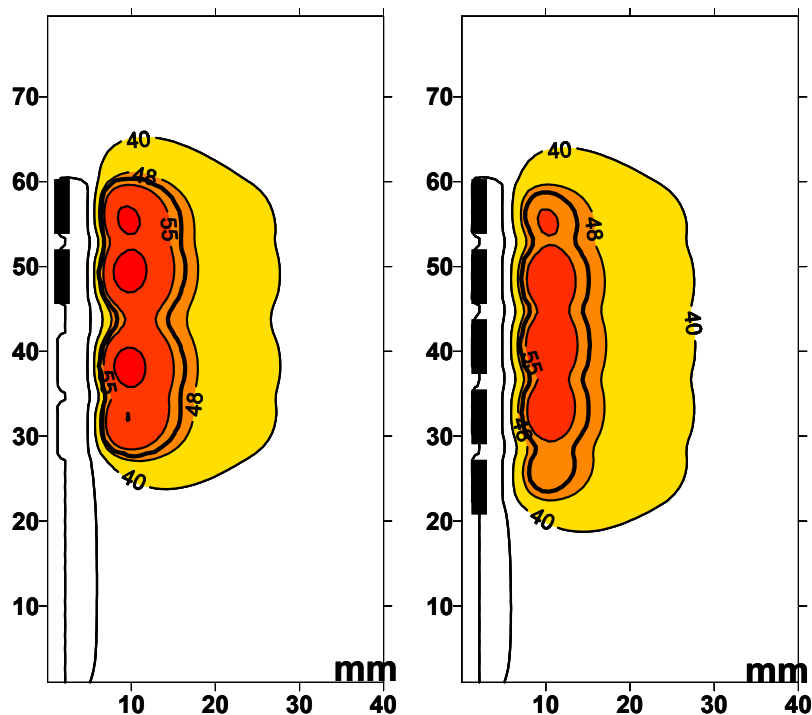become more complicated. By creating an applicator where the transducer assembly can translate without moving the catheter, multiple heat treatments could be done to heat the prostate along the length of a transurethral applicator. This strategy would simplify the applicator construction and MR temperature monitoring requirements. To evaluate this strategy, the R-Z model was used to simulate a two transducer array heating in one area, was subsequently translated, and then treated a second area. An alternative strategy would be to incorporate five transducers along the length of the applicator. The thermal dose patterns and maximum temperature maps from these two applicator configurations are shown in Figure 7.9. Both strategies appeared to offer similar heating patterns and are viable solutions for controlling thermal lesion formation along the length of a transurethral ultrasound applicator.

7.3.4 3D Model

A 3D biothermal model for ultrasound heating applicators was developed in this work. This model has the potential to accurately describe heating patterns from multisectored ultrasound applicators and possibly offer treatment planning simulations. Due to technical limitations of the finite difference method as outlined in Chapter 2, the 3D model was utilized in this work on a limited basis. However, as the technical limitations are overcome, the model created and developed in this work can serve as the basis for future simulation studies. Examples of the amount of information that can be obtained from the 3D model
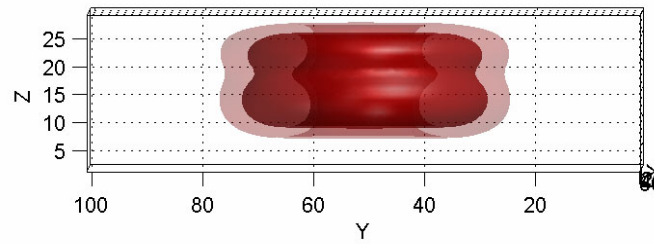
Figure 7.10: Surface plot representation of 3D biothermal simulation of an interstitial ultrasound applicator (6 mm OD) with two tubular transducers.
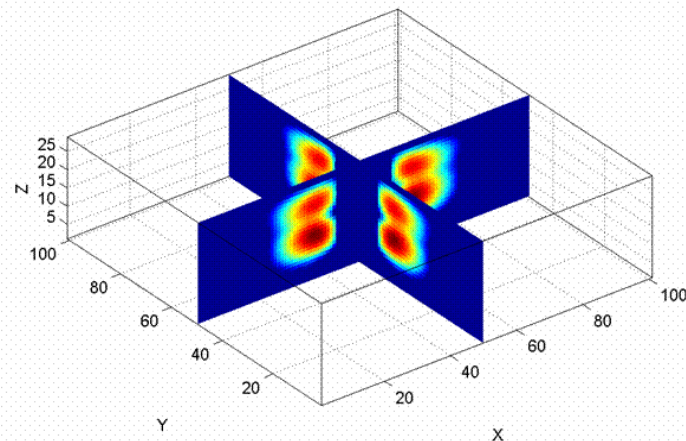
Figure 7.11: 3D slice representation of the simulation shown in Figure 7.10. The figure was created in MATLAB and any slices throughout the volume could be chosen.

are shown in Figures 7.10 and 7.11. In these experiments, a tubular interstitial ultrasound applicator (6 mm OD) heated generalized tissue. Using MATLAB to visualize the simulation results renders a surface area plot as well as slices through any part of the heated volume.

7.4 Conclusions

Multisectored transurethral ultrasound applicators offer incredible flexibility of control over heating deposition for thermal therapy. The biothermal model developed and modified in this work is a powerful tool for identifying and exploring this flexibility and new heating strategies. The simulations throughout this work all display excellent correlation to experimental studies and give quantitative insight into the heating penetration of thermal lesions. In addition, the controllers incorporated into the model display the potential of using non-invasive MR temperature monitoring for applicator feedback control. The model also explores heating strategies that take advantage of the MR compatibility of the applicators and offers practical solutions.

Chapter 8

Conclusions

8.1 Research Summary

Multisectored tubular ultrasound transducers provide an accurate technique of shaping a thermal lesion in three dimensions without requiring movement of the device during treatment. These transducers can be incorporated into different types of delivery devices, including interstitial and transurethral heating applicators. Multisectored ultrasound applicators were designed in this work for use with MR temperature monitoring. Due to some of the technical limitations and specifications of MR temperature imaging, these devices were developed to be stationary during treatment, provide excellent control over the shape of a heating pattern with MR temperature feedback, and offer simple MR

guided treatment setup.

In order to evaluate the utility of multisectored ultrasound applicators, a finite difference biothermal model based on the Pennes bioheat equation in cylindrical coordinates was modified as detailed in Chapter 2 of this work. The model accounts for changes in attenuation and perfusion with changes in thermal dose. In this work, bang-bang, pilot point, and manual control systems were developed and programmed into both 2D R-θ and R-Z models. The models were also developed to incorporate multisectored tubular ultrasound transducers with independent power control. The multisectored transducers could be programmed with a variable number of sectors and different sector sizes. The 3D model developed in this work offers the first steps of creating an accurate simluation tool for evaluating ultrasound heating applicators and heat treatment planning.

Interstitial ultrasound applicators offer accurate heat delivery directly to a target tissue. Unlike HIFU applicators, interstitial ultrasound applicators have the advantage of being inserted directly in the target site, which eliminates concerns about ultrasound properties as the energy travels through tissue interfaces. In addition, interstitial applicators can heat a large volume in a single treatment in a much shorter time than HIFU devices. In most cases, the applicator setup, design, and power driving systems are simpler for interstitial devices. The advantages of HIFU devices are non-invasive treatment options and very accurate control over the size and shape of heating patterns. In Chapter 3,

new interstitial ultrasound device designs were thoroughly evaluated with biothermal simulations, *ex vivo* heating experiments, and *in vivo* experiments conducted under MR temperature monitoring. The multisectored ultrasound transducers provided a novel heating strategy, where a heating pattern could be shaped during a single heat treatment without mechanically manipulating the interstitial device during treatment. In Chapter 3, internally-cooled and catheter-cooled interstitial applicator designs with multisectored ultrasound transducers with individual sector power control demonstrated excellent conformity of heating pattern deposition. These new device designs and treatment strategies were compared with a novel rotating interstitial ultrasound applicator in Chapter 4. These devices improve thermal therapy by offering shorter treatment times, accurate heat deposition, and an adaptable strategy for heating with MR temperature monitoring.

In Part II of this work, the strategies incorporated into interstitial heating devices were translated into transurethral prostate thermal therapy applicators. A new transurethral catheter featuring concentric water flow cooling was designed in this work. The device was constructed to be flexible and MR compatible for use with MR temperature monitoring. Also, a unique hub was developed that allowed rotation and translation of the ultrasound transducer for accurate setup and placement. Following other transurethral ultrasound device designs and utilizing MR temperature monitoring for feedback control of prostate heating, the devices created in this work were specifically designed and

developed for use with MR temperature monitoring. Other transurethral ultrasound applicators have been designed to rotate during treatment to deliver conformal therapy. This can cause issues with MR temperature monitoring because of the PRF method's sensitivity to motion in the images and the extension of treatment times. Multisectored transurethral ultrasound applicators allow for similar angular control over heating patterns as rotating devices, decrease treatment times, and are stationary during treatment. Finally, the capability of these applicators in combination with prostate thermal treatment strategies was explored with biothermal model simulations. The control systems incorporated in the model demonstrated the potential for using real-time MR temperature feedback to control individual sectors on the multisectored applicators.

The work presented in this dissertation includes the design and development of new interstitial and transurethral heating devices, thorough characterization of applicator capabilities, novel thermal treatment strategies, preclinical animal studies, and development of MR temperature monitoring feedback systems coupled with ultrasound heating devices.

8.2 Future Directions

Future directions of the studies and devices presented in this work include moving the experiments from preclinical studies to first stage clinical

treatment strategies. Catheter and device designs need to be finalized for robustness and mass production for the clinical studies. MR temperature monitoring systems need to be further evaluated for their accuracy. Temperature feedback control systems can be developed to provide additional treatment accuracy, improving the safety and practicality of heat treatments. This work establishes a new heating device design and strategy for advancing the clinical acceptance of thermal therapy under MR guidance.

Bibliography

[1]   D. M. Agnese and W. E. Burak, Jr. Ablative approaches to the minimally invasive treatment of breast cancer. *Cancer J*, 11(1): 77-82, 2005.

[2]   M. Ahmed and S. N. Goldberg. Thermal ablation therapy for hepatocellular carcinoma. *J Vasc Interv Radiol*, 13(9 Pt 2): S231-244, 2002.

[3]   O. Algan, H. Fosmire, K. Hynynen, B. Dalkin, H. Cui, G. Drach, B. Stea and J. R. Cassady. External beam radiotherapy and hyperthermia in the treatment of patients with locally advanced prostate carcinoma. *Cancer*, 89(2): 399-403, 2000.

[4]   G. Alivizatos, N. Ferakis, D. Mitropoulos, A. Skolarikos, K. Livadas and I. Kastriotis. Feedback microwave thermotherapy with the prostalund compact device for obstructive benign prostatic hyperplasia: 12-month response rates and complications. *J Endourol*, 19(1): 72-78, 2005.

[5]   Y. Anzai, R. Lufkin, A. DeSalles, D. R. Hamilton, K. Farahani and K. L. Black. Preliminary experience with mr-guided thermal ablation of brain tumors. *AJNR Am J Neuroradiol*, 16(1): 39-48; discussion 49-52, 1995.

[6]   G. Aus. Current status of hifu and cryotherapy in prostate cancer--a review. *Eur Urol*, 50(5): 927-934; discussion 934, 2006.

[7]   A. Blana, B. Walter, S. Rogenhofer and W. F. Wieland. High-intensity focused ultrasound for the treatment of localized prostate cancer: 5-year experience. *Urology*, 63(2): 297-300, 2004.

[8]   B. A. Bornstein, P. S. Zouranjian, J. L. Hansen, S. M. Fraser, L. A. Gelwan, B. A. Teicher and G. K. Svensson. Local hyperthermia, radiation therapy, and chemotherapy in patients with local-regional recurrence of breast carcinoma. *Int J Radiat Oncol Biol Phys*, 25(1): 79-85, 1993.

[9]   Y. Y. Botros, J. L. Volakis, P. VanBaren and E. S. Ebbini. A hybrid computational model for ultrasound phased-array heating in presence of strongly scattering obstacles. *IEEE Trans Biomed Eng*, 44(11): 1039-1050, 1997.

[10]   S. L. Brown, J. W. Hunt and R. P. Hill. Differential thermal sensitivity of tumour and normal tissue microvascular response during hyperthermia. *Int J Hyperthermia*, 8(4): 501-514, 1992.

[11]   R. Bruskewitz, M. M. Issa, C. G. Roehrborn, M. J. Naslund, R. Perez-Marrero, B. P. Shumaker and J. E. Oesterling. A prospective, randomized 1-year clinical trial comparing transurethral needle ablation to transurethral resection of the prostate for the treatment of symptomatic benign prostatic hyperplasia. *J Urol*, 159(5): 1588-1593; discussion 1593-1584, 1998.

[12]   C. Chaussy, S. Thuroff, X. Rebillard and A. Gelet. Technology insight: High-intensity focused ultrasound for urologic cancers. *Nat Clin Pract Urol*, 2(4): 191-198, 2005.

[13]   J. C. Chen, J. A. Moriarty, J. A. Derbyshire, R. D. Peters, J. Trachtenberg, S. D. Bell, J. Doyle, R. Arrelano, G. A. Wright, R. M. Henkelman, R. S. Hinks, S. Y. Lok, A. Toi and W. Kucharczyk. Prostate cancer: Mr imaging and thermometry during microwave thermal ablation-initial experience. *Radiology*, 214(1): 290-297, 2000.

[14]   L. Chen, D. M. Bouley, B. T. Harris and K. Butts. Mri study of immediate cell viability in focused ultrasound lesions in the rabbit brain. *J Magn Reson Imaging*, 13(1): 23-30, 2001.

[15]   R. Chopra, M. J. Bronskill and F. S. Foster. Feasibility of linear arrays for interstitial ultrasound thermal therapy. *Med Phys*, 27(6): 1281-1286, 2000.

[16]   R. Chopra, M. Burtnyk, M. A. Haider and M. J. Bronskill. Method for mri-guided conformal thermal therapy of prostate with planar transurethral ultrasound heating applicators. *Phys Med Biol*, 50(21): 4957-4975, 2005.

[17]   R. Chopra, C. Luginbuhl, F. S. Foster and M. J. Bronskill. Multifrequency ultrasound transducers for conformal interstitial thermal therapy. *IEEE Trans Ultrason Ferroelectr Freq Control*, 50(7): 881-889, 2003.

[18]   R. Chopra, C. Luginbuhl, A. J. Weymouth, F. S. Foster and M. J. Bronskill. Interstitial ultrasound heating applicator for mr-guided thermal therapy. *Phys Med Biol*, 46(12): 3133-3145, 2001.

[19]   R. Chopra, J. Wachsmuth, M. Burtnyk, M. A. Haider and M. J. Bronskill. Analysis of factors important for transurethral ultrasound prostate heating using mr temperature feedback. *Phys Med Biol*, 51(4): 827-844, 2006.

[20]   J. Crezee, R. S. Kaatee, J. F. van der Koijk and J. J. Lagendijk. Spatial steering with quadruple electrodes in 27 mhz capacitively coupled interstitial hyperthermia. *Int J Hyperthermia*, 15(2): 145-156, 1999.

[21]   C. Damianou and K. Hynynen. The effect of various physical parameters on the size and shape of necrosed tissue volume during ultrasound surgery. *J Acoust Soc Am*, 95(3): 1641-1649, 1994.

[22]   C. A. Damianou, N. T. Sanghvi, F. J. Fry and R. Maass-Moreno. Dependence of ultrasonic attenuation and absorption in dog soft tissues on temperature and thermal dose. *J Acoust Soc Am*, 102(1): 628-634, 1997.

[23]   D. R. Daum and K. Hynynen. Theoretical design of a spherically sectioned phased array for ultrasound surgery of the liver. *Eur J Ultrasound*, 9(1): 61-69, 1999.

[24]   J. J. De La Rosette, D. L. Floratos, J. L. Severens, L. A. Kiemeney, F. M. Debruyne and M. Pilar Laguna. Transurethral resection vs microwave thermotherapy of the prostate: A cost-consequences analysis. *BJU Int*, 92(7): 713-718, 2003.

[25]   J. J. de la Rosette, M. P. Laguna, S. Gravas and M. J. de Wildt. Transurethral microwave thermotherapy: The gold standard for

minimally invasive therapies for patients with benign prostatic hyperplasia? *J Endourol*, 17(4): 245-251, 2003.

[26] D. L. Deardorff and C. J. Diederich. Angular directivity of thermal coagulation using air-cooled direct-coupled interstitial ultrasound applicators. *Ultrasound Med Biol*, 25(4): 609-622, 1999.

[27] D. L. Deardorff and C. J. Diederich. Ultrasound applicators with internal water-cooling for high-powered interstitial thermal therapy. *IEEE Trans Biomed Eng*, 47(10): 1356-1365, 2000.

[28] J. Delannoy, C. N. Chen, R. Turner, R. L. Levin and D. Le Bihan. Noninvasive temperature imaging using diffusion mri. *Magn Reson Med*, 19(2): 333-339, 1991.

[29] B. Denis de Senneville, B. Quesson and C. T. Moonen. Magnetic resonance temperature imaging. *Int J Hyperthermia*, 21(6): 515-531, 2005.

[30] W. C. Dewey. Arrhenius relationships from the molecule and cell to the clinic. *Int J Hyperthermia*, 10(4): 457-483, 1994.

[31] M. W. Dewhirst. Future directions in hyperthermia biology. *Int J Hyperthermia*, 10(3): 339-345, 1994.

[32] M. W. Dewhirst, B. L. Viglianti, M. Lora-Michiels, M. Hanson and P. J. Hoopes. Basic principles of thermal dosimetry and thermal thresholds for tissue damage from hyperthermia. *Int J Hyperthermia*, 19(3): 267-294, 2003.

[33] C. J. Diederich. Interstitial ultrasound applicators are practical from an engineering perspective for treating large tumours. *Int J Hyperthermia*, 12(2): 305-306, 1996.

[34] C. J. Diederich. Ultrasound applicators with integrated catheter-cooling for interstitial hyperthermia: Theory and preliminary experiments. *Int J Hyperthermia*, 12(2): 279-297; discussion 299-300, 1996.

[35] C. J. Diederich and E. C. Burdette. Transurethral ultrasound array for prostate thermal therapy: Initial studies. *Ieee Transactions on Ultrasonics Ferroelectrics and Frequency Control*, 43(6): 1011-1022, 1996.

[36] C. J. Diederich and E. C. Burdette. Transurethral ultrasound array for prostate thermal therapy: Initial studies. *IEEE Transactions on Ultrasonics Ferroelectrics & Frequency Control*, 43(6): 1011-1022, 1996.

[37] C. J. Diederich and K. Hynynen. Ultrasound technology for hyperthermia. *Ultrasound Med Biol*, 25(6): 871-887, 1999.

[38] C. J. Diederich, W. H. Nau, A. B. Ross, P. D. Tyreus, K. Butts, V. Rieke and G. Sommer. Catheter-based ultrasound applicators for selective thermal ablation: Progress towards mri-guided applications in prostate. *Int J Hyperthermia*, 20(7): 739-756, 2004.

[39] C. J. Diederich, R. J. Stafford, W. H. Nau, E. C. Burdette, R. E. Price and J. D. Hazle. Transurethral ultrasound applicators with directional heating patterns for prostate thermal therapy: In vivo evaluation using magnetic resonance thermometry. *Med Phys*, 31(2): 405-413, 2004.

[40]   G. D'Ippolito and S. N. Goldberg. Radiofrequency ablation of hepatic
       tumors. *Tech Vasc Interv Radiol*, 5(3): 141-155, 2002.

[41]   E. S. Ebbini and C. A. Cain. Optimization of the intensity gain of multiple-
       focus phased-array heating patterns. *Int J Hyperthermia*, 7(6): 953-973, 1991.

[42]   X. Fan and K. Hynynen. Control of the necrosed tissue volume during
       noninvasive ultrasound surgery using a 16-element phased array. *Med
       Phys*, 22(3): 297-306, 1995.

[43]   V. Ficarra, S. Z. Antoniolli, G. Novara, A. Parisi, S. Fracalanza, G.
       Martignoni and W. Artibani. Short-term outcome after high-intensity
       focused ultrasound in the treatment of patients with high-risk prostate
       cancer. *BJU Int*, 98(6): 1193-1198, 2006.

[44]   S. W. Flanagan, P. L. Moseley and G. R. Buettner. Increased flux of free
       radicals in cells subjected to hyperthermia: Detection by electron
       paramagnetic resonance spin trapping. *FEBS Lett*, 431(2): 285-286, 1998.

[45]   H. Fosmire, K. Hynynen, G. W. Drach, B. Stea, P. Swift and J. R. Cassady.
       Feasibility and toxicity of transrectal ultrasound hyperthermia in the
       treatment of locally advanced adenocarcinoma of the prostate. *Int J Radiat
       Oncol Biol Phys*, 26(2): 253-259, 1993.

[46]   W. M. Gedroyc. Magnetic resonance guidance of thermal ablation. *Top
       Magn Reson Imaging*, 16(5): 339-353, 2005.

[47]   A. Gelet, J. Y. Chapelon, R. Bouvier, O. Rouviere, D. Lyonnet and J. M.
       Dubernard. Transrectal high intensity focused ultrasound for the

treatment of localized prostate cancer: Factors influencing the outcome. *Eur Urol*, 40(2): 124-129, 2001.

[48]   D. J. Goldberg. Lasers for facial rejuvenation. *Am J Clin Dermatol*, 4(4): 225-234, 2003.

[49]   J. D. Hazle, C. J. Diederich, M. Kangasniemi, R. E. Price, L. E. Olsson and R. J. Stafford. Mri-guided thermal therapy of transplanted tumors in the canine prostate using a directional transurethral ultrasound applicator. *J Magn Reson Imaging*, 15(4): 409-417, 2002.

[50]   T. R. Herrmann, A. J. Gross, D. Schultheiss, P. M. Kaufmann, U. Jonas and M. Burchardt. Transurethral microwave thermotherapy for the treatment of bph: Still a challenger? *World J Urol*, 24(4): 389-396, 2006.

[51]   A. Hines-Peralta and S. N. Goldberg. Review of radiofrequency ablation for renal cell carcinoma. *Clin Cancer Res*, 10(18 Pt 2): 6328S-6334S, 2004.

[52]   M. D. Hurwitz, I. D. Kaplan, J. L. Hansen, S. Prokopios-Davos, G. P. Topulos, K. Wishnow, J. Manola, B. A. Bornstein and K. Hynynen. Hyperthermia combined with radiation in treatment of locally advanced prostate cancer is associated with a favourable toxicity profile. *Int J Hyperthermia*, 21(7): 649-656, 2005.

[53]   M. D. Hurwitz, I. D. Kaplan, G. K. Svensson, K. Hynynen and M. S. Hansen. Feasibility and patient tolerance of a novel transrectal ultrasound hyperthermia system for treatment of prostate cancer. *Int J Hyperthermia*, 17(1): 31-37, 2001.

[54]   K. Hynynen. Acoustic power calibrations of cylindrical intracavitary ultrasound hyperthermia applicators. *Med Phys*, 20(1): 129-134, 1993.

[55]   K. Hynynen, D. DeYoung, M. Kundrat and E. Moros. The effect of blood perfusion rate on the temperature distributions induced by multiple, scanned and focused ultrasonic beams in dogs' kidneys in vivo. *Int J Hyperthermia*, 5(4): 485-497, 1989.

[56]   R. O. Illing, T. A. Leslie, J. E. Kennedy, J. G. Calleary, C. W. Ogden and M. Emberton. Visually directed high-intensity focused ultrasound for organ-confined prostate cancer: A proposed standard for the conduct of therapy. *BJU Int*, 98(6): 1187-1192, 2006.

[57]   R. D. Issels, M. Schlemmer and L. H. Lindner. The role of hyperthermia in combined treatment in the management of soft tissue sarcoma. *Curr Oncol Rep*, 8(4): 305-309, 2006.

[58]   M. Kangasniemi, C. J. Diederich, R. E. Price, R. J. Stafford, D. F. Schomer, L. E. Olsson, P. D. Tyreus, W. H. Nau and J. D. Hazle. Multiplanar mr temperature-sensitive imaging of cerebral thermal treatment using interstitial ultrasound applicators in a canine model. *J Magn Reson Imaging*, 16(5): 522-531, 2002.

[59]   D. S. Kellner, N. A. Armenakas, M. Brodherson, J. Heyman and J. A. Fracchia. Efficacy of high-energy transurethral microwave thermotherapy in alleviating medically refractory urinary retention due to benign prostatic hyperplasia. *Urology*, 64(4): 703-706, 2004.

[60]   A. M. Kinsey, C. J. Diederich, V. Rieke, W. H. Nau, K. Butts Pauly, D. M. Bouley and G. Sommer. Transurethral ultrasound applicators for dynamic 3d control of prostate thermal therapy under mr guidance. *Med Phys*, In review, 2007.

[61]   A. M. Kinsey, C. J. Diederich, P. D. Tyreus, W. H. Nau, V. Rieke and K. B. Pauly. Multisectored interstitial ultrasound applicators for dynamic angular control of thermal therapy. *Med Phys*, 33(5): 1352-1363, 2006.

[62]   M. C. Kolios, M. D. Sherar and J. W. Hunt. Blood flow cooling and ultrasonic lesion formation. *Med Phys*, 23(7): 1287-1298, 1996.

[63]   M. C. Kolios, A. E. Worthington, D. W. Holdsworth, M. D. Sherar and J. W. Hunt. An investigation of the flow dependence of temperature gradients near large vessels during steady state and transient tissue heating. *Phys Med Biol*, 44(6): 1479-1497, 1999.

[64]   C. Lafon, F. Chavrier, F. Prat, J. Y. Chapelon and D. Cathignol. Theoretical comparison of two interstitial ultrasound applicators designed to induce cylindrical zones of tissue ablation. *Med Biol Eng Comput*, 37(3): 298-303, 1999.

[65]   C. Lafon, S. Chosson, F. Prat, Y. Theillere, J. Y. Chapelon, A. Birer and D. Cathignol. The feasibility of constructing a cylindrical array with a plane rotating beam for interstitial thermal surgery. *Ultrasonics*, 37(9): 615-621, 2000.

[66]   C. Lafon, L. de, Y. Theillere, F. Prat, J. Y. Chapelon and D. Cathignol. Optimizing the shape of ultrasound transducers for interstitial thermal ablation. *Med Phys*, 29(3): 290-297, 2002.

[67]   C. Lafon, L. Koszek, S. Chesnais, Y. Theillere and D. Cathignol. Feasibility of a transurethral ultrasound applicator for coagulation in prostate. *Ultrasound Med Biol*, 30(1): 113-122, 2004.

[68]   C. Lafon, Y. Theillere, F. Prat, A. Arefiev, J. Y. Chapelon and D. Cathignol. Development of an interstitial ultrasound applicator for endoscopic procedures: Animal experimentation. *Ultrasound Med Biol*, 26(4): 669-675, 2000.

[69]   B. Larson, C. Huidobro, C. Acevedo, D. Busel, L. Mynderses, J. Collins and T. Larson. In vivo temperature mapping of prostate during treatment with thermatrx tmx-2000 device: Heat field and mri determinations of necrotic lesions. *J Endourol*, 19(8): 1021-1025, 2005.

[70]   B. T. Larson, D. G. Bostwick, A. G. Corica and T. R. Larson. Histological changes of minimally invasive procedures for the treatment of benign prostatic hyperplasia and prostate cancer: Clinical implications. *J Urol*, 170(1): 12-19, 2003.

[71]   T. R. Larson. Rationale and assessment of minimally invasive approaches to benign prostatic hyperplasia therapy. *Urology*, 59(2 Suppl 1): 12-16, 2002.

[72] R. J. Lee, M. Buchanan, L. J. Kleine and K. Hynynen. Arrays of multielement ultrasound applicators for interstitial hyperthermia. *IEEE Trans Biomed Eng*, 46(7): 880-890, 1999.

[73] P. P. Lele. Advanced ultrasonic techniques for local tumor hyperthermia. *Radiol Clin North Am*, 27(3): 559-575, 1989.

[74] M. A. Leonardi and C. B. Lumenta. Stereotactic guided laser-induced interstitial thermotherapy (slitt) in gliomas with intraoperative morphologic monitoring in an open mr: Clinical expierence. *Minim Invasive Neurosurg*, 45(4): 201-207, 2002.

[75] W. L. Lin, R. B. Roemer and K. Hynynen. Theoretical and experimental evaluation of a temperature controller for scanned focused ultrasound hyperthermia. *Med Phys*, 17(4): 615-625, 1990.

[76] H. L. Liu, Y. Y. Chen, J. Y. Yen and W. L. Lin. Pilot point temperature regulation for thermal lesion control during ultrasound thermal therapy. *Med Biol Eng Comput*, 42(2): 178-188, 2004.

[77] N. McDannold and K. Hynynen. Quality assurance and system stability of a clinical mri-guided focused ultrasound system: Four-year experience. *Med Phys*, 33(11): 4307-4313, 2006.

[78] N. McDannold, R. L. King and K. Hynynen. Mri monitoring of heating produced by ultrasound absorption in the skull: In vivo study in pigs. *Magn Reson Med*, 51(5): 1061-1065, 2004.

[79]   D. Melodelima, C. Lafon, F. Prat, A. Birer and D. Cathignol. Ultrasound cylindrical phased array for transoesophageal thermal therapy: Initial studies. *Phys Med Biol*, 47(23): 4191-4203, 2002.

[80]   D. Melodelima, F. Prat, A. Birer, Y. Theillere and D. Cathignol. Comparison of two methods of treatment for intraluminal thermal ablation using an ultrasound cylindrical phased array. *Ultrasonics*, 42(1-9): 937-942, 2004.

[81]   W. H. Nau, C. J. Diederich and E. C. Burdette. Evaluation of multielement catheter-cooled interstitial ultrasound applicators for high-temperature thermal therapy. *Med Phys*, 28(7): 1525-1534, 2001.

[82]   W. H. Nau, C. J. Diederich, A. B. Ross, K. Butts, V. Rieke, D. M. Bouley, H. Gill, B. Daniel and G. Sommer. Mri-guided interstitial ultrasound thermal therapy of the prostate: A feasibility study in the canine model. *Med Phys*, 32(3): 733-743, 2005.

[83]   W. H. Nau, C. J. Diederich and P. R. Stauffer. Directional power deposition from direct-coupled and catheter-cooled interstitial ultrasound applicators. *Int J Hyperthermia*, 16(2): 129-144, 2000.

[84]   J. Overgaard. The current and potential role of hyperthermia in radiotherapy. *Int J Radiat Oncol Biol Phys*, 16(3): 535-549, 1989.

[85]   J. Overgaard, D. Gonzalez Gonzalez, M. C. Hulshof, G. Arcangeli, O. Dahl, O. Mella and S. M. Bentzen. Randomised trial of hyperthermia as adjuvant to radiotherapy for recurrent or metastatic malignant melanoma.

European society for hyperthermic oncology. *Lancet*, 345(8949): 540-543, 1995.

[86]   J. Overgaard and M. Overgaard. Hyperthermia as an adjuvant to radiotherapy in the treatment of malignant melanoma. *Int J Hyperthermia*, 3(6): 483-501, 1987.

[87]   D. L. Parker, V. Smith, P. Sheldon, L. E. Crooks and L. Fussell. Temperature distribution measurements in two-dimensional nmr imaging. *Med Phys*, 10(3): 321-325, 1983.

[88]   H. H. Pennes. Analysis of tissue and arterial blood temperatures in the resting human forearm. 1948. *J Appl Physiol*, 85(1): 5-34, 1998.

[89]   R. D. Peters, E. Chan, J. Trachtenberg, S. Jothy, L. Kapusta, W. Kucharczyk and R. M. Henkelman. Magnetic resonance thermometry for predicting thermal damage: An application of interstitial laser coagulation in an in vivo canine prostate model. *Magn Reson Med*, 44(6): 873-883, 2000.

[90]   R. D. Peters, R. S. Hinks and R. M. Henkelman. Ex vivo tissue-type independence in proton-resonance frequency shift mr thermometry. *Magn Reson Med*, 40(3): 454-459, 1998.

[91]   L. J. Pisani, A. B. Ross, C. J. Diederich, W. H. Nau, F. G. Sommer, G. H. Glover and K. Butts. Effects of spatial and temporal resolution for mr image-guided thermal ablation of prostate with transurethral ultrasound. *J Magn Reson Imaging*, 22(1): 109-118, 2005.

[92]   W. H. Press. *Numerical recipies in c: The art of scientific computing.* Cambridge University Press, Cambridge, 1997.

[93]   B. Quesson, J. A. de Zwart and C. T. Moonen. Magnetic resonance temperature imaging for guidance of thermotherapy. *J Magn Reson Imaging*, 12(4): 525-533, 2000.

[94]   V. Rieke, K. K. Vigen, G. Sommer, B. L. Daniel, J. M. Pauly and K. Butts. Referenceless prf shift thermometry. *Magn Reson Med*, 51(6): 1223-1231, 2004.

[95]   D. I. Rosenthal, F. J. Hornicek, M. Torriani, M. C. Gebhardt and H. J. Mankin. Osteoid osteoma: Percutaneous treatment with radiofrequency energy. *Radiology*, 229(1): 171-175, 2003.

[96]   A. B. Ross, C. J. Diederich, W. H. Nau, H. Gill, D. M. Bouley, B. Daniel, V. Rieke, R. K. Butts and G. Sommer. Highly directional transurethral ultrasound applicators with rotational control for mri-guided prostatic thermal therapy. *Phys Med Biol*, 49(2): 189-204, 2004.

[97]   A. B. Ross, C. J. Diederich, W. H. Nau, V. Rieke, R. K. Butts, G. Sommer, H. Gill and D. M. Bouley. Curvilinear transurethral ultrasound applicator for selective prostate thermal therapy. *Med Phys*, 32(6): 1555-1565, 2005.

[98]   J. A. Saal and J. S. Saal. Intradiscal electrothermal treatment for chronic discogenic low back pain: Prospective outcome study with a minimum 2-year follow-up. *Spine*, 27(9): 966-973; discussion 973-964, 2002.

[99] S. A. Sapareto and W. C. Dewey. Thermal dose determination in cancer therapy. *Int J Radiat Oncol Biol Phys*, 10(6): 787-800, 1984.

[100] M. H. Seegenschmidt, P. Fessenden and C. C. Vernon. *Principles and practices of thermoradiotherapy and thermochemotherapy*. Springer-Verlag, Berlin, 1995.

[101] M. Sherar, F. F. Liu, M. Pintilie, W. Levin, J. Hunt, R. Hill, J. Hand, C. Vernon, G. van Rhoon, J. van der Zee, D. G. Gonzalez, J. van Dijk, J. Whaley and D. Machin. Relationship between thermal dose and outcome in thermoradiotherapy treatments for superficial recurrences of breast cancer: Data from a phase iii trial. *Int J Radiat Oncol Biol Phys*, 39(2): 371-380, 1997.

[102] M. D. Sherar, J. Trachtenberg, S. R. Davidson, C. McCann, C. K. Yue, M. A. Haider and M. R. Gertner. Interstitial microwave thermal therapy for prostate cancer. *J Endourol*, 17(8): 617-625, 2003.

[103] P. K. Sneed and T. L. Phillips. Combining hyperthermia and radiation: How beneficial? *Oncology (Williston Park)*, 5(3): 99-108; discussion 109-110, 112, 1991.

[104] P. K. Sneed, P. R. Stauffer, M. W. McDermott, C. J. Diederich, K. R. Lamborn, M. D. Prados, S. Chang, K. A. Weaver, L. Spry, M. K. Malec, S. A. Lamb, B. Voss, R. L. Davis, W. M. Wara, D. A. Larson, T. L. Phillips and P. H. Gutin. Survival benefit of hyperthermia in a prospective randomized

trial of brachytherapy boost +/- hyperthermia for glioblastoma multiforme. *Int J Radiat Oncol Biol Phys*, 40(2): 287-295, 1998.

[105] S. B. Solomon. Thermal ablation: A potential solution for managing the small renal tumor. *Nat Clin Pract Urol*, 2(1): 2-3, 2005.

[106] E. A. Stewart, J. Rabinovici, C. M. Tempany, Y. Inbar, L. Regan, B. Gostout, G. Hesley, H. S. Kim, S. Hengst and W. M. Gedroyc. Clinical outcomes of focused ultrasound surgery for the treatment of uterine fibroids. *Fertil Steril*, 85(1): 22-29, 2006.

[107] T. Straube and T. Kahn. Thermal therapies in interventional mr imaging. Laser. *Neuroimaging Clin N Am*, 11(4): 749-757, 2001.

[108] P. D. Tyreus and C. J. Diederich. Theoretical model of internally cooled interstitial ultrasound applicators for thermal therapy. *Phys Med Biol*, 47(7): 1073-1089, 2002.

[109] P. D. Tyreus, W. H. Nau and C. J. Diederich. Effect of applicator diameter on lesion size from high temperature interstitial ultrasound thermal therapy. *Med Phys*, 30(7): 1855-1863, 2003.

[110] T. Uchida, S. Baba, A. Irie, S. Soh, N. Masumori, T. Tsukamoto, H. Nakatsu, H. Fujimoto, T. Kakizoe, T. Ueda, T. Ichikawa, N. Ohta, T. Kitamura, M. Sumitomo, M. Hayakawa, T. Aoyagi, M. Tachibana, R. Ikeda, K. Suzuki, N. Tsuru, S. Ozono, K. Fujimoto, Y. Hirao, K. Monden, Y. Nasu, H. Kumon, K. Nishi, S. Ueda, H. Koga and S. Naitoh. Transrectal

high-intensity focused ultrasound in the treatment of localized prostate cancer: A multicenter study. *Hinyokika Kiyo*, 51(10): 651-658, 2005.

[111]   T. Uchida, M. Muramoto, H. Kyunou, M. Iwamura, S. Egawa and K. Koshiba. Clinical outcome of high-intensity focused ultrasound for treating benign prostatic hyperplasia: Preliminary report. *Urology*, 52(1): 66-71, 1998.

[112]   C. A. Van den Berg, J. B. Van de Kamer, A. A. De Leeuw, C. R. Jeukens, B. W. Raaymakers, M. van Vulpen and J. J. Lagendijk. Towards patient specific thermal modelling of the prostate. *Phys Med Biol*, 51(4): 809-825, 2006.

[113]   J. F. van der Koijk, J. de Bree, J. Crezee and J. J. Lagendijk. Numerical analysis of capacitively coupled electrodes for interstitial hyperthermia. *Int J Hyperthermia*, 13(6): 607-619, 1997.

[114]   J. van der Zee. Heating the patient: A promising approach? *Ann Oncol*, 13(8): 1173-1184, 2002.

[115]   J. van der Zee and G. D. Gonzalez. The dutch deep hyperthermia trial: Results in cervical cancer. *Int J Hyperthermia*, 18(1): 1-12, 2002.

[116]   J. van der Zee, D. Gonzalez Gonzalez, G. C. van Rhoon, J. D. van Dijk, W. L. van Putten and A. A. Hart. Comparison of radiotherapy alone with radiotherapy plus hyperthermia in locally advanced pelvic tumours: A prospective, randomised, multicentre trial. Dutch deep hyperthermia group. *Lancet*, 355(9210): 1119-1125, 2000.

[117] J. van der Zee and G. C. van Rhoon. Cervical cancer: Radiotherapy and hyperthermia. *Int J Hyperthermia*, 22(3): 229-234, 2006.

[118] M. Van Vulpen, A. A. De Leeuw, B. W. Raaymakers, R. J. Van Moorselaar, P. Hofman, J. J. Lagendijk and J. J. Battermann. Radiotherapy and hyperthermia in the treatment of patients with locally advanced prostate cancer: Preliminary results. *BJU Int*, 93(1): 36-41, 2004.

[119] C. C. Vernon, J. W. Hand, S. B. Field, D. Machin, J. B. Whaley, J. van der Zee, W. L. van Putten, G. C. van Rhoon, J. D. van Dijk, D. Gonzalez Gonzalez, F. F. Liu, P. Goodman and M. Sherar. Radiotherapy with or without hyperthermia in the treatment of superficial localized breast cancer: Results from five randomized controlled trials. International collaborative hyperthermia group. *Int J Radiat Oncol Biol Phys*, 35(4): 731-744, 1996.

[120] P. Wust, B. Hildebrandt, G. Sreenivasa, B. Rau, J. Gellermann, H. Riess, R. Felix and P. M. Schlag. Hyperthermia in combined treatment of cancer. *Lancet Oncol*, 3(8): 487-497, 2002.

[121] R. Yee, S. Connolly and H. Noorani. Clinical review of radiofrequency catheter ablation for cardiac arrhythmias. *Can J Cardiol*, 19(11): 1273-1284, 2003.

[122] A. R. Zlotta and B. Djavan. Minimally invasive therapies for benign prostatic hyperplasia in the new millennium: Long-term data. *Curr Opin Urol*, 12(1): 7-14, 2002.
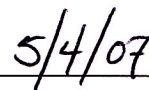
Publishing Agreement

It is the policy of the University to encourage the distribution of all theses and dissertations. Copies of all UCSF theses and dissertations will be routed to the library via the Graduate Division. The library will make all theses and dissertations accessible to the public and will preserve these to the best of their abilities, in perpetuity.

Please sign the following statement:

I hereby grant permission to the Graduate Division of the University of California, San Francisco to release copies of my thesis or dissertation to the Campus Library to provide access and preservation, in whole or in part, in perpetuity.

_____   __5/4/07__

Author Signature   Date